Electronic Thesis and Dissertation Repository

8-15-2019 10:15 AM

In-line Monitoring of Lubricant Addition Through Passive Vibration Measurements in a V-blender

Austin Cameron
The University of Western Ontario

Supervisor
Briens, Lauren
The University of Western Ontario

Graduate Program in Chemical and Biochemical Engineering
A thesis submitted in partial fulfillment of the requirements for the degree in Master of Engineering Science
© Austin Cameron 2019

Follow this and additional works at: https://ir.lib.uwo.ca/etd

Part of the Chemical Engineering Commons

Abstract

Process analytical technologies can improve product monitoring and process efficiency in pharmaceutical manufacturing. Passive vibration measurements were evaluated for their potential as a technique to monitor lubricant dispersal in a V-blender. An accelerometer was attached to the lid of a V-blender shell to measure vibrations from particle collisions. Lubricants formed a layer around the surface of particles, altering energy dissipation upon impact. With mixing, vibrational amplitudes approached a stable value indicating a mixing end-point. Mixing profiles were sensitive to changes in particle type, particle size and distribution, and lubricant concentrations for ideal particles and pharmaceutical granules. Axial loading configurations provided better mixing performance compared to radial configurations. An optimal fill level for effective convective mixing was determined through vibration measurements. Overall, this research demonstrated the potential of using passive vibration measurements as a monitoring technique for lubricant dispersal in pharmaceutical manufacturing to improve control and efficiency of the mixing process.

Keywords

Summary for Lay Audience

Prior to compression in tablet manufacturing, a lubricant is added and mixed in a V-blender to ensure the mixture is ejected from the tablet die smoothly. Mixing is conducted batch-wise and must be analyzed off line afterwards to ensure the mixture is uniform and will produce desired tablet properties, thereby a costly and time-consuming step within the manufacturing process. To improve process efficiency, inline monitoring methods using passive acoustic emissions or vibration measurements could be implemented. These methods are non-destructive, non-invasive, and have a reduced capital cost compared to other monitoring techniques.

An accelerometer was attached to the lid of a V-blender shell to measure vibrations from particle collisions. As particles tumbled, they impacted the lid of the V-shell transmitting a portion of energy into stress waves measured as vibrations by the sensor. When a lubricant was introduced, the lubricant formed a layer around the surface of particles, altering energy dissipation upon impact. With further mixing, the lubricant layer around the particles becomes more complete and uniform. Vibrational amplitudes then approached a stable value indicating a mixing end-point, allowing for the process to be monitored. Vibration measurements were sensitive to changes in particle type, particle size, and lubricant concentrations for ideal particles due to changes in momentum and energy transmission.

Vibration measurements were investigated to determine the effect of loading configuration and fill level on lubricant mixing performance. Axial loading lubricant configurations provided better mixing performance compared to radial configurations due to inherent V-blender mixing mechanisms. An optimal fill level for effective convective mixing was determined to be 21 – 23 vol %.

Lubricant dispersal for pharmaceutical granules was monitored using vibration measurements. Granules required a much smaller mixing time than ideal particles due to differences in particle surface morphology. Mixing profiles were sensitive to particle size, lubricant concentration, and segregation effects in both signal amplitude and variation. Overall, this research demonstrated the potential of using passive vibration measurements as a monitoring technique for lubricant dispersal in pharmaceutical manufacturing to improve control and efficiency of the mixing process.

Co-Authorship Statement

Chapters 3, 4, and 5 have been either submitted or published in refereed journals. The individual contributions of each author are stated.

Chapter 3

Monitoring magnesium stearate blending in a V-blender through passive vibration measurements

Authors: Austin Cameron, Lauren Briens

Status: Published online in *AAPS PharmSciTech* on July 26, 2019.

Austin Cameron performed all experimental work including data analysis. Lauren Briens provided consultation and guidance on experimental work and data analysis. The manuscript was written and revised by Austin Cameron and reviewed by Lauren Briens.

Chapter 4

An investigation of magnesium stearate mixing performance in a V-blender through passive vibration measurements

Authors: Austin Cameron, Lauren Briens

Status: Published online in *AAPS PharmSciTech* on May 24, 2019.

Austin Cameron performed all experimental work including data analysis. Lauren Briens provided consultation and guidance on experimental work and data analysis. The manuscript was written and revised by Austin Cameron and reviewed by Lauren Briens.

Chapter 5

Monitoring lubricant addition in pharmaceutical tablet manufacturing through passive vibration measurements in a V-blender

Authors: Austin Cameron, Lauren Briens

Status: To be submitted for publication in Powder Technology.

Austin Cameron performed all experimental work including data analysis. Lauren Briens provided consultation and guidance on experimental work and data analysis. The manuscript was written and revised by Austin Cameron and reviewed by Lauren Briens.

Acknowledgments

I would like to first thank my supervisor, Dr. Lauren Briens for her continuous support and encouragement. Without her expertise or guidance, the completion of this thesis would not be possible. I would also like to thank Dr. Paul Charpentier for serving on my advisory committee.

I would like to acknowledge the Natural Sciences and Engineering Research Council (NSERC) and the Western University Graduate Research fund for their financial contributions and support.

Thank you to Souheil Afara for his willingness and availability to provide technical assistance. I would also like to thank Ivan Barker at Surface Science Western for examining my particles.

Finally, I would like to thank my parents, family, and friends whose advice and support were of great help throughout the course of this research. This research is dedicated to the bright memory of my grandmother Lorna Closs, through unwavering support believed in my ability to be successful in all my pursuits. Her care from a young age has invaluably contributed to this academic achievement in many ways.

Table of Contents

List of Tables

List of Figures

Chapter 1

1   Introduction

The pharmaceutical tablet manufacturing process consists of a variety of stages conducted batch-wise as shown in Figure 1.1, adapted from Aulton, 2002 (1). Samples must be withdrawn and tested offline extensively after each stage to ensure the product will comply with quality standards. If the sample does not meet the required specifications, the entire batch must be discarded, and the process begins anew.

```
        ┌─────────────┐        ┌ Active Ingredient
        │   Mixing    │◄───────┤
        └─────────────┘        └ Filler
               │
               ▼
        ┌─────────────┐
        │ Granulation │◄──────── Liquid Binder
        └─────────────┘
               │
               ▼
        ┌─────────────┐
        │   Drying    │
        └─────────────┘
               │
               ▼
        ┌─────────────┐
        │   Milling   │
        └─────────────┘                ┌ Dry Binder
               │                        │ Disintegrant
               ▼                        │
        ┏━━━━━━━━━━━━━┓        ┤ Lubricant
        ┃   Mixing    ┃◄───────┤
        ┗━━━━━━━━━━━━━┛        │ Antiadherent
               │                        └ Glidant
               ▼
        ┌─────────────┐
        │  Tabletting │
        └─────────────┘
               │
               ▼
        ┌─────────────┐
        │   Coating   │
        └─────────────┘
```
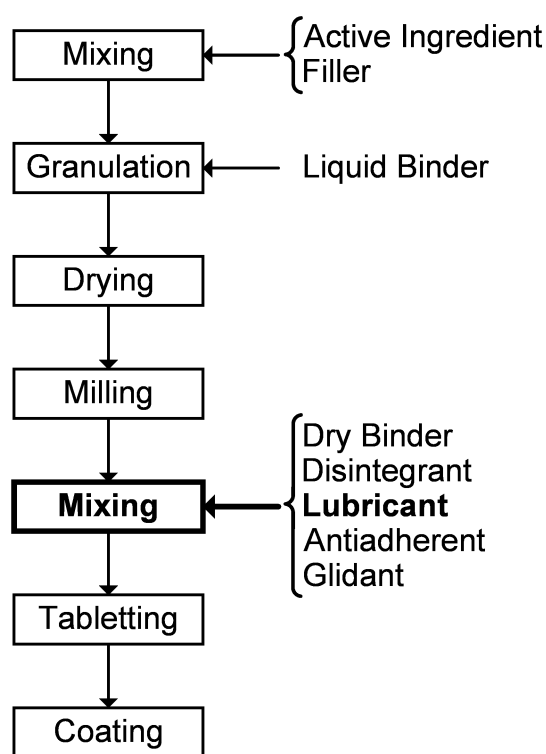
Figure 1.1: Schematic of a typical tablet manufacturing pathway

In the final mixing stage, excipients are added to the granules such as binders, disintegrants, lubricants, antiadherents, and glidants (Figure 1.1); the focus of this research being on the addition of a lubricant. These excipients are added to prepare the mixture for tableting. This mixing step is critical to control as it is the last stage before tableting and can ultimately dictate final tablet properties. Mixing must then be

monitored and controlled to ensure production of tablets with uniform weight and content uniformity, as well as consistent and reproducible properties.

1.1   Lubricant Addition

Prior to tablet compression, a lubricant is added to ensure the tablet is ejected from the press smoothly without sticking or breakage. The lubricant decreases friction between the tablet surface and the die wall reducing the ejection force. Two mechanisms exist in which lubricants affect tablet compression: liquid film lubrication and boundary lubrication (2,3). In liquid film lubrication, a liquid lubricant can form a continuous thin fluid layer in which the lubricant separates the tablet surface and the metal surface. In boundary lubrication, lubricant particles often penetrate surface asperities forming non-continuous and continuous layers between surfaces and interfaces of the excipients and the tablet die. Magnesium stearate is an FDA approved boundary lubricant and is used since it has a high lubricant efficiency, is inexpensive, and chemically stable (4). Magnesium stearate is a is a salt that contains two equivalents of stearate which is the anion of stearic acid and one magnesium cation. The magnesium cation group allows magnesium stearate particles to easily adsorb into surface asperities of particles before adhering to the surface of particles orienting in mono and multilayers (4,5). These layers result in a reduction of contact areas, reducing friction between particles and the tablet press allowing for the tablet to be ejected smoothly. Due to its large surface area, effective lubricant coatings are developed quickly giving magnesium stearate a high lubrication efficiency.

Although necessary in tablet manufacturing, lubricant addition can negatively affect final tablet properties. Due to its hydrophobic nature, magnesium stearate has been known to negatively affect dissolution and disintegration time of tablets (6,7). In addition, as magnesium stearate reduces contact points and friction between particles, it also negatively affects tablet hardness (8-10). These effects are worsened with magnesium stearate concentration and mixing time as magnesium stearate becomes more incorporated into the mixture. Lubricant addition should then be optimized and monitored as magnesium stearate is effective and small amounts and is difficult to disrupt once adhered to the surface of particles (9,11).

1.2   Tumbling Mixers

Lubricant addition is carried out primarily in tumbling mixers. Tumbling mixers are mounted on a rotating axle where particles mix due to gravity. Tumbling mixers can vary in their geometry where V-blenders are composed of two shells connected at angles between 75-90° and can differ in shell size. The V-blender is used since it is well established and provides effective mixing for lubricant dispersal but gentle mixing for fragile granules used in the tablet manufacturing process. As particles tumble in a V-blender, there are two mixing mechanisms due to the inherent geometry of the V-blender as shown in Figure 1.2. One occurs from 0-180° of rotation where the mixer goes from an upright position to that of inverted. Here, mixing is dominated by a convective mechanism of particles being randomly distributed through free fall as they separate to each arm of the shell. The other phase occurs through 180-360° of rotation as the mixer goes from an inverted to an upright position. The particles converge at the bottom and only a fraction of the particles cross the axis of symmetry through axial dispersion. Therefore, mixing in a V-blender is much more effective in each arm of the shell than across the axis of symmetry (12-16).
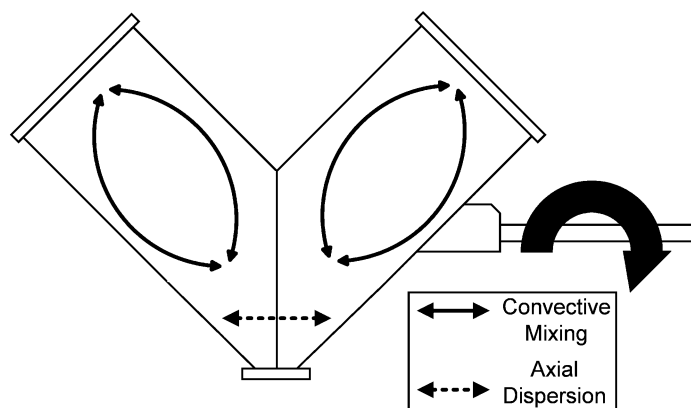
Figure 1.2: Schematic of a V-blender mixing mechanisms with axis of rotation

Due to its inherent mixing mechanisms, mixing performance in a V-blender is affected by fill level, mixing time, rotation speed, and loading configuration (12-16). In addition, as the V-blender relies on gravity to provide effective mixing, trajectory segregation can occur depending on particle size, shape and surface morphology (17,18). Large

differences in particle size, density, and distribution width from the granulation stage cause heavier, more dense particles to fall faster within the mixer and separate from their smaller or lighter counterparts. Since lubricants improve flowability (5,11,19) mixtures are more susceptible to segregate during lubricant addition. These parameters could then have serious implications on lubricant addition in a V-blender and should be optimized and controlled to ensure effective lubricant dispersal.

1.3   Process Monitoring

1.3.1   Assessing Blend Homogeneity

Once a lubricant is mixed, the homogeneity of the blend must first be assessed to ensure it meets product regulations. Samples are first withdrawn using a thief probe, consisting of two concentric tubes, with aligning holes depending upon if its an open or closed position. Upon insertion, the thief probe is rotated to align the sample ports on both tubes, a sample of powder flows into the cavity, and the probe is withdrawn. Once extracted, these samples are analyzed using destructive methods such as high-performance liquid chromatography (HPLC) and UV spectroscopy. These methods suffer from many drawbacks, which have been investigated and studied extensively (20-22). The insertion of the probe itself can disturb the bed leading to segregation, channeling, and introduce contamination. Multiple samples are then required at various positions throughout the bed to provide a representation of the entire blend, but again becomes error prone. These methods then become laborious, time consuming, and costly. As well, if the blend is found not to be uniform, the material is discarded, and the entire mixing process must be repeated.

1.3.2   Process Analytical Technologies

To monitor, control, and optimize pharmaceutical mixing processes, process analytical techniques (PAT) are being developed. PAT are systems that implement sensors to monitor and detect changes in real time in manufacturing processes with the aim of increasing product quality and efficiency while removing issues associated with extractive sampling (23). For mixing, PAT could determine mixing end-points in real

time, resulting in fewer rejected batches allowing for better control and improved efficiency of the manufacturing process.

PAT to determine uniformity and homogeneity within mixing that have been studied extensively include near infrared spectroscopy (NIR), Raman spectroscopy, magnetic nuclear resonance imaging (MRI), and radioactive tracers. Chapter 2 will provide an in-depth review of the development and applications of PAT in mixing.

1.4 Passive Vibration Measurements

The focus of this research is the development of passive vibration measurements or acoustic emissions to monitor lubricant addition in tablet manufacturing. Passive vibrations offer many advantages over other PATs as they are completely non-invasive, non-destructive, and have a lower capital cost compared to other methods (24).

Due to sudden localized changes in stress, energy in the form of vibrational waves are generated, transmitted, and received as they propagate through matter (25). In tumbling mixers, vibrations are created from the transfer of energy between particle-particle collisions, particle-equipment collisions, and equipment noise (26). Monitoring mixing using passive vibration measurements refers to the differences in measured signal amplitudes from a heterogeneous state to a homogenous state.

Crouter and Briens (27) assessed the feasibility of passive vibration measurements to monitor lubricant addition for sugar spheres and pharmaceutical granules. Measured signals changed as the lubricant was dispersed. Some of the mixing profiles showed significant scatter making it difficult to extract important information about the mixing. The measurements showed potential to monitor mixing, but more research and development was clearly needed.

1.4.1 Sensors

In this research, vibrations were measured using an ICP (Integrated Circuit Piezoelectric) accelerometer manufactured by PCB Piezotronics. These sensors utilize the piezoelectric effect of quartz to generate an electrical output which is proportional to the applied force

on the accelerometer. The force applied to the sensor alters the alignment of positive and negative ions in the quartz. The applied acceleration results in a charge separation in which ions accumulate on an electrode and are then transmitted to a signal conditioner (28). The accelerometer was affixed to the V-blender lid using adhesive wax. The lid was chosen as the mounting location as it allows for the transfer of the least attenuated and most distinct vibrations to the sensor based on the mixing mechanisms inherent within the V-blender (29). Adhesive wax was used for mounting as it provided the desired stiffness and minimal interference for the sensor while not requiring modification of existing equipment.

1.4.2   Acquisition Frequency and Sampling Rate

In this research, signal vibrations were captured within the audible range (20 – 20,000 Hz) as frequency analysis outside this frequency range did not provide any identifiable trends in preliminary experiments (29). Signals measured from the accelerometer are a continuous analog signal, which must be converted to a digital format during computer processing. To prevent signal aliasing, the sampling rate required for the audible frequency range is 40,000 Hz based on the Nyquist theorem. The accelerometer had a range of 0.35 – 12,000 Hz and a sampling rate of 40,000 Hz was used.

1.4.3   Signal Filtering

Some noise in low frequency bands is attributed to equipment noise which must be filtered to extract valuable process data. A high-pass, 6 tap Daubechies level 12 wavelet decomposition filter was chosen (30) to remove emissions less than 3 Hz. A wavelet filter works by removing an approximation of the signal based on a sine wave. The filter decomposes the signal into components in the time-frequency domain. Using thresholding technique, wavelet components containing noise are removed. The original signal without noise is reconstructed using an inverse filter. The small portion of the signal that remains after filtering is due to the signal not being a perfect sine wave. Level 12 decomposition was chosen as a balance between computing times without affecting the time or frequency encoded information.

1.5   Coefficient of Restitution

To elucidate the energy transfer occurring in collisions within the tumbling V-blender, and consequently the measured vibrations by the accelerometer, a parameter, the coefficient of restitution (COR) was estimated and used in this research. The COR models particle collisions based on a variety of characteristics that affect the kinetic energy dissipated in a collision as governed by Newton's law of restitution. It is measured as a ratio of the energy retained after a collision to that of pre-collision. When a collision becomes more elastic, that is most of the energy is retained after collision, the COR approaches one. Conversely, the COR becomes zero when all the energy is dissipated, and the collision is entirely inelastic.

Particle collisions within a tumbling V-blender can be modelled by particle collisions with plates. Here, the COR is primarily dependent on the mechanism of energy dissipated within a collision based on material properties. Upon collision, energy from the particle is mainly dissipated through stress waves that propagate throughout the material. More minor forms include flexural wave propagation, air drag, and rotational velocity depending on environmental conditions. Ductile particles are more susceptible to undergo plastic deformation upon contact with the plate transferring much more energy than retained, resulting in a more inelastic collision and therefore a low COR. This is compared to harder, more elastic particles where much of the energy is retained by the particle, where the collision is more elastic resulting in a higher COR (31). This is true up until a certain threshold where a critical velocity is reached, and the material yields under stress. Heavier particles with increased density and size result in a lower COR as these particles possess a higher kinetic energy upon impact resulting in a larger contact deformation due to added mass. This is particularly important in thin plates as increased mass causes bending of the plate and flexural vibrations can propagate back and forth to the point of contact resulting in an additional energy loss and a lower COR (32,33). Similarly, with increasing impact velocity, because of the increased trajectory height, more energy is transferred to the plate than retained, causing a lower COR (32-34). As well, with increasing impact angle, the COR decreases since less energy is transferred to the normal component of the collision allowing for an increased rebound in the tangential

component (34). The coefficient of restitution and inelasticity of collisions can be summarized by the inelasticity parameter, developed by Zener (35):

$$e = \frac{\pi^{\frac{3}{5}}}{3^{\frac{1}{2}}} \left(\frac{r}{2t}\right)^2 \left(\frac{v_0}{v\prime}\right)^{\frac{1}{5}} \left(\frac{\rho_{pa}}{\rho_{pl}}\right)^{\frac{3}{5}} \left(\frac{E_{pa}}{E_{pa}+E_{pl}}\right)^{\frac{2}{5}}$$ (eq. 1.1)

where r is the particle radius, t is the plate thickness, v_0 is the incident velocity, v' is the rebound velocity, ρ_{pa} is particle density, ρ_{pl} is plate density, and E_{pa} and E_{pl} are the elastic modulus of the particle and plate respectively. An increase in the inelasticity parameter corresponds to a more inelastic collision resulting in a lower COR.

When lubricants adhere to the surface of particles, they affect the intrinsic properties of the particles such as the elastic modulus making collisions more inelastic. Additional energy dissipation occurs into the magnesium stearate layer where less energy is retained by the particle post collision resulting in a lower measured COR. With additional mixing, this layer becomes more developed in thickness and uniformity further dampening collisions resulting in an even lower energy dissipation and measured COR (36).

Conventionally, the definition of the COR is measured by the ratio of the particle's velocity after and before collision. From the laws of motion and momentum, the COR can also be represented by the ratio of the particle's rebound height to the initial drop height. Similarly, the COR can be represented as the ratio of time between successive rebounds which can be measured by an accelerometer through vibrations caused by collisions (37).

Therefore, the COR can effectively model energy transfer in a collision which can be measured by an accelerometer through vibrations produced from the energy transfer of the particles with the V-shell. Energy dissipated into the V-shell through vibrations are measured by the accelerometer, and the energy retained by the particle after collision is measured by the COR. An increase in parameters such as impact velocity and mass result in a lower COR and subsequently an increase in the vibrations measured as more energy is dissipated than retained by the particle. When magnesium stearate is added and mixed, energy is dissipated into the formed magnesium stearate layer than transmitted into the

V-shell lid or retained by the particle. Subsequently, both the COR and measured vibrations decrease. The COR is then an important parameter in modelling the energy transfer in a system and consequently modelling the vibrations measured based on mixing dynamics and changes in process parameters of a V-blender.

1.6   Thesis Objectives and Overview

Preliminary research demonstrated the feasibility of passive vibration measurements to monitor lubricant addition in a V-blender (27). Further work is required to understand how passive vibration measurements monitoring lubricant addition is affected by various process parameters and challenges to gain process knowledge leading toward industrial implementation. The objectives are addressed over the subsequent chapters as follows:

Chapter 2 provides a summary of the development of PAT for mixing processes and the advantages and disadvantages of each.

Chapter 3 uses vibration measurements to monitor lubricant addition in a V-blender for ideal particles of sugar spheres and glass beads of differing sizes mixed with increasing amounts of lubricant. Emphasis was put on understanding energy transfer, mixing mechanisms, and coating morphology in lubricant addition through the coefficient of restitution, flowability, and SEM images.

Chapter 4 investigates the effect of inherent V-blender mixing limitations on the mixing performance of a lubricant through loading configuration and V-shell fill level. This was assessed by monitoring the process with vibration measurements of glass beads mixed with magnesium stearate.

Chapter 5 applies the knowledge of previous chapters to monitor lubricant addition in a V-blender through passive vibration measurements for pharmaceutical granules. The effect of lubricant concentration, particle size, and segregation effects were determined and compared with glass beads as a model particle.

Chapter 6 provides a general discussion and conclusions from this research with recommendations for future work.

1.7   References

1. Aulton, M. *Pharmaceutics: The Science of Dosage Form Design*. Edinburgh; New York: Churchill Livingstone 2002; 379 – 396.
2. Miller T, York P. Pharmaceutical tablet lubrication. Int J Pharm 1988; 41(1-2): 1-19.
3. Staniforth, J, Cryer S, Ahmed H, Davies S. Aspects of pharmaceutical tribology. Ind Drug Dev Pharm 1989; 15(14-16): 2265 – 2294.
4. Perrault M, Bertrand F, Chaouki J. An investigation of magnesium stearate mixing in a V-blender through gamma-ray detection. Powder Technol 2010; 200(3): 234 -245.
5. Morin G, Briens L. The effect of lubricants on powder flowability for pharmaceutical application. AAPS PharmSciTech 2013; 14(3): 1158-1168.
6. Kikuta JL, Kitamori N. Effect of mixing time on the lubricating properties of magnesium stearate and the final characteristics of the compressed tablets. Drug Dev Ind Pharm 1994; 20: 343-355.
7. Abe H, Otsuka M. Effects of lubricant-mixing time on prolongation of dissolution time and its prediction by measuring near infrared spectra from tablets. Drug Dev Ind Pharm 2012; 38: 412-419.
8. Jarosz PJ, Parrott EL. Effect of lubricants on tensile strengths of tablets. Drug Dev Ind Pharm 1984; 10: 259-273.
9. Johansson ME. Influence of the granulation technique and starting material properties on the lubricating effect of granular magnesium stearate. J Pharm Pharmacol 1985; 37: 681-685.
10. Perrault M, Bertrand F, Chaouki, J. An experimental investigation of the effect of the amount of lubricant on tablet properties. Drug Dev Ind Pharm 2011; 37(2): 234-242.
11. Pingali KC, Saranteas K, Foroughi R, Muzzio FJ. Practical methods for improving flow properties of active pharmaceutical ingredients. Drug Dev Ind Pharm 2009; 35(12): 1460-1469.
12. Brone D, Wightman C, Connor K, Alexander A, Muzzio FJ, Robinson P. Using flow perturbations to enhance mixing of dry powders in V-blenders. Powder Technol 1997; 91: 165-172.
13. Brone D, Alexander A, Muzzio FJ. Quantitative Characterization of mixing of dry powders in v-blenders. AIChE J 1998; 44:271-278.
14. Kuo H, Knight P, Parker D, Seville J. Solids circulation and axial dispersion of cohesionless particles in a V-mixer. Powder Technol 2005; 152: 133-140.
15. Lemieux M, Bertrand F, Chaouki J, Gosselin P. Comparative study of the mixing of free-flowing particles in a V-blender and a bin-blender. Chem Eng Sci 2007; 62: 1783-1802.
16. Lemieux M, Leonard G, Doucet J, Leclaire L, Viens F, Chaouki J, Bertrand F. Large-scale numerical investigation of solids mixing in a V-blender using the discrete element method. Powder Technol 2008; 181:205-216.

17. Ottino JM, Khakhar DV. Mixing and segregation of granular materials. Annu Rev Fluid Mech 2000; 32: 55-91.
18. Bridgewater J. Mixing and segregation mechanisms in particle flow. Granular Matter 1994; 161-193.
19. Faqih AM, Mehrotra A, Hammond SV, Muzzio FJ. Effect of moisture and magnesium stearate concentration on flow properties of cohesive granular materials. Int J Pharma 2007; 336(2): 338-345.
20. Deveswaran R, Bharath S, Basavaraj BV, Abraham S, Furtado S, Madhavan V. Concepts and Techniques of Pharmaceutical Powder Mixing Process: A Current Update. J Pharm Tech 2009; 2: 245-249.
21. Garcia T, Wilkinson S, Scott J. The Development of a Blend-Sampling Technique to Assess the Uniformity of a Powder Mixture. Drug Dev Ind Pharm 2001; 27:4, 297-307.
22. Muzzio FJ, Goodridge CL, Alexander A, Arratia P, Yang H, Sudah O, Mergen G. Sampling and characterization of pharmaceutical powders and granular blends. Int J Pharm 2003; 250: 51-64.
23. Bakeev K. Overview of Process Analysis and PAT. *Process Analytical Technology: Spectroscopic Tools and Implementation Strategies for the Chemical and Pharmaceutical Industries*. Wiley: 2010; 1–14.
24. Crouter A, Briens L. Methods to assess mixing of pharmaceutical powders. AAPS PharmSciTech 2019; 20:84.
25. Kinsler L, Frey A, Coppens A, Sanders J. Fundamentals of acoustics. New York City, United States of America: Wiley; 1999.
26. Tily P, Porada S, Scruby C, Lidington S. Monitoring of mixing processes using acoustic emission. In: Harnby N, Benkreira H, Carpenter K, Mann R, eds. Fluid Mixing III. Rugby: The Institute of Chemical Engineers 1988; 75-94.
27. Crouter A, Briens L. Monitoring lubricant using passive acoustic emissions in a V-blender. Powder Technol 2016; 301: 1119 – 1129.
28. PCB Piezotronics, Inc. (2019). Introduction to ICP Accelorometers. Retrieved Jan 15, 2019 from http://www.pcb.com/Resources/Technical-Information/Tech_Accel
29. Crouter A, Briens L. Passive acoustic emissions from particulates in a V-blender. Drug Dev Ind Pharm 2015; 11: 1809 – 1818.
30. Daubechies I. The wavelet transform, time-frequency localization and signal analysis. IEEE Trans Inf Theory 1990; 36: 961-1005.
31. Marinack M, Musgrave R, Higgs C. Experimental investigations on the coefficient of restitution of single particles. Tribology Transactions. 2013; 56(4): 572 – 580.
32. Sondergaard R, Chaney K, Brennen C. Measurements of spheres bouncing off flat plates. Journal of Applied Mechanics. 1990; 112(3): 694 – 699.
33. Muller P, Bottcher R, Russell A, True M, Aman S, Tomas J. Contact time at impact of spheres on large thin plates. Adv Powder Tech 2016; 27(4): 1233 – 1243.
34. Salman A, Verba A, Lukenics Z, Szabo M. Effects of impact velocity and angle on collision. Period Polytech Chem Eng 1991; 35(1-2): 43 – 51.

35. Zener C. The intrinsic inelasticity of large plates. Phys Rev 1941; 59: 669 – 673.
36. Crouter A, Briens L. Monitoring lubricant addition using passive acoustic emissions in a V-blender. Powder Technol 2016; 301: 1119-1129.
37. Aguiar C, Laudares F. Listening to the coefficient of restitution and the gravitational acceleration of a bouncing ball. Am J Phys 2003; 71: 499 – 501.

Chapter 2

2 Process Analytical Technologies (PAT)

2.1 Introduction

Mixing is a critical process step in tablet manufacturing to ensure proper blend homogeneity resulting in tablets with reproducible and desirable properties. This is particularly important for certain excipients and active pharmaceutical ingredients (API) including lubricants which are added in low concentrations, where proper uniformity is difficult to achieve (1). Lubricant mixing performance is a complex function between mixer and lubricant process parameters which negatively affect final tablet properties (2-5). Strict and extensive validation testing is then required to ensure proper content uniformity before the sample can move to tableting.

The Barr laboratories trial in 1993 (6) caused the Food and Drug Administration (FDA) to modify its policies on blend uniformity and sampling methods. However, limitations in current sampling techniques still exist due to sampling biases. Currently, blend homogeneity is assessed offline by first extracting samples with thief probes and analyzing through conventional spectroscopic techniques. However, this assessment suffers from drawbacks attributed to local segregation of pharmaceutical mixtures leading to errors within sampling. The insertion of the thief probe may cause channeling in which particles from upper layers are dragged into lower layers with further insertion depths of the probes (7). As well, upon sampling, larger particles in the mixture preferentially flow into the sampling cavity due to segregation (8). These mechanisms can lead to contamination and content variation, making it difficult to obtain representative samples (9). Therefore, sub-sampling and multiple samples at various points in the powder bed are required, making analysis costly and time consuming. Furthermore, current assessments can only ensure the homogeneity at single points in time. Mixtures can undergo further segregation with further handling, discharge, and transport leading to reduced final product quality.

To remove issues associated with extractive sampling, provide better control over processes through monitoring, process analytical technologies (PATs) have been developed for designing, analyzing, and controlling manufacturing through timely measurements during processing of critical quality and performance attributes with the goal of ensuring final product quality (10). There have been advances and growing interest in PAT due to initiatives put forth by regulated bodies such as the FDA introducing a framework and quality by design for PAT in 2004 (10) and more recently through published guidance of ICH Q13 Continuous Manufacturing of Drug Substances and Products and ICH Q14 Analytical Procedure Development which complement Q8-Q11 (11). PAT include systems that implement sensors to monitor and detect changes real time in manufacturing processes. For mixing processes, PAT would allow for better monitoring and control resulting in fewer rejected batches and improve product quality.

Many technologies have been investigated to evaluate the content uniformity and homogeneity of mixtures and identify an optimal mixing end-point. These technologies include spectroscopic, velocimetric, and tomographic process analytical technologies along with passive vibration measurements.

2.2   Spectroscopic Techniques

Spectroscopic techniques are based on the interaction of electromagnetic radiation with matter. Interaction of electromagnetic energy results in vibrations and frequencies of molecules due to absorption and emission of photons. Individual components resonate at unique wavelengths allowing for the identification of these components in a mixture. Near infrared spectroscopy (NIR) has been well established as a monitoring technique, with others including Raman spectroscopy and laser induced fluorescence (LIF).

2.2.1   Near-Infrared Spectroscopy

NIR utilizes the unique absorption of light in the infrared spectrum to identify components in a mixture and monitor mixing processes. When samples are irradiated with NIR light, some NIR light is absorbed by molecules, bringing them to a higher vibrational state. Vibrations can result in molecule stretching, compression, and bending between molecule bonds. NIR signal is then proportional to the degree of bending and

stretching based through the change in bond distance and angle (12). Based on composition, powders absorb and respond to NIR differently particularly powders with O-H, N-H, C-H, and S-H bonds (13). Therefore, NIR produces large amounts of overlapping, weak absorbance spectral data which require pre-treatment and extensive analysis to extract useful information to be implemented as a potential monitoring technique to assess homogeneity in mixing processes (14). NIR for the monitoring of mixing has been studied extensively for various types of mixers. Table 2.1 summarizes NIR monitoring in tumbling mixers, where various pre-processing and spectral analysis methods must be implemented to extract useful process information.

Table 2.1: NIR spectroscopy applications for tumbling mixing monitoring

Reference	API (s)	Excipients	Mixer	Assessment parameter	Pre-treatment Method	Spectral Analysis
Hailey *et al.* (15)	API from Pfizer	Lactose, maize starch	Y-cone blender	Homogeneity	SNV, DT	MBSD
Sekulic *et al.* (16)	Sodium benzoate	Avicel, lactose, MgSt	V-blender	Homogeneity	Dx^2y	MBSD
Wargo and Drennen (17)	Hydrochlorothiazide	Croscarmellose sodium, lactose, sodium, MgSt	Twin shell blender	Homogeneity	Dx^2y	BEST, PCA
De Maesschalck *et al.* (18)	API	Aerosil, lactose, maize starch	Tumbling blender	Homogeneity	Dx^2y, SNV, DT	Dissimilarity, MSD, PCA
Sekulic *et al.* (19)	API	Avicel, DCP, sodium glycolate, MgSt	Flo-bin blender	Homogeneity	Dx^2y, SNV, DT	MBSD, Dissimilarity, PCA, SIMCA
El-Hagrasy *et al.* (20)	Salicylic acid	Fast-Flo lactose	V-blender	Homogeneity	Dx^2y, SNV, MSC	MBSD, PCA, SIMCA
El-Hagrasy *et al.* (21)	Salicylic acid	Fast-Flo lactose	V-blender	Homogeneity	Dx^2y, SNV, MSC	PCA
El-Hagrasy *et al.* (22)	Salicylic acid	Fast-Flo lactose	V-blender	Homogeneity	Dx^2y	SIMCA, PC-MBEST
El-Hagrasy and Drennen (23)	Salicylic acid	Fast-Flo lactose	V-blender	Homogeneity	Dx^2y	PCR, PLS, MLR

Table 2.1 (continued)

Reference	API (s)	Excipients	Mixer	Assessment Parameter	Pre-treatment Method	Spectral Analysis
Shi *et al.* (24)	Acetaminophen	Avicel, lactose, MgSt	Bin blender	End-point	S-G, SNV	MBSD, PLS, RSD
Liew *et al.* (25)	Chlorpheniramine maleate	Avicel, lactose, MgSt	Bin blender	Homogeneity	SNV	PLSR
Sulub *et al.* (26)	API	Crospovidone, lactose, MCC	Bin blender	End-point	Dx^2y, S-G, SNV	PLS
Igne *et al.* (27)	Acetaminophen	Croscarmellose sodium, lactose, MCC, MgSt	V-blender	End-point	S-G, SNV	SIM PLISMA
Jaumot *et al.* (28)	Acetaminophen	Croscarmellose sodium, lactose, MCC, MgSt	V-blender	Homogeneity end-point	MSC	ALS
Bakri *et al.* (29)	Naproxen	Avicel, mannitol, MgSt, croscarmellose sodium	Bin blender	Homogeneity	Dx^2y, S-G, SNV	PLS
Besseling *et al.* (30)	API	Avicel, crospovidone, DCP, polyplasdone XL, silica, sodium bicarbonate, talc	Tumbling blender	Homogeneity end-point	S-G, SNV	PLS
Murayama *et al.* (31)	Ascorbic acid	MgSt, mannitol	V-blender	Homogeneity end-point	Dx^2y, S-G	MBSD
Sibik *et al.* (32)	API	Lactose, talc	Bin blender	End-point	DT, S-G, SNV	MBSD

Table 2.1 (continued)

Reference	API (s)	Excipients	Mixer	Assessed Parameter	Pre-treatment Method	Spectral Analysis
Tewari *et al.* (33)	API	Croscarmellose sodium, MgSt, mannitol	V-blender	End-point		PCR, PLS
Lee *et al.* (34)	Chlorpheniramine maleate	Avicel, lactose	Double cone blender	Homogeneity		PLSR

* MgSt magnesium stearate, MCC microcrystalline cellulose, DCP dibasic calcium phosphate, SNV standard normal variate, DT detrending, Dx^2y second derivative, MSC multiplicative scatter correction, S-G Savitzky-Golay pre-treatment, MBSD moving block standard deviation, PLS partial least squares analysis, RSD relative standard deviation, PLSR partial least squares regression, SIM PLISMA simple-to-use interactive self-modelling mixture analysis, ALS alternating least squares, PCR principal component regression, MLR multiple linear regression, BEST boot-strap error adjusted single sample technique, PC-MBEST principle component modified BEST

2.2.1.1   NIR Spectra Pre-treatment

Variability in particle size distribution, packing density, shape, and morphology can result in detrimental light scattering (14). This unwanted variation results in additive, scaling, and shifting effects of the spectrum effectively masking process information. It is critical to select an appropriate pre-treatment method before spectral analysis. The most common methods used include derivatives, detrending, normalization, standard normal variate (SNV), and multiplicative scatter correction (MSC).

MSC removes undesirable scattering effects through a linear regression of estimation coefficients of the additive and multiplicative contributions using a reference spectrum (35):

$$x_{org} = b_o + b_{ref,1} \cdot x_{ref} + c \qquad\qquad \text{(eq 2.1)}$$

where x_{org} is the original sample spectra, x_{ref} is the reference spectrum, b_0 and $b_{ref,1}$ are scaling factors, and c is unmodelled part of the relation. Once estimation coefficients are obtained, MSC corrects the original signal:

$$x_{corr} = \frac{x_{org} - b_o}{b_{ref,1}} \qquad\qquad \text{(eq. 2.2)}$$

where x_{corr} is the corrected spectral signal.

SNV removes baseline contributions by scaling and centering spectra by subtracting the mean and dividing by the standard deviation of the entire spectra (36):

$$x_{corr} = \frac{x_{org} - a_0}{a_1} \qquad\qquad \text{(eq. 2.3)}$$

a_0 is the spectral mean, and a_1 is the spectral standard deviation. Normalization differs from SNV in the fact it removes the scale, but the spectra is not shifted (a_0 is set to zero).

Spectral derivatives are applied to resolve peak overlap and enhance resolution. First derivatives remove added baselines in the signal, and second derivatives allow for the removal of both the baseline and linear drift between samples. However, derivatives

result in a reduction of signal to noise ratio and original spectral shape. To correct this, the Savitzky-Golay method (37) can be implemented which involves a smoothing step. A polynomial of varying degree is fitted to a window of raw data allowing for derivatives to be easily calculated.

Detrending fits a low degree polynomial to all data points in a NIR spectrum and the corrected signal is the result of subtracting the polynomial fit from the original spectrum. Detrending is normally used complementary with SNV (14).

NIR spectra pre-treatments are necessary to extract valuable process data, however, selection of the proper method is dependent on the application and processing capabilities. Higher degree fits and corrections reduce the signal to noise ratio and eliminate background signal more effectively, however, would introduce increased processing times.

2.2.1.2 NIR Spectra Analysis

Once pre-treated, NIR spectra are analyzed and visualized to show changes in homogeneity with mixing. Once the signal stabilizes over time, a mixing end-point can be identified. However, due to the abundance of data produced in NIR spectra, the appropriate method must be applied to best visualize and represent process data. Most common methods are dissimilarity, moving block standard deviation (MBSD), principal component analysis (PCA), and partial least squares (PLS), or variants that are modified to some extent.

Dissimilarity is calculated by taking the normalized spectra during mixing and projecting them orthogonally onto a normalized target spectrum (38):

$$Diss_i = x_i - (x_i \times t_i^T)t_i \qquad\qquad (eq. 2.4)$$

where x_i is the measured normalized spectra during mixing and t_i is the target spectra. The calculated dissimilarity plots are plotted against mixing time. The obtained profiles allow for identification of steady state mixing where homogeneity is uniform.

A MBSD calculates the standard deviation computes the standard deviation of each wavelength i for a set of n consecutively recorded spectra over a sliding window of specified length:

$$S_i = \sqrt{\frac{\sum_{j=1}^{n}(x_{ij} - \bar{x}_i)^2}{n-1}}$$ (eq. 2.5)

Where x_{ij} is the absorbance at wavelength i in spectrum j, and $\bar{x}_i$ is the mean absorbance for the n spectra at the same wavelength. The standard deviation of each window is then plotted with time until the profile reaches a plateau indicating uniform homogeneity and a mixing end-point. Moving standard deviations are advantageous over other methods in the fact that they do not require a reference spectrum (39).

Multivariate analysis can be used as an analysis technique for NIR spectral data. PCA transforms a large matrix X of pretreated spectra data that has N rows of observations, with K columns of variables, into a lower dimensional matrix consisting of scores and loadings (T matrix) which retain maximal information about the variables. These observations can be projected onto a n-observation dimensional space and fitted to reveal information. For three measurements, it can be represented in a three-dimensional space. The observations are fitted with a line of best fit that minimizes the variance of the observation. Each data point is a 90° projection of this component, where scores represent the distance of each data point to the first component. A second component is perpendicular to the first, in which these two components form a plane in the three-dimensional space. The distance of each data point to this plane is a measure of the residual errors (17). The score plot can be used to compare similarity of spectra. Score plots similar to one another and equally distributed, indicate that the mixture spectra is indistinguishable representing a uniform homogeneity.

PLS extends PCA to incorporate a Y matrix of outcome or calibration data. The Y matrix is used to define other components known as u-scores (U matrix). The conventional scores in PCA are used to predict the u-scores which predict the response variable Y. For PLS, the covariance of the scores in the X and Y space is maximized to provide the greatest possible relation between each variable (23). Once again, second components are

obtained forming a plane providing score information on the relation between matrix X and Y.

2.2.1.3   NIR Disadvantages

NIR spectroscopy has been well established as a monitoring technique for mixing processes, however, is still limited by some disadvantages. NIR spectra require extensive pre and post-processing treatment making interpretation of data more difficult and increasing processing time. As well, NIR would require modifications to equipment as windows or ports are required for measurements by the sensor. Modifications would then increase costs and regulatory steps. Finally, the probe tip, sensor window or port must be clear to provide accurate measurements, which is difficult to control particularly in tablet manufacturing mixing when dealing with fine, cohesive, powders.

2.2.2   Raman Spectroscopy

Raman spectroscopy utilizes the polarizability of particles that result in different excitation levels of emitted photons when particles are exposed to monochromatic light. When exposed to monochromatic light, light is primarily scattered elastically in a sample, where the energy of the emitted proton, and therefore the frequency, is the same as the incident light. This is known as Rayleigh scattering. However, a very small fraction of the scattered light results in emitted protons that differ in frequency and energy. When monochromatic light interacts with particles, electrons absorb or release energy from incident photons changing the virtual energy state of the electron for a finite amount of time until photons are emitted at different frequencies and energies, resulting in the electron returning to a different energy state than the initial (40). Stokes lines occur when the electron absorbs energy and the frequency of the scattered photon is greater than that of the incident. Conversely, Anti-Stokes lines occur when electrons release energy and the frequency of the photon is less than that of the incident beam. These lines are represented by distinct peaks that are specific to the particle sampled. Raman spectroscopy can be then used to identify specific molecules and monitor differences in homogeneity as vibrational frequencies are specific to molecular composition.

Raman spectroscopy has been implemented for various pharmaceutical manufacturing processes including fluidization (41), granulation (42), coating (43,44) extrusion/spheronization (45), hot-melt extrusion (46), and freeze drying (47). However, only a few studies on mixing and determining end-point homogeneity have been conducted. Vergote *et al.* (48) utilized Raman spectroscopy to monitor mixing of a binary mixture of diltiazem pellets and paraffinic wax beads in a planetary mixer. Large variations of the mean square of differences of spectra were seen until the signals reached a plateau indicating a mixing end-point which was confirmed by high-performance liquid chromatography. Hausman *et al.* (49) used Raman spectroscopy to determine the blend uniformity of low dose azimilide dihydrochloride in a pharmaceutical blend in a tumbling V-blender. Using principal component regression, De Beer *et al.* (50) evaluated the in-line concentrations of the API ibuprofen in a pharmaceutical aqueous suspension. De Beer *et al.* (51) employed Raman spectroscopy to monitor the blend homogeneity of diltiazem hydrochloride in a high shear powder mixing process. A soft independent modelling of class analogy was developed to assess uniformity and identify mixing end-points, confirmed by near-infrared measurements. Dallin *et al.* (52) identified mixing end-points of increasing amounts of aspirin in Avicel in a convective mixer.

Like near-infrared spectroscopy, Raman spectroscopy suffers from the same disadvantages including requiring a window or a port into the mixing vessel and resulting fouling of the probe. Multiple measurements are then required for representative measurements making analysis more extensive. In addition, fluorescence can interfere and mask the Raman signals when certain materials allow for the complete absorption of the photon followed by emission (40). However, Raman spectroscopy has a greater chemical specificity over NIR and is useful in multi component mixtures since Raman produces strong individual peaks.

2.3 Velocimetric Techniques

Velocimetric techniques locate and track a tracer particle over time elucidating mixing dynamics. Tracers can include coloured particles in optical image analysis and radioactive tracers for positron emission particle tracking (PEPT).

2.3.1   Optical Image Analysis

Image processing can be a non-invasive technique for monitoring mixing processes. Image processing utilizes the difference in colour contrast of particles to determine homogeneity throughout the duration of mixing to identify an end-point. Alternatively, particle contrast can allow for particles to act as tracers effectively monitoring mixing through tracking velocity profiles.

In image analysis, a camera acts as a sensor to monitor mixing in which images are then analyzed through various image analysis software. Proper calibration (53) and selection of post-analysis (54) is crucial in the performance of image analysis as a monitoring technique. Chen and Yu (55) mixed Ti/SiO_2 and C/SiO_2 with mechanical vibration and hand-shaking and analyzed samples after mixing offline through image analysis in an optical microscope. A binary analysis was performed using thresholding which set darker Ti particles to a value of one, and lighter white silica to zero. Based on the uniformity of the produced binary values, a mixing efficiency was determined. This demonstrated the potential for image analysis to identify the homogeneity of a mixture. Bulent *et al.* (56) monitored the mixing of plaster with dyes inline through a modified impeller mixer with a viewing port. The grayscale intensity changed during mixing until a stable value was reached indicating a mixing end-point. The image of interest restricted viewing not providing a good representation of the entire mixture. Realpe and Velazquez (53) implemented better calibration by using PCA followed by PLS resulting in calibration spectrums of mean grey values that mimicked NIR spectra. Mixtures of lactose, starch, microcrystalline cellulose, and coloured dyes were monitored using the mean grey value. Mixing profiles were confirmed by NIR spectroscopy. Le Coent *et al*. (57) improved post-analysis through implementing a technique called the box counting method. An image is divided into boxes of a certain length and the fractal information is used to determine information on the degree of homogeneity. Box lengths are varied, and the fractal dimension is calculated several times. An erosion technique was then used to isolate data points to retain big objects, reducing data points, allowing for significant variation of the fractal dimension as a function of homogeneity. This method was applied to monitor the mixing of two powders of similar density and size, with one coloured in a

stirred vessel. Mixing efficiency was affected by stirring speed. Xiaoyan *et al.* (58) compared analysis methods variance and contact on the image analysis performance of monitoring white and red plastic beads in a rotary drum. Variance is similar to the box counting method, where images are divided into cells and the variance of coloured particle concentration is calculated and changes over time. Contact counts the interfaces of different components on pixel level, where if a mixture is well mixed contact interfaces are high. Both methods obtained appropriate mixing profiles, where contact improved accuracy but required more processing time.

Image analysis has also been used to monitor mixing through particle tracing. Remy *et al*. (58) monitored the mixing of clear and coloured glass beads in a glass vessel agitated by an impeller. Halogen light produced glares on glass beads allowing their velocity profiles to be traced by image analysis. Consecutive images of the flow field were taken, and average particle displacement vectors were calculated to monitor mixing. Mixing was affected by particle and vessel wall roughness, and impeller speed.

Image analysis has demonstrated potential to monitor mixing processes non-invasively, however, is limited by disadvantages. Image analysis monitoring requires particles to be different colours. Most pharmaceutical mixes are composed of various white powders, restricting the use of image analysis to limited applications. As well, image analysis requires a transparent vessel or port to record images. This leads to modification of equipment resulting in higher costs. Furthermore, images are only taken at the port window or powder surface, in which measurements are not indicative of the entire powder composition. Multiple measurements at different locations may then be needed, but at the added cost of image equipment and vessel modification. Much like other monitoring techniques, better calibration and analysis methods provide more accurate measurements, but increase processing time.

2.3.2   Radioactive Particle Tracers

Positron emission particle tracking (PEPT) is a radioactive tracer technique that has been developed to study particle dynamics and flow. Radioactive tracers are composed of isotopes rich with proton rich nuclei which radioactively decay through beta positive

emission. When the emitted positron annihilates with an electron, 2 colinear gamma rays are emitted. Arrays of positron detectors along mixing vessels allow for the annihilation site to be estimated and tracked with time (59). Tracers are developed to closely match the particles in size and density to reflect the motion of the bulk mixture (60). As well, gamma radiation can penetrate relatively easy through most materials making it a non-invasive method for monitoring.

PEPT has been used to examine mixing dynamics. Portillo *et al.* (61) investigated the effect of impeller rotation speed, powder flow rate, powder cohesion, and residence time for mixing lactose in a continuous mixer using a radioactive tracer. Perrault *et al.* (62) assessed the potential of radioactive tracers as an inline monitoring method for the mixing of magnesium stearate into microcrystalline cellulose and lactose in a V-blender. Here, the magnesium stearate was used as the radioactive tracer by first being activated in a nuclear reactor. Mixing was found to be affected by both the mixer rotational speed and the pre-blend composition.

Radioactive tracers can effectively be used to study mixing dynamics; however, the requirement of sensor arrays limits the scale of the technique to lab-development. As well, gamma radiation scattering can occur introducing error into measurements making the monitoring technique less accurate. Furthermore, as radioactive tracers can only indicate flow and mixing patterns, not content uniformity, prevents this technique to be used to monitor a mixing end-point.

2.4   Tomographic Techniques

Tomographic techniques utilize the information from the transmission and reflectance from the penetration of an energy wave to reconstruct image cross sections of a sample. The energy in Magnetic Resonance Imaging (MRI) comes from a magnetic field and X-rays for X-ray computed tomography.

2.4.1   Magnetic Resonance Imaging

MRI utilizes specific frequencies of atomic nuclei which are influenced by magnetic fields. Atomic nuclei naturally possess a magnetic moment around a magnetic field. The

nuclei rotate and spin at unique frequencies, called the Larmor frequency, which is dependent on the strength of the magnetic field. Spatial variation within the magnetic field results in the nuclei to spin at different frequencies. Certain nuclei such as hydrogen resonate stronger compared to others (phosphorous and fluorine). MRI then uses the distribution of these signals as a function of frequency and relates it to the spatial distribution of the nuclei (63). At a given spatial resolution, a three-dimensional image can be produced in voxels (proportional to a pixel in a 2D image), each representing a sample within a mixture. This spatial variation allows for particles' motion to be tracked subsequently detecting differences in mixture composition, which can be implemented as a monitoring method.

Particles must first be 'visible' to MRI prior to capturing motion. As elements containing hydrogen produce stronger signals, studies primarily use particles containing oil, or are coated and doped externally. Hill *et al.* (64) rotated 1 mm MRI sensitive spherical pills with inert 3 mm plastic spheres in a drum to monitor segregation patterns. Not only was segregation dependent on rotation speed, mixing and segregation patterns were more complex compared to surface observations as revealed by MRI. Using a Turbula mixer, Sommier *et al.* (65) monitored mixing of sugar beads. A portion of sugar beads were first doped with silicon oil to be detected by MRI. For beads of the same size, a mixing end-point was determined. In addition, it was found that mixing and segregation patterns were affected by rotation speed, bead size, and number of rotations. Porion *et al.* (66) further developed mixing and segregation mechanisms in a Turbula mixer using MRI. Poppy seeds with a high oil content and sugar spheres of different sizes were tumbled in the mixer and MRI images were affected by a variety of process parameters. Kawaguchi *et al.* (67) investigated segregation and mixing patterns in a rotating drum differing in geometry. Inert polystyrene and MRI visible vitamin E filled microcapsules were rotated in the drum and imaged. Mixing patterns within the drum were affected by drum geometry. Using a binary segregated mixture of melamine particles and capsules filled with oil, Hardy *et al.* (68) monitored the mixing process in a rotating drum through MRI. The images generated approached uniformity quickly indicating a mixing end-point.

As outlined by preliminary studies, there is potential for monitoring mixing processes through MRI. MRI is completely non-invasive, penetrates deep into samples, there is no preferred orientation for measurement, and requires no mechanical markers. However, monitoring with MRI suffers from multiple disadvantages. MRI requires 'visible' particles which may not be representative of particles in the process. To produce a measurable signal, particles should contain large amounts of protons, primarily done by having an internal or external oil content. External doping or coatings can negatively affect particle flowability and API content uniformity. MRI monitoring also limits the size of the mixing vessel. The size of the mixing vessel can only be as large as the size of the induced magnetic field to provide adequate penetration depth. In addition, MRI requires extensive signal analyses and expensive equipment. Finally, of the studies conducted, primarily binary mixtures of spherical, free flowing particles were used which are not representative of pharmaceutical mixing highlighting the limitations of MRI technology to the lab scale.

2.4.2   X-Ray Computed Tomography

X-rays have shown in preliminary investigations a potential to monitor mixing processes. X-rays utilize a higher form of electromagnetic energy which can past through most objects. X-rays are absorbed in varying amounts depending on the density and atomic number of the particle they pass through. This difference in absorbance allows for cross-sectional images of samples to be constructed which can indicate the homogeneity of certain mixtures (69).

Yang and Fu (70) investigated the effect of particle size and loading configuration on mixing performance of microcrystalline cellulose in a scaled down V-blender. Microcrystalline cellulose particles were labelled with lead (II) acetate trihydrate to increase microcrystalline cellulose particles' radiological density due to its high X-ray attenuation coefficient. A linear correlation between the gray scale of X-ray cross-section images and percentage of lead impregnated particles was obtained indicating the degree of homogeneity. It was determined that large particles and layer-filled configurations led to better mixing than column-filled configurations. Chester *et al.* (69) investigated mixing in a double cone blender filled with pellets and spherical particles using X-ray

tomography. A portion of each batch was impregnated with molybdenum as ammonium heptamolybdate to increase particle X-ray visibility. Increased fill levels promoted segregation leading to poorer mixing. Better mixing performance was achieved for axial configurations compared to radial configurations. Liu *et al.* (71) studied the mixing of microcrystalline cellulose and starch granules in a rotating cylinder using synchrotron X-ray computed microtomography. The synchrotron radiation results in higher intensity than traditional X-ray tomography. Mixing improved with increased rotation rate. Segregation increased with longer mixing time.

X-ray tomography is a potential, fast, and non-destructive method to identify homogeneity. However, the application for monitoring mixing is limited. Monitoring mixing in real-time is difficult to achieve as the time required for a single scan is very long. As well, depending on particle composition, the particles may have to be doped to increase X-ray visibility. Finally, extensive and expensive equipment is required.

2.5   Passive Vibration Measurements

Due to sudden localized changes in stress, energy in the form of vibrational waves are generated, transmitted, and received as they propagate through matter (72). Waves propagate through media varying in direction from the energy source. Longitudinal waves travel parallel to the direction of the wave, while transverse waves propagate perpendicular to the energy source. Longitudinal waves can exist in any phase, whereas transverse waves can only occur in solids. Rayleigh waves exist as a combination of longitudinal and transverse waves forming ellipses in surfaces of semi-infinite media (72).

Waves can be characterized by their speed, frequency, wavelength, and amplitude. Frequency is the reciprocal of the time required for one complete cycle of a sinusoidal tone. Frequencies can be categorized based on their magnitude: below 20 Hz (infrasonic), between 20 – 20,000 Hz (audible), and above 20,000 Hz (ultrasonic) (73). The wavelength is the distance between successive crests or peaks of the same height in a wave. The speed at which waves propagate can be related to both the frequency and wavelength:

$$c = \lambda f \hspace{6cm} \text{(eq. 2.6)}$$

where c is the speed, λ is the wavelength, and f is the frequency of the wave. The speed of the wave is also affected by the phase elasticity E (Bulk modulus in liquids, Young's modulus in solids) and the density ρ of the medium in which the wave propagates:

$$c = \sqrt{\frac{E}{\rho}} \hspace{6cm} \text{(eq 2.7)}$$

The amplitude of a wave is the maximum displacement of a wave measured from the equilibrium position. This is an important characteristic, as the energy from a vibrational wave is proportional to the square of the wave's amplitude. When a vibrational wave moving in one fluid strikes the surface or interface of a different material, a portion of the energy is transmitted into the second material and a portion is reflected (74). Energy from the vibrational wave is dissipated or attenuated with changes in time and distance from the source. Attenuation is primarily caused by energy being converted into other forms of energy including heat, sound, and scattering. When waves encounter a discontinuity in a medium, they scatter in different directions than the incident wave (73).

Passive vibration regarding monitoring is the measurement of vibrations created by the process itself. This is similar to passive acoustic emission monitoring, where acoustics is specific to vibrations created in the audible range as detected by the human ear, and vibration measurements is a more direct measure of energy dissipation and transmission at a point of interest at all frequencies. In mixing processes, acoustic emissions or vibration measurements results from particle-particle collisions, particle- equipment collisions, and equipment noise (75). The monitoring of these processes through passive vibration measurements and acoustic emissions refers to the differences in signal amplitudes from a heterogeneous state to a homogenous state.

There have been limited studies conducted on acoustic emission and vibration measurements monitoring. Of the conducted research, much has been confined to convective mixers rather than tumbling mixers. Tily *et al.* (75) monitored the mixing of various powders in a Kenwood mixer. Root mean square values changed with further

mixing until a plateau was reached indicating a mixing end-point. Bellamy *et al.* (76) monitored mixing of cellulose and aspirin in a high shear blender using near infrared spectroscopy and acoustic emissions. Both methods identified mixing profiles, where acoustic mixing profiles were obtained over a range of frequencies in the power spectrum with time. Using the same technique, Allan *et al.* (77) used acoustic emissions to monitor the mixing of citric acid, aspirin, and Avicel in a convective blender. Mixing profiles were generated in real time, where acoustic emissions initially increased and reached a plateau as the mixture became homogenous. In a tumbling V-blender, Crouter and Briens (78) monitored lubricant dispersal onto sugar spheres and granule formulations. Mixing profiles were obtained, and mixing end-points determined.

Passive vibration measurements or acoustic emissions monitoring has demonstrated potential to monitor mixing processes in both tumbling and convective mixers. This method is completely non-invasive and non-destructive as sensors are attached on the outside of the mixing vessel, and offer a lower equipment cost and setup compared to other inline monitoring methods. However, large volumes of data are produced increasing processing and analysis time to extract useful information. In addition, vibration measurements can be less sensitive than spectroscopic methods, as they do not directly measure chemical properties. Further refinement and development are therefore required to successfully implement vibration measurement mixing monitoring.

2.6 Conclusions

Mixing performance is crucial to control and monitor in pharmaceutical tablet manufacturing to ensure a proper content uniformity is achieved through identification of a mixing end-point. This is particularly important where excipients are added in small quantities including lubricants, where blending is difficult to achieve, and mixing process parameters can negatively affect final tablet properties. To remove issues associated with extractive sampling, process analytical technologies are being developed to monitor and control processes improving process efficiency. Many technologies have been used to evaluate mixing performance as summarized in Table 2.2 adapted from Crouter and Briens (79).

Table 2.2: Summary of Process Analytical Technologies to evaluate mixing processes

PAT	Measured Parameter	Application	Advantages	Disadvantages
Near infrared Spectroscopy	Absorption energy	• Homogeneity • End-point • Composition	• Online monitoring capability • Applicable for multicomponent mixtures	• Modification of equipment • Difficult interpretation • Probe window fouling
Raman Spectroscopy	Scattered light	• Homogeneity • End-point • Composition	• Online monitoring capability • Applicable for multicomponent mixtures	• Modification of equipment • Difficult interpretation • Probe window fouling • Susceptible to fluorescence
Optical Image Analysis	Colour	• Homogeneity • Velocity profile	• Low cost • Simple to use	• Modification of equipment • Required component contrast • Sensor window fouling
Radioactive Tracers	Positron detection	• Velocity profile	• Non-invasive	• Restricted to development • Limited to one component assessment
Magnetic Resonance Imaging	Magnetic Field	• Homogeneity • Velocity profile	• Non-invasive • 3D image	• Expensive • Restricted to development • MRI sensitive particles required • Limited to one component assessment

Table 2.2 (continued)

PAT	Measured Parameter	Application	Advantages	Disadvantages
X-ray Computed Tomography	X-ray	• Homogeneity	• Non-invasive • 3D image	• Expensive • X-ray sensitive particles required • Real-time measurements not possible • Limited to one component assessment
Vibration Measurements	Vibrations and sound	• Homogeneity • End-point	• Non-invasive	• Large volume of data • Not well developed

2.7 References

1. Li J, Wu Y. Lubricant in pharmaceutical solid dosage forms. Lubricants 2014; 2: 21 – 43.
2. Brone D, Wightman C, Connor K, Alexander A, Muzzio FJ, Robinson P. Using flow perturbations to enhance mixing of dry powders in V-blenders. Powder Technol 1997; 91: 165-172.
3. Brone D, Alexander A, Muzzio FJ. Quantitative Characterization of mixing of dry powders in v-blenders. AIChE J 1998; 44:271-278.
4. Jarosz PJ, Parrott EL. Effect of lubricants on tensile strengths of tablets. Drug Dev Ind Pharm 1984;10(2):259-73.
5. Kikuta JI, Kitamori N. Effect of mixing time on the lubricating properties of magnesium stearate and the final characteristics of the compressed Fts. Drug Dev Ind Pharm 1994;20(3):343-55.
6. United States of America vs. Barr Laboratories Inc. Civil Action for the District of New Jersey; 1993.
7. Deveswaran R, Bharath S, Basavaraj BV, Abraham S, Furtado S, Madhavan V. Concepts and Techniques of Pharmaceutical Powder Mixing Process: A Current Update. J Pharm Technol 2009; 2: 245-249.
8. Garcia T, Wilkinson S, Scott J. The Development of a Blend-Sampling Technique to Assess the Uniformity of a Powder Mixture. Drug Dev Ind Pharm 2001; 27:4, 297-307.
9. Muzzio FJ, Goodridge CL, Alexander A, Arratia P, Yang H, Sudah O, Mergen G. Sampling and characterization of pharmaceutical powders and granular blends. Int J Pharm 2003; 250: 51-64.
10. U.S Department of Health and Human Services, Food and Drug Administration, Center for Drug Evaluation and Research (CDER), Center for Veterinary Medicine (CVM), Office of Regulatory Affairs (ORA). A framework for innovative pharmaceutical manufacturing and quality assurance; 2004. Available from: https://www.fda.gov/media/71012/download
11. International Conference of Harmonisation. Guidelines ICH 8-14. Accessed July 21, 2019 from: https://www.ich.org/products/guidelines/quality/article/quality-guidelines.html
12. Siesler H, Ozaki Y, Kawata S, Heise H. Near-infrared spectroscopy: principles, instruments, and applications. Wiley 2008.
13. Berntsson O, Danielsson L, Lagerholm B, Folestad S. Quantitative in-line monitoring of powder blending by near-infrared reflection spectroscopy. Powder Technol 2002; 123: 185 – 193.
14. Rinnan A, van den Berg F, Engelsen S. Review of the most common pre-processing techniques for near infrared spectra. TrAC 2009; 28: 1201 – 1222.
15. Hailey P, Doherty P, Tapsell P, Oliver T, Aldridge P. Automated system for the on-line monitoring of powder blending processes using near-infrared spectroscopy. Part I. System development and control. J Pharm Biomed Anal 1996; 14: 551 – 559.

16. Sekulic S, Ward H, Brannegan D, Stanley E, Evans C, Sciavolino S et al. On-line monitoring of powder blend homogeneity by near-infrared spectroscopy. Anal Chem 1996; 68(3): 509 – 513.
17. Wargo D, Drennen J. Near-infrared spectroscopic characterization of pharmaceutical powder blends. J Pharm Biomed Anal 1996; 14: 1415 – 1423.
18. De Maesschalck R, Cuesta Sanchez F, Massart D, Doherty P, Hailey P. On-line monitoring of powder blending with near-infrared spectroscopy. Appl Spectrosc 1998; 52: 725 – 731.
19. Sekulic S, Wakeman J, Doherty P, Hailey P. Automated system for the on-line monitoring of powder blending processes using near-infrared spectroscopy. Part II. Qualitative approaches to blend evaluation. J Pharm Biomed Anal 1998; 17: 1285 – 1309.
20. El-Hagrasy A, Morris H, D'Amico F, Lodder R, Drennen J. Near-infrared spectroscopy and imaging for the monitoring of powder blend homogeneity. J Pharm Sci 2001; 90: 1298 – 1307.
21. El-Hagrasy A, D'Amico F, Drennen JK. A process analytical technology approach to near-infrared process control of pharmaceutical powder blending. Part 1: D-optimal design for characterization of powder mixing and preliminary spectral data evaluation. J Pharm Sci 2006; 95: 392 – 406.
22. El-Hagrasy A, Delago-Lopez M, Drennen J. A process analytical technology approach to near-infrared process control of pharmaceutical powder blending. Part 2: qualitative near-infrared models for prediction of blend homogeneity. J Pharm Sci. 2006; 95: 407 – 421.
23. El-Hagrasy A, Drennen J. A process analytical technology approach to near-infrared process control of pharmaceutical powder blending. Part 3: quantitative near-infrared calibration for prediction of blend homogeneity and characterization of powder mixing kinetics. J Pharm Sci 2006; 95: 422 – 434.
24. Shi Z, Cogdill R, Short S, Anderson C. Process characterization of powder blending by near-infrared spectroscopy: blend end-points and beyond. J Pharm Biomed Anal 2008; 47: 738 – 745.
25. Liew C, Karande A, Heng P. In-line quantification of drug and excipients in cohesive powder blends by near infrared spectroscopy. Int J Pharm. 2010; 386: 138 – 148.
26. Sulub Y, Konigsberger M, Cheney J. Blend uniformity end-point determination using near-infrared spectroscopy and multivariate calibration. J Pharm Biomed Anal. 2011; 55: 429 – 434.
27. Igne B, Talwar S, Drennen J, Anderson C. Online monitoring of pharmaceutical materials using multiple NIR sensors- part II: blend end-point determination. J Pharm Innov 2013; 8: 45 – 55.
28. Jaumot J, Igne B, Anderson C, Drennen C, de Jaun A. Blending process modeling and control by multivariate curve resolution. Talanta 2013; 117: 492 – 504.
29. Bakri B, Weimer M, Hauck G, Reich G. Assessment of powder blend uniformity: comparison of real-time NIR blend monitoring with stratified sampling in

combination with HPLC and at-line NIR chemical imaging. Eur J Pharm Biopharm 2015; 97: 78 – 89.

30. Besseling R, Damen M, Tran T, Nguyen T, van den Dries K, Oostra W, et al. An efficient, maintenance free and approved method for spectroscopic control and monitoring of blend uniformity: the moving F-test. J Pharm Biomed Anal. 2015; 114: 471 – 481.

31. Murayama K, Ishikawa D, Genkawa T, Sugino H, Komiyama M, Ozaki Y. Image monitoring of pharmaceutical blending processes and the determination of an end point by using a portable near-infrared imaging device based on a polychromator-type near-infrared spectrometer with a high-speed and high-resolution photo diode array detector. Molecules 2015; 20: 4007 – 19.

32. Sibik J, Chalus P, Maurer L, Murthy A, Krimmer S. Mechanistic approach in powder blending PAT: bi-layer mixing and asymptotic end point prediction. Powder Technol 2017; 308: 306 – 317.

33. Tewari J, Strong R, Boulas P. At-line determination of pharmaceuticals small molecules' blending end point using chemometric modeling combined with Fourier transform near infrared spectroscopy. Spectrochim Acta A 2017; 173: 886 – 91.

34. Lee W, Widjaja E, Heng P, Chan L. Near infrared spectroscopy for rapid and in-line detection of particle size distribution variability in lactose during mixing. Int J Pharm 2019; 566: 454 – 462.

35. Geladi P, MacDougall D, Martens H. Linearization and scatter-correction for near-infrared reflectance spectra of meat. Appl Spectrosc 1985; 39(3): 491 – 500.

36. Barnes R, Dhanoa M, Lister S. Standard normal variate transformation and de-trending of near-infrared diffuse reflectance spectra. Appl Spectrosc 1989; 43(5): 772 – 777.

37. Savitzky A, Golay M. Smoothing and differentiation of data by simplified least squares procedure. Anal Chem 1964; 36(8): 1627 – 1639.

38. Paclik P, Duin R. Dissimilarity-based classification of spectra: computational issues. Real-Time Imaging 2003; 9: 237 – 244.

39. Blanco M, Gozalez B, Bertran E. Monitoring powder blending in pharmacetical processes by use of near infrared spectroscopy. Talanta 2002; 56: 203-212.

40. Hollas, J. Rotational Raman Spectroscopy. In *Modern Spectroscopy*. Wiley 2004; 122 - 137.

41. Aaltonen J, Kogermann K, Strachan C, Rantanen J. In-line monitoring of solid-state transitions during fluidisation. Chem Eng Sci 2007; 62(1–2): 408–415.

42. Walker G, Bell S, Greene K, Jones D, Andrews G. Characterisation of fluidised bed granulation processes using in-situ Raman spectroscopy. Chem Eng Sci 2009; 64(1): 91–98.

43. El Hagrasy A, Chang S, Desal D, Kiang S. Raman spectroscopy for the determination of coating uniformity of tablets: Assessment of product quality and coating pan mixing efficiency during scale-up. J Pharm Innovation 2006; 1(1): 37–42.

44. Mller J, Knop K, Thies J, Uerpmann C, Kleinebudde P.Feasibility of Raman spectroscopy as PAT tool in active coating Raman spectroscopy as PAT tool in active coating. Drug Dev Ind Pharm 2010; 36(2): 234–243.

45. Marola M, Sandler N, Heinämäki J, Yliruusi J, Römer M, Rantanen J. Pellet manufacturing by extrusion-spheronization using process analytical technology. AAPS PharmSciTech 2006; 6(2): 174–183.

46. Vervaet C, Saerens L, Lenain B, Beer T, Dierickx L, Remon, J. Raman spectroscopy for the in-line polymer–drug quantification and solid state characterization during a pharmaceutical hot-melt extrusion process. Eur J Pharm Biopharm 2010; 77(1): 158–163.

47. Romero-Torres S, Wikström H, Grant E, Taylor L. Monitoring of mannitol phase behavior during freeze-drying using non-invasive Raman spectroscopy. PDA J Pharm Sci Technol 2015; 61(2): 131–145.

48. Vergote G, De Beer T, Vervaet C, Remon J, Baeyens W, Diericx N,Verpoort F. In-line monitoring of a pharmaceutical blending process using FT-Raman spectroscopy. Eur J Pharm 2004; 21(4): 479–485.

49. Hausman D, Cambron R, Sakr A. Application of Raman spectroscopy for on-line monitoring of low dose blend uniformity. Int J of Pharm 2005; 298(1): 80–90.

50. De Beer T, Baeyens W, Ouyang J, Vervaet C, Remon J. Raman spectroscopy as a process analytical technology tool for the understanding and the quantitative in-line monitoring of the homogenization process of a pharmaceutical suspension. Analyst 2006; 131(10): 1137–1144.

51. De Beer T, Bodson C, Dejaegher B, Walczak B, Vercruysse P, Burggraeve A, Lemos A, Delattre L, Heyden Y, Remon J, Vervaet C, Baeyens W. Raman spectroscopy as a process analytical technology (PAT) tool for the in-line monitoring and understanding of a powder blending process. J Pharm Biomed Anal 2008; 48(3): 772–779.

52. Dallin P, Nordon A, Littlejohn D, Andrews J, Bellamy J, Allan P. In situ monitoring of powder blending by non-invasive Raman spectrometry with wide area illumination. J Pharm Biomed Anal 2012; 76: 28–35.

53. Realpe A, Velazquez C. Image processing and analysis for determination of concentrations of powder mixtures. Powder Technol 2003; 134: 193 – 200.

54. Xiaoyan L, Chaoyu Z, Jiesi Z. Quantitative comparison of image analysis methods for particle mixing in rotary drums. Powder Technol 2015; 282: 32 – 36.

55. Chen C, Yu C. Two-dimensional image characterization of powder mixing and its effects on solid-state reactions. Mater Chem Phys 2004; 85: 227 – 237.

56. Bulent A, Silleli H, Koc C, Dayioglu M. Monitoring of dry powder mixing with real-time image processing. J Appl Sci 2007; 7: 1218 – 1223.

57. Le Coent A, Rivoire A, Briancon S, Lieto J. An original image-processing technique for obtaining the mixing time: the box-counting with erosions method. Powder Technol 2005; 152: 62 – 71.

58. Remy B, Canty T, Khinast J, Glasser B. Experiments and simulations of cohesionless particles with varying roughness in a bladed mixer. Chem Eng Sci 2010; 65: 4557 – 71.

59. Broadbent C, Bridgewater J, Parker D, Keningley S, Knight P. A phenomenological study of a batch mixer using a positron camera. Powder Technol 1993; 76: 317 – 329.

60. Fan L, Chen S, Sckhoff N, Watson C. Evaluation of a motionless mixer using a radioactive tracer technique. Powder Technol 1971; 4: 345 – 350.

61. Portillo P, Vanrase A, Ingram A, Sevile J, Ierapetritou M, Muzzio F. Investigation of the effect of impeller rotation rate, powder flow rate, and cohesion on powder flow behaviour in a continuous blender using PEPT. Chem Eng Sci 2010; 65: 5658 – 68.

62. Perrault M, Bertrand F, Chaouki J. An investigation of magnesium stearate mixing in a V-blender through gamma-ray detection. Powder Technol 2010; 200: 234 – 245.

63. Nakagawa M, Altobelli SA, Caprihan A, Fukushima E, Jeong EK. Non-invasive measurements of granular flows by magnetic resonance imaging. Exp Fluids 1993; 16: 54-60.

64. Hill KM, Caprihan A, Kakalios J. Bulk segregation in rotated granular material measured by magnetic resonance imaging. Phys Rev Lett 1977; 78: 50-53.

65. Sommier N, Porion P, Evesque P, Leclerc B, Tchoreloff P, Couarraze G. Magnetic resonance imaging investigation of the mixing-segregation process in a pharmaceutical blender. Int J Pharm 2001; 222: 243-258.

66. Porion P, Sommier N, Faugere AM, Evesque P. Dynamics of size segregation and mixing of granular materials in a 3D-blender by NMR investigation. Powder Technol 2004; 141: 55-68.

67. Kawaguchi T, Tsutsumi K, Tsuji Y. MRI measurement of granular motion in rotating drum. Part Part Syst Charact 2006; 23: 266-271.

68. Hardy EH, Hoferer J, Kasper G. The mixing state of fine powders measured by magnetic resonance imaging. Powder Technol 2007; 177: 12-22.

69. Chester A, Kowalski J, Coles M, Muegge E, Muzzio F, Brone D. Mixing dynamics in catalyst impregnation in double-cone blenders. Powder Technol 1999; 102: 85 – 94.

70. Yang C, Fu X. Development and validation of a material labeling method for powder process characterization using x-ray computed tomography. Powder Technol 2004; 146:10 – 19.

71. Liu R, Yin X, Li H, Shao Q, York P, He Y, et al. Visualization and quantitative profiling of mixing and segregation of granules using synchrotron radiation X-ray microtomography and three dimensional reconstruction. Int J Pharm 2013; 445(1-2): 125 – 133.

72. Kinsler L, Frey A, Coppens A, Sanders J. *Fundamentals of acoustics*. New York City, United States of America: Wiley; 1999.

73. Boyd J, Varley J. The uses of passive measurement of acoustic emissions from chemical engineering processes. Chem Eng Sci 2001; 56(5): 1749-1767.

74. Barron R. *Industrial noise control and acoustics*. New York City, United States of America: Marcel Dekker, Inc.; 2003.

75. Tily P, Porada S, Scruby C, Lidington S. Monitoring of mixing processes using acoustic emission. In: Harnby N, Benkreira H, Carpenter K, Mann R, eds. Fluid Mixing III. Rugby: The Institute of Chemical Engineers 1988; 75-94.

76. Bellamy L, Nordon A, Littlejohn D. Non-invasive monitoring of powder mixing with near infrared spectroscopy and acoustics. Spectrosc Eur 2004: 25-27.

77. Allan P, Bellamy L, Nordon A, Littlejohn D. Non-invasive monitoring of the mixing of pharmaceutical powders by broadband acoustic emission. Analyst 2010; 135: 518-524.

78. Crouter A, Briens L. Monitoring lubricant addition using passive acoustic emissions in a V-blender. Powder Technol 2016; 301: 1119-1129.

79. Crouter A, Briens L. Methods to assess mixing of pharmaceutical powders. AAPS PharmSciTech. 2019; 20:84.

Chapter 3

3 Monitoring Magnesium Stearate Blending in a V-blender through Passive Vibration Measurements

Publication status: A version of this chapter was published online in *AAPS PharmSciTech* on July 26, 2019.

3.1 Introduction

Within the pharmaceutical industry, mixing is a crucial unit operation, particularly in tablet manufacturing. Prior to tableting, a lubricant is added to the blend, to ensure that tablet is ejected out of the die properly. These blends occur in batches, having to be stopped and tested through off line sampling after every batch to ensure that the blend is uniform, consistent, and will produce products with desired properties. Inline monitoring methods would improve process efficiency, accurately characterizing powder blends continuously and non-intrusively.

Mixing is generally done in two types of mixers: convective and tumbling. Convective mixers rely upon an impeller to mix powders in a fixed vessel. Here, the impeller configuration and bowl geometry can be adapted to the application. Tumbling mixers rely upon gravity to cascade the powders through a vessel attached to a rotating axel, mainly differing in their shell geometry. Tumbling mixers are primarily used for the last mixing step within the tablet manufacturing process due to their gentle mixing. As well, tumbling mixers have been shown to provide better mixing (1), ensuring that the blend is uniform (2-4), compared to other mixer configurations.

Just before tableting, a lubricant, commonly magnesium stearate, is added to the powder mixture. The magnesium stearate first adsorbs onto the surface of the particles in the formulation. Then, shear from the mixing motion can induce delamination of the magnesium stearate particles, impacting the adsorbed film developing on the particles in the formulation (5). It has been hypothesized that lubricant particles first fill cavities in surface irregularities before forming a continuous layer (5,6), thereby reducing contact points and friction, allowing the tablet to be ejected cleanly from the press. Although lubricants are necessary in the tableting process, there are many negative effects

associated with their use. High levels of magnesium stearate decrease tablet strength (7-9) and increase tablet disintegration time (7). It is therefore critical to use the appropriate amount of lubricant, as well as accurately monitor the mixing process to ensure that tablets have desirable, reproduceable properties.

The uniformity of powder blends is currently assessed by extracting samples offline using a thief probe, and then these samples are analyzed using conventional methods such as high-performance liquid chromatography (HPLC) and UV-spectroscopy. However, these methods suffer from many drawbacks, which have been investigated and studied extensively (10-12). The insertion of the probe itself can disturb the bed leading to segregation, channeling, and introduce contamination. Multiple samples are required at various positions throughout the bed to provide a representation of the entire blend, but again becomes error prone. These methods then become laborious, time consuming, and costly. As well, if the blend is found not to be uniform, the material is discarded, and the entire mixing process must be repeated.

There has been a growing interest in inline monitoring methods to increase process efficiency, product quality, and consistency, eliminating the issues associated with offline sampling. Of the technologies investigated, the most prominent include near infrared spectroscopy (NIR) (13-15), Raman spectroscopy, (16-18), magnetic resonance imaging (MRI) (19-21), and radioactive tracers (5,22,23). Although these methods can characterize the powder bed effectively, there are multiple disadvantages. The methods require probes or window ports for the sensors to analyze data which become intrusive, adding additional components/modifying existing equipment, increasing cost. These technologies also require extensive processing capabilities to analyze data. Finally, the capital costs of the sensor and equipment required to record data is high.

Acoustic emissions or vibration measurements during mixing can result from particle-particle collisions, particle-equipment collisions, as well as equipment noise. The monitoring of mixing using acoustic emissions or vibrations refers to the differences in signal amplitudes from a heterogeneous state to a homogeneous state. This is primarily done through a sensor attached to the outside of the mixer, making it a non-invasive and

non-destructive method, with a decreased capital cost. Although data analysis is required, this is generally less complex compared to other inline monitoring methods.

The coefficient of restitution (COR) effectively models the loss of kinetic energy in a collision through the ratio of the pre-collision energy to the energy retained after the collision. If the collision is completely elastic, this ratio approaches 1, where no energy is dissipated and transmitted to the sensor resulting in a small measured amplitude. Conversely, if the collision is perfectly inelastic, the COR is equal to zero, none of the energy is retained by the particle, as energy is dissipated with more transmitted to the sensor resulting in large measured vibration amplitudes. As well, if the impacting velocity is increased, more energy is transmitted to the sensor resulting in a lower COR (24-27).

Most of the research monitoring mixing using acoustic emissions has been conducted on convective rather than tumbling mixers. Using a lab scale orbital mixer with a binary mixture, Tily *et al.* (28) identified that the primary source of acoustic emissions resulted from particle-wall collisions. The emissions transitioned from an initial to a final stable level, identifying the mixing endpoint. Bellamy *et al.* (13) compared NIR to acoustic emissions using a high shear blender to mix cellulose and a second component. Both methods were sensitive to particle size and could be used simultaneously to predict an endpoint. By using a convective mixer to mix aspirin and citric acid with Avicel, Allan *et al.* (29) found that acoustic signals increased with increased impeller speed, mass, density, and size.

Crouter and Briens (30) studied mixing using a V-blender and sugar spheres, microcrystalline cellulose, and lactose. It was found that increasing the size and density of particles, increased the measured acoustic or vibration amplitudes due to increased kinetic energy transferred to the sensor upon impact. Similarly, increasing the fill level or decreasing the shell size decreased the signal amplitudes as the particles had lower impact velocities due to their shorter trajectories before collision with the equipment. Crouter and Briens were able to monitor the mixing of magnesium stearate into sugar spheres and granule formulations using acoustic emissions or vibrations (31). The

measured vibration profiles showed distinct changes with the addition of the magnesium stearate. Cameron and Briens further validated these findings by mixing magnesium stearate with glass beads. Mixing end-points and measured vibrational amplitudes were affected by fill level and magnesium stearate loading configuration due to mixing mechanisms within a V-blender (32).

This study aims to further evaluate and determine the inline and real-time potential of vibration measurements to monitor the mixing of magnesium stearate into a mixture using a tumbling V-blender. The development of a method to monitor mixing inline and in real-time would improve production efficiency while ensuring a consistent, high quality product.

3.2   Materials and Methods

3.2.1   Particles

The particles that were used in experimental trials included glass beads and sugar spheres. The particles and their properties are listed in Table 3.1. All particles were approximately spherical. The moisture content of the particles was determined using a Mettler-Toledo HG63 halogen moisture analyzer. All particle types and conditions reported a moisture content less than 2 % based on weight-loss drying at 105 °C. In this study, magnesium stearate was chosen as the lubricant as it is widely used in the pharmaceutical industry because of its chemical stability and low cost.

Table 3.1: Particle properties

Particle	Size (mm)	Bulk Density (g/cm^3)	Apparent Density (g/cm^3)	Average Mass of 1 Particle (mg)
1 mm glass beads	1	1.49	2.5	2.3
2 mm glass beads	2	1.49	2.5	12
3 mm glass beads	3	1.49	2.5	39
4 mm glass beads	4	1.49	2.5	86
60 – 80 mesh sugar spheres	0.18 – 0.25	0.77	1.5	0.0078
30 – 35 mesh sugar spheres	0.50 – 0.60	0.77	1.5	0.13
20 – 25 mesh sugar spheres	0.71 – 0.85	0.77	1.5	0.37
16 – 20 mesh sugar spheres	0.85 – 1.18	0.77	1.5	0.82
14 – 18 mesh sugar spheres	1.00 – 1.40	0.77	1.5	1.5

3.2.2   V-blender

A Patterson-Kelley V-blender rotating at a fixed speed of 25 rpm with an 8 Qt (7.6 L) stainless steel shell was used for the trials. The V-shell was filled to 25 % of its volume with the specified particles. For mixing trials, magnesium stearate was added to the particles in varying amounts from 1-2 % by weight and distributed evenly on the top of the particle bed.

3.2.3   Sensors and Data Acquisition System

Vibrations were measured using a PCB Piezotronics accelerometer (model 353B34) with a frequency range of 0.35-12,000 Hz, combined with an ICP signal conditioner (model 480E09) at an acquisition frequency of 40,000 Hz. Signals were captured using Labview 8.5 with a National Instruments DAQ-6036E card. The accelerometer was securely attached to the V-shell lid using adhesive wax at a radial position of r/R = 0.74 (Figure 3.1). To focus on vibrations from particle interactions within the V-shell, the signals were filtered using a Daubechies wavelet filter (30).
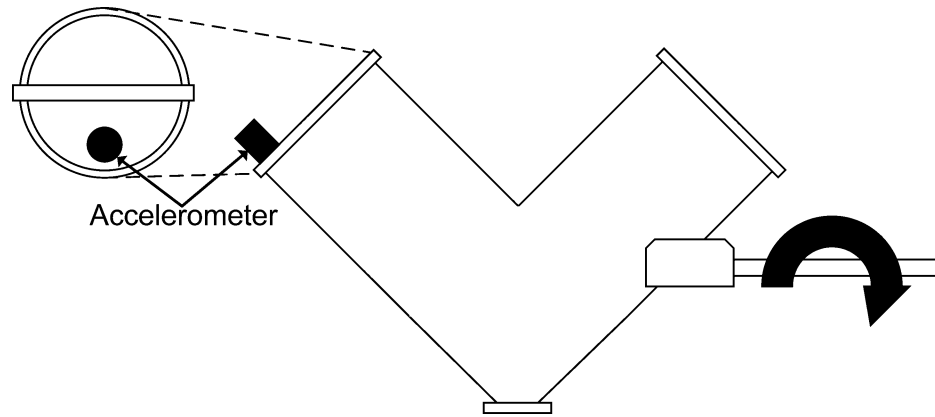
Figure 3.1: V-blender with accelerometer location and axis of rotation

3.2.4   Coefficient of Restitution (COR)

The COR was estimated from drop tests of the particles onto the lid and normal to the surface of the V-blender with the accelerometer (Figure 3.2). Particles were dropped far away from the support to minimize the effect of the support on measurements (33). The drop height (H) was constant at 11.1 cm from the lid of 3.1 mm in thickness. The time between successive peak amplitudes as particles rebounded was used to determine the COR (24). Oblique drop tests were conducted at 60°, and vibrational amplitudes recorded. This was repeated for a total of 15 times, for each particle type and condition.
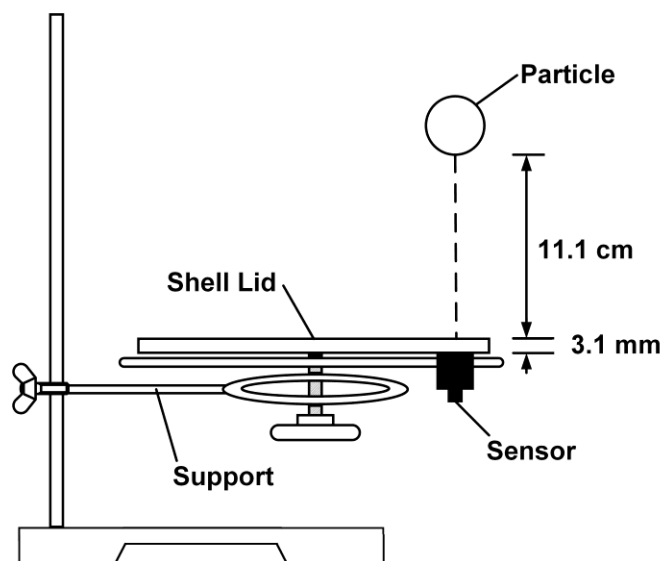
Figure 3.2: Schematic of apparatus used to measure the coefficient of restitution

3.2.5 Flowability

The flowability of the particulates was estimated using the avalanche time measured using the Revolution Powder Analyzer from Mercury Scientific. A sample size of 118 cm^3 was loaded into the sampling drum that had a diameter of 11 cm and a width of 3.5 cm. The drum was rotated at 0.3 rpm until a total of 50 avalanches had occurred; an avalanche was defined as a rearrangement of more than 0.65 volume percent of the sample in the drum. Optical measurements of the powder surface were taken at a resolution of 648 x 488 at 60 frames per second. Software calculated the avalanche time from the optical measurements. Samples were measured in triplicate.

3.2.6 SEM Imaging

Scanning electron microscope (SEM) images of glass beads were taken using a Hitachi SU8230 Regulus Ultra-High-Resolution Scanning electron microscope. Glass beads were mounted on a plate using carbon adhesive discs before analysis. Images allowed for surface morphology of the beads to be examined to determine differences between magnesium stearate concentration and mixing time.

3.3 Results

For each rotation within the blender, three features were observed in the filtered signals measured by the accelerometer (30) related to particle motion with each revolution of the mixer. Feature 1 is attributed to particles impacting the lid upon inversion of the mixer. Feature 2 arises from vibrations created when particles slide along the mixer walls and Feature 3 is produced when particles recombine and impact the bottom plate of the mixer (Figure 3.3). Representative features were obtained and reported by averaging the three largest amplitudes per feature per revolution. Feature 1 showed the largest amplitudes which also increased with particle mass (Figure 3.4). The amplitudes of Features 2 and 3 (not shown) were much smaller and did not show a consistent trend with particle mass.
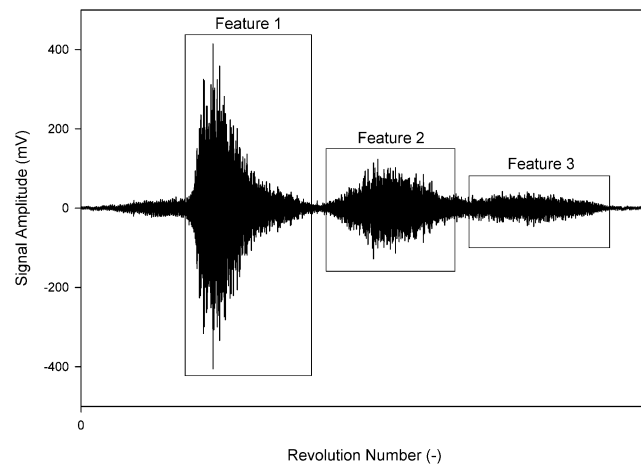

Figure 3.3: Filtered signal of 2 mm glass beads related to particle motion
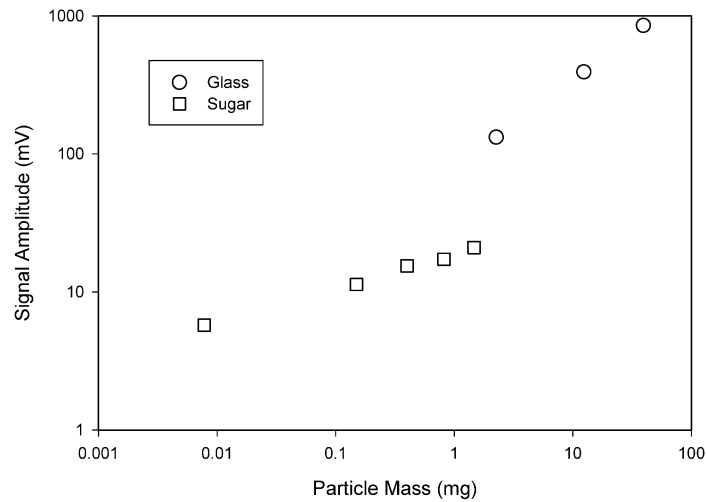
Figure 3.4: Effect of particle mass on amplitude of Feature 1 vibrations

Figure 3.5 summarizes the effect of mass on vibration amplitudes by comparing the amplitudes of heavier 1 mm glass beads with the lighter 16-20 mesh sugar spheres (average diameter of 1.02 mm). The feature amplitudes of glass beads were larger than that of the sugar spheres. Feature 1 showed the largest amplitudes and the largest difference between the two particles.

Figure 3.5: Effect of density on amplitude of feature vibrations for 1 mm glass beads and 16 - 20 mesh sugar spheres; averages shown with ± 1 standard deviation

The particles were mixed with magnesium stearate. The vibrations were measured during mixing and the amplitudes of Feature 1 were calculated. Figure 3.6 shows the effect of magnesium stearate on the measurements using 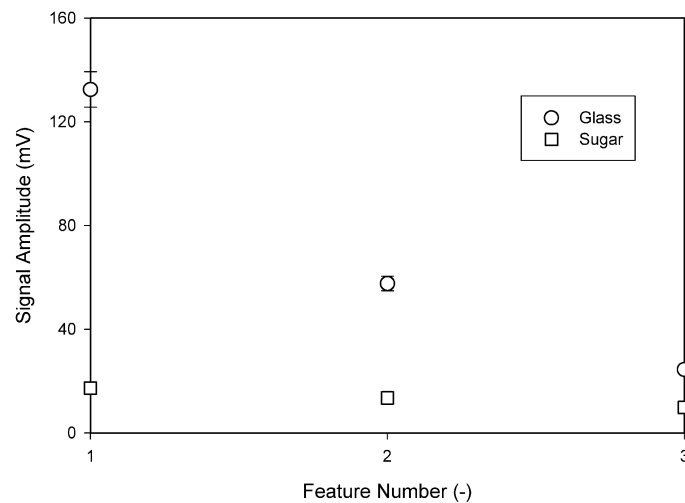the 16-20 mesh sugar spheres as an example. With mixing, the amplitudes decreased rapidly below the initial signal amplitude until a low relatively stable mixing plateau was achieved. As more magnesium stearate was added, the signal amplitude decreased to a lower value and fewer V-shell revolutions were needed to reach an approximate low plateau. Similar trends in the amplitudes of Feature 1 were observed when magnesium stearate was mixed with the other sizes of sugar spheres. The revolution at which the amplitude became approximately constant was more easily identified for larger than 0.22 mm in diameter particles (0.01 mg in mass) and for larger additions of the magnesium stearate.
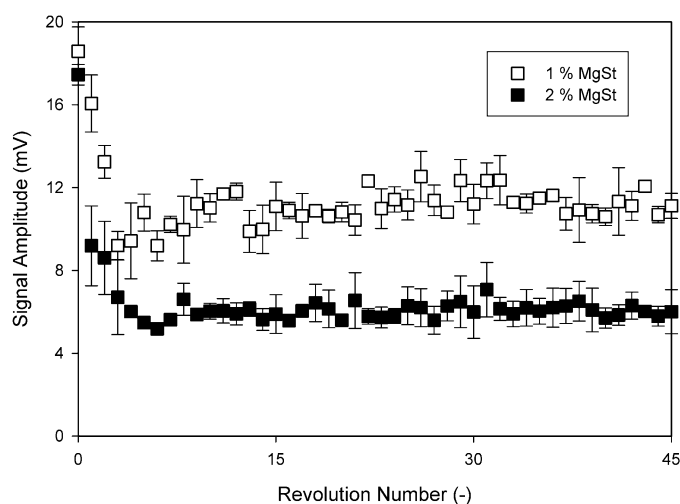
Figure 3.6: Feature 1 vibration amplitudes at 1 wt % and 2 wt % magnesium stearate for 16 - 20 mesh sugar spheres; ± standard deviation

The 14-18 mesh sugar spheres (average diameter of 1.2 mm) and 1 mm glass beads were each mixed with approximately 30 g of magnesium stearate. The vibrations were recorded during mixing and the amplitudes of Feature 1 were estimated. Figure 3.7 shows that for both particle types, the mixing plateaus were reached at approximately the same time, where the steady state amplitude for glass beads was slightly higher than sugar spheres.

Figure 3.7: Feature 1 vibration amplitudes of 1 mm glass beads and 14 - 18 mesh sugar spheres both mixed with approximately 30 g of magnesium stearate; ± standard deviation

SEM images of the 2 mm glass beads were taken before and after 45 revolutions of mixing with increasing amounts of magnesium stearate. In addition, SEM images of the 1 mm glass beads were taken at various times or shell revolutions during the mixing. The images showed that magnesium s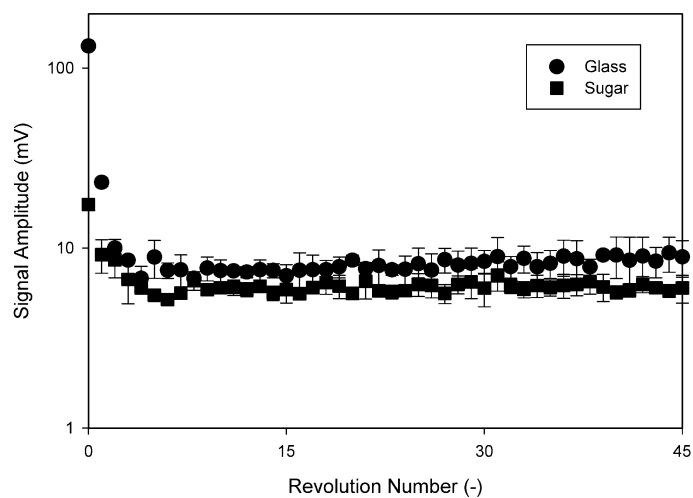tearate flakes adhered to the surfaces of the particles (Figure 3.8). With increasing amounts of magnesium stearate, the coverage of the magnesium stearate on the particles became more uniform and complete. As only a maximum of 2 wt % magnesium stearate was added, a continuous layer was not formed. With increasing revolutions or mixing time, the magnesium stearate layer became more complete and uniform, until a continuous layer formed just beyond 10 revolutions as shown in Table 3.2. Glass beads were shown as an example for imaging as contrast allowed the magnesium stearate layer to be easily distinguished from the surface of the glass bead when compared to sugar spheres. However, similar layering of the magnesium stearate on the surfaces was observed for all particles.

a)

b)

c)
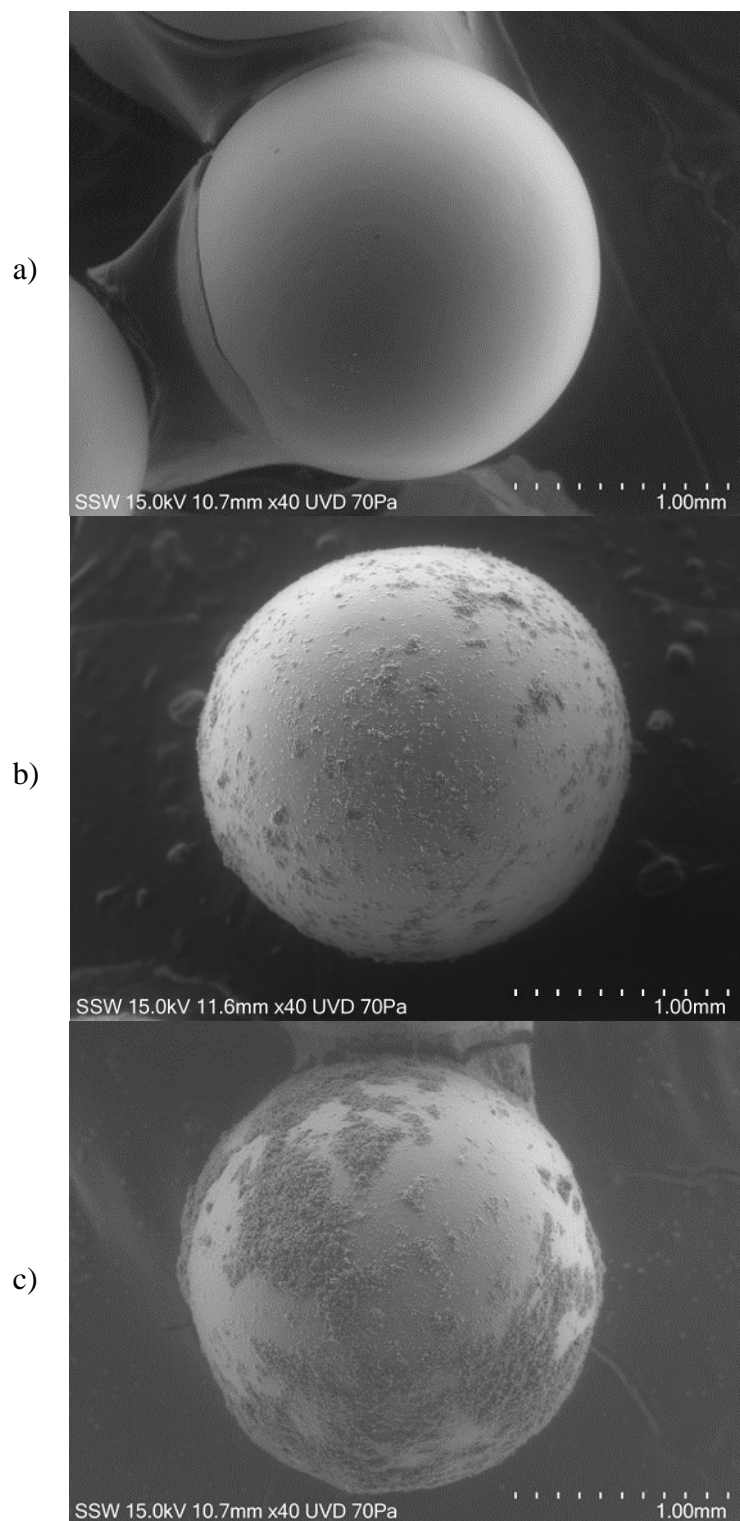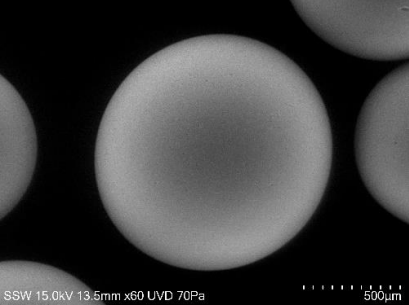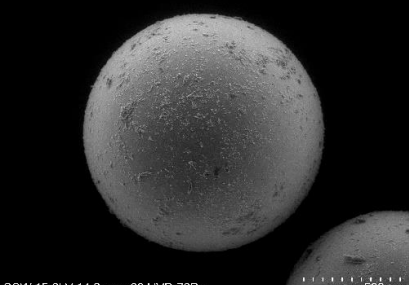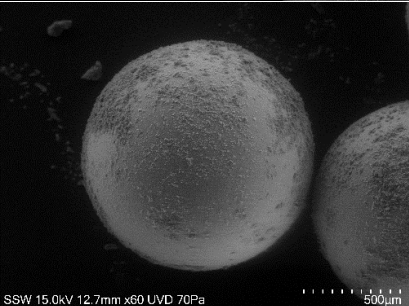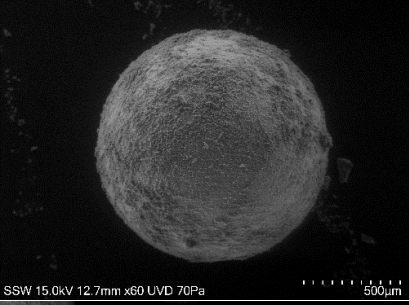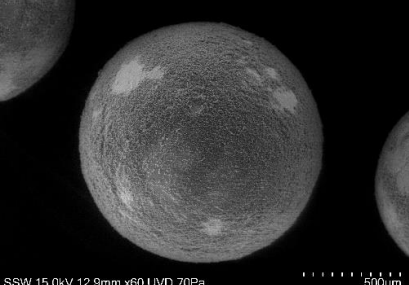
Figure 3.8: SEM images of a glass bead before a) and after mixing with magnesium stearate at b) 1 and c) 2 wt %; 40 x magnification

Table 3.2: SEM images of 1 mm glass beads mixed with 1 wt % MgSt at different revolutions; 60 x magnification

Revolution (#)	SEM Image	Observation
0		Surface of glass completely bare and smooth
2		Magnesium stearate particles begin to adhere to surface of glass bead
5		Magnesium stearate layer becomes more complete
10		Magnesium stearate almost completely covers surface of glass bead
45		Magnesium stearate layer is complete and uniform apart from exposed spots due to contact with other particles and surfaces

The COR was measured for both sugar spheres and glass beads, as shown in Figure 3.9. For the glass beads, the COR was approximately 0.7. The COR values for the sugar spheres were slightly lower than those of glass beads just below 0.6 and had high standard deviations; the standard deviation of the measurements increased as the size decreased as it became harder to pick up and release individual particles to complete the measurements. It was not possible to accurately measure values for particles with a mass less than 0.4 mg.
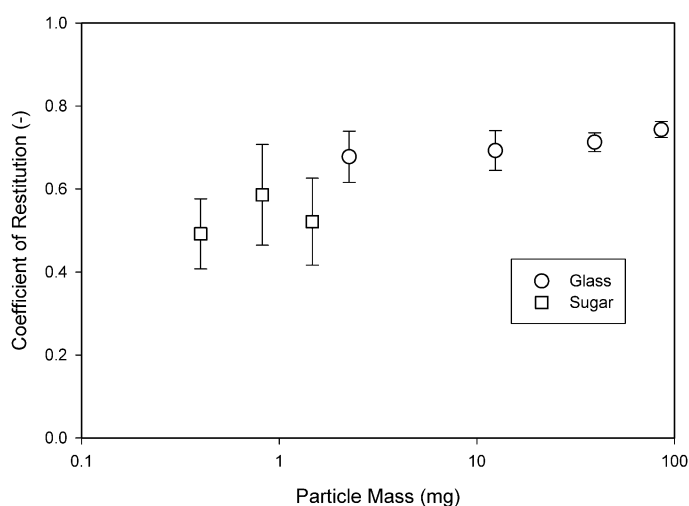
Figure 3.9: Coefficient of restitution for unmixed particles by mass; averages shown with ± standard deviation

The COR was measured again for particles mixed with magnesium stearate after 45 revolutions. For the glass beads, the addition of 1 % MgSt decreased the COR to an average of 0.6 and then slightly lower with an increase in the amount of magnesium stearate from 1 to 2 wt % (Figure 3.10). The standard deviation of the measurements using glass beads mixed with magnesium stearate was high. For the sugar spheres, it appeared that the COR decreased slightly with the addition of MgSt.
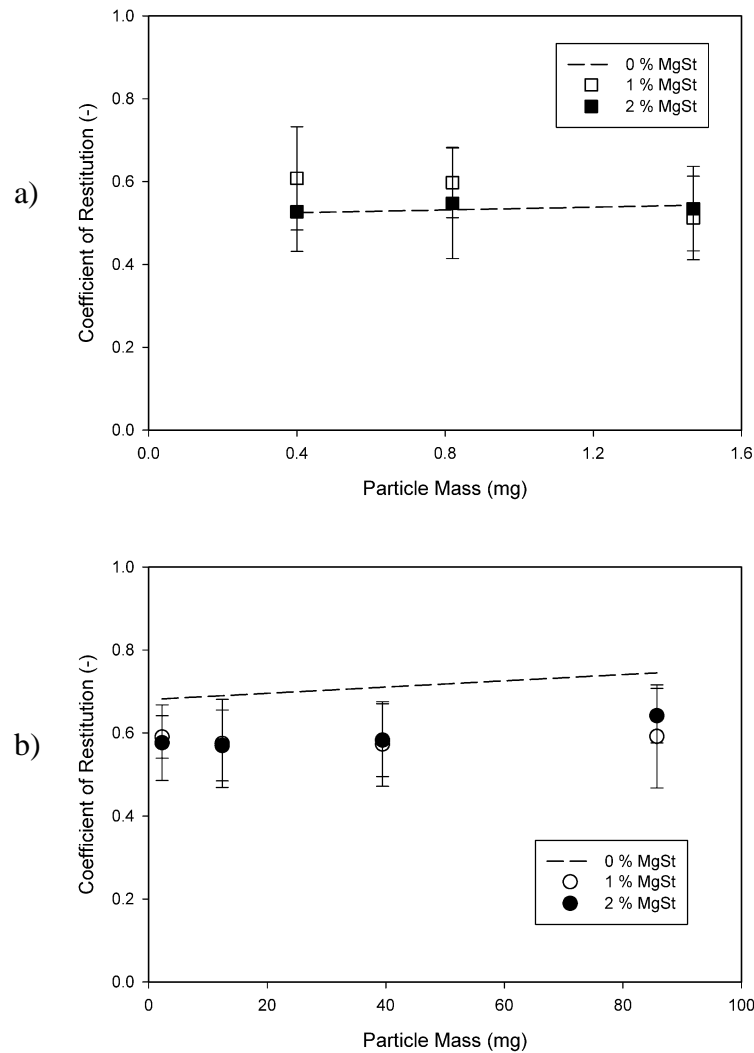
Figure 3.10: Coefficient of restitution of a) sugar spheres and b) glass beads each mixed with 1 % and 2 % magnesium stearate by weight; averages shown with ± 1 standard deviation

The COR and the corresponding vibration measurements for individual drop tests were directly compared. For glass beads, as shown in Figure 3.11, the signal amplitude increased with particle mass, while the COR remained relatively constant. The error for signal amplitude also increased with particle size. Similar trends were obtained for the sugar spheres mixed with magnesium stearate (Figure 3.12).
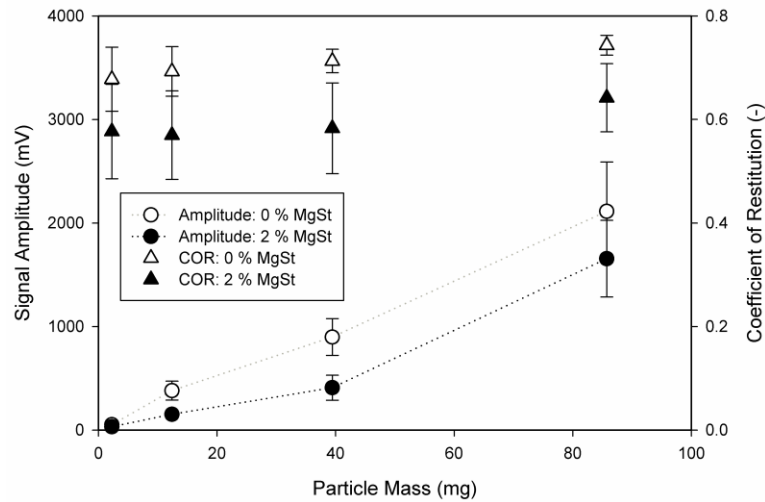
Figure 3.11: Coefficient of restitution and Feature 1 vibration amplitude data for individual glass bead drop tests with 0 wt % and 2 wt % magnesium stearate
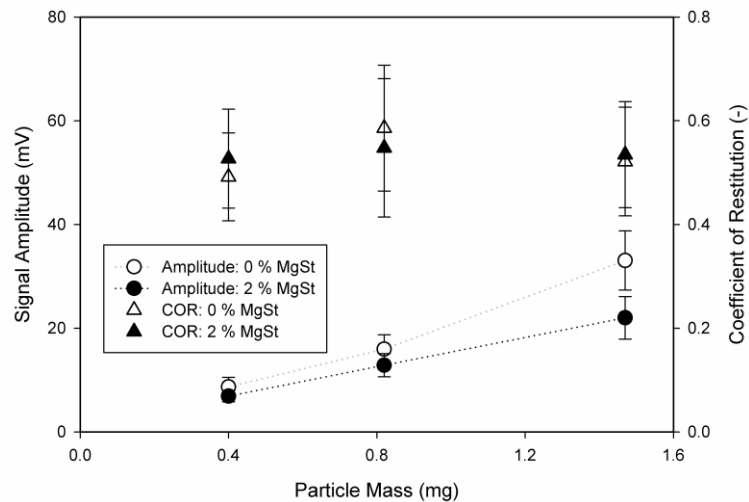
Figure 3.12: Coefficient of restitution and Feature 1 vibration amplitude data for individual sugar sphere drop tests with 0 wt % and 2 wt % magnesium stearate

Drop tests were performed with glass beads with an angled surface as shown in Figure 3.13. The measured vibration amplitudes were significantly lower for collisions with an angled surface compared to collisions normal to the particle's initial trajectory. The differences increased with particle mass, as did measurement error.
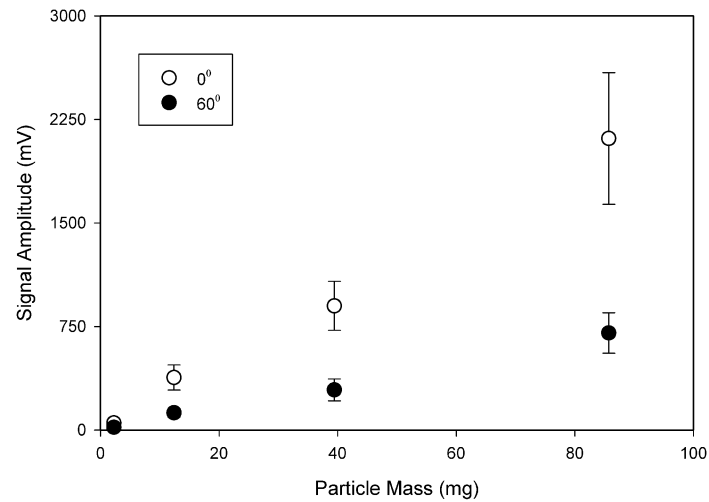
Figure 3.13: Effect of angle on Feature 1 signal amplitude for individual glass bead drop tests; averages shown with ± 1 standard deviation

The flowability of the sugar spheres mixed with magnesium stearate was measured using the Revolution Powder Analyzer. Figure 3.14 shows that when magnesium stearate was added, flowability either worsened or improved depending on particle size.
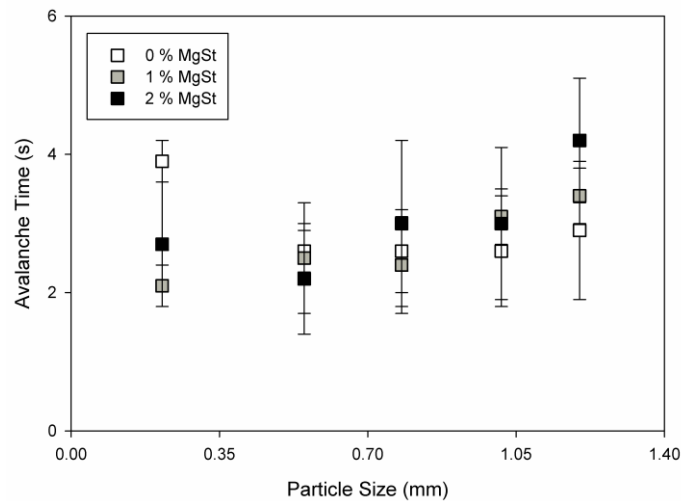
Figure 3.14: The effect of magnesium stearate addition on the flowability of sugar spheres

3.4 Discussion

The signal amplitudes of the vibrations of Feature 1 were the largest of the three identified features. As the V-shell of the blender rotates, the particles tumble. As the V-shell rotates to an upside-down position, the particles fall a relatively long distance and impact the lid at high velocities and corresponding high kinetic energies. With the impact or collision, some of the energy remains with the particle allowing it to rebound to a certain height while the remaining energy is dissipated through plastic deformation and stress wave propagation. Critical velocities were not reached to exceed the yield stress of the particles and did not result in deformation. Stress waves, however, propagated through the lid creating vibrations that were measured by the accelerometer. As the transmission distance from impact to the accelerometer was short, attenuation of the vibrations was minimized, and the measured vibrations had relatively large amplitudes.

The amplitudes of the vibrations of Feature 3 were also due to the particles falling within the blender V-shell and impact or collision with the bottom of the V-shell. The vibrations from particles impacting the bottom plate would have been relatively large. However, the vibrations measured by the accelerometer were small due to significant attenuation; the vibrations travelled through the plate attached to the shell by a rubber gasket and then up the sides of the shell before reaching the sensor on the lid. In addition, due to geometry of the V-shell, many particles would collide with the lower shell wall instead of the bottom plate. As shown in Figure 3.13, vibrations propagated following collision with an angled surface (such as the lower shell wall) are lower than those that would be propagated and measured following collision normal to the particle trajectory (as with collision with the lid or bottom plate). The energy dissipated therefore differed as the impact was not normal to the surface and the collision could also include some sliding or rolling component at the inclined surface.

The amplitudes of Feature 2 were different from those of Features 1 and 3 due to particle motion. Vibrations of Feature 2 were due to sliding and rolling motion of the particles along the wall of the V-shell. With this motion, particles impact the shell, but at low velocities as the bulk motion impedes high individual particle velocities, and usually the impact is tangential to the surface. The energy dissipated through wave propagation is

therefore relatively low and is attenuated through the vessel wall before measured by the accelerometer attached to the lid.

The amplitudes of the vibrations of Feature 1 were affected by the mass of the particles as varied through particle size and density (Figure 3.4). Kinetic energy is proportional to the mass of a particle. Therefore, particles with a larger mass either through size or density impacted the V-shell lid with higher energies resulting in more energy dissipated through vibrations which were measured by the accelerometer.

Considering experimental errors, the coefficient of restitution was determined to be approximately constant with particle mass (Figure 3.9). The relative independence with mass was supported by literature. The Zener model uses intrinsic properties of the particles to estimate an inelasticity parameter in a model to estimate the coefficient of restitution (34). According to the Zener model, the estimated coefficient of restitution for glass beads colliding with a metal plate of 3.1 mm thickness as per the V-blender lid, would be approximately constant between 0.93 and 0.99 for the specified 1-4 mm particle diameter range. The measured values were lower than the theoretical values due to experimental errors and the idealistic conditions of the model which does not incorporate, for example, air drag and particle rotational velocity.

Although the coefficient of restitution was determined to be approximately constant with particle mass, there was significant increase in measured vibrations with increasing particle mass (Figures 3.11 and 3.12). As the particle mass increased, the overall energy of the particle at the instant of the collision increased, but the ratio of the energy retained by the particle after collision to the energy dissipated changed; with increased energy levels, waves are more easily propagated through the lid (33), increasing the amplitude of the vibrations that were then measured by the sensor.

Figures 3.6 shows that the measured amplitude of vibrations of Feature 1 decreased when magnesium stearate was mixed into the particles. The measured amplitudes decreased to about 12 mV with the addition of 1 % magnesium stearate regardless of particle size or density. The measured amplitudes further decreased to about 5 mV with the addition of more magnesium stearate at a concentration of 2 %.

The magnesium stearate particles adhere to the surface of the particles, as shown in the SEM images in Figure 3.8. This non-uniform layer alters the properties of the particles and collisions become more inelastic. When a particle mixed with magnesium stearate collides with the V-shell lid, some energy is now dissipated into the deformation of the magnesium stearate layer adhered on the particles; the energy retained by the particle remained about the same and therefore less energy dissipated through wave propagation resulting in smaller vibrations measured by the accelerometer. A comparison of Figures 3.9 and 3.10 shows that the coefficient of restitution remained approximately constant with particle mass and with the addition of the magnesium stearate. Upon impact, the magnesium stearate particles would disperse in the adhered layer. As the magnesium stearate was increased to 2 wt %, the layer became more complete/uniform in the coverage of the particles; more energy is dissipated in deformation of the magnesium stearate layer resulting in even less energy dissipated through wave propagation as shown in Figures 3.11 and 3.12.

Figure 3.6 shows that the measured amplitudes of Feature 1 vibrations decreased with the addition of magnesium stearate for the 16-20 mesh sugar spheres. At 1 wt % magnesium stearate, the measured amplitudes became constant at about 12 mV near 10 revolutions. At 2 wt % the magnesium stearate the amplitudes decreased to about 5 mV near 7 revolutions. Preliminary experiments with coloured sugar spheres provided supporting visual observations: the point at which Feature 1 vibrations reached a plateau approximately corresponded to magnesium stearate flakes adhering to all of the particles and visually uniformly dispersed. The preliminary experiments and results were confirmed by SEM photos. As shown with glass beads in Table 3.2, the magnesium stearate particles began to adhere to the particles, becoming more complete and uniform with mixing time until a continuous layer was formed just beyond 10 revolutions indicating a mixing end-point which corresponds to the vibration measurements. With further increases in mixing time, the magnesium stearate layer thickness is upheld through friction and contact between particles and particles with the V-shell. Beyond 10 revolutions, the thickness of the magnesium stearate layer increases until the layer becomes more susceptible to shear and breakage through particle contact, resulting in the thickness of the layer being maintained as shown in Table 3.2 of a glass bead imaged at

45 revolutions. This corresponds to measured vibrational amplitudes being relatively stable beyond mixing endpoints.

The number of revolutions required to mix magnesium stearate with the particles decreased as the amount of magnesium stearate increased. The increased number of magnesium stearate particles provided more contact opportunities with the sugar spheres or glass beads. Contact allows the magnesium stearate flakes to adhere to the other particles and then further contact combined with any shearing and delamination transfers magnesium stearate flakes to other particles. More contact opportunities therefore provide a higher dispersal rate of the magnesium stearate leading to shorter required mixing times. Figure 3.7 shows that the amplitude profiles were similar for mixing the same amount magnesium stearate with either 1 mm glass beads or 14-18 mesh sugar spheres (average diameter of 1.2 mm), with both particles reaching a plateau at approximately the same time. This can be attributed to the similar volume to surface ratio of the particles, where magnesium stearate flakes simply adhere to their surfaces; mixing performance of particles of the same size is similar regardless of mass. The differences in the plateau level of the signals can be attributed to the added mass of the glass particles compared to the sugar spheres; although thoroughly mixed with equal amounts of magnesium stearate, energy dissipated into the accelerometer upon collision is primarily due to the increased kinetic energy from the added mass rather than the adhered magnesium stearate layer.

It has been proposed that as magnesium stearate is mixed into another powder that its flaky particles could continue to shear creating more particles to continue the layering around the primary powder particles. As this mechanism alters the magnesium stearate particulate layer around the primary powder particles, upon collisions, the energy dissipated into the coating layer would change. As a result, the energy dissipated through wave propagation measured as vibrations by the accelerometer would then change. Figure 3.6 shows that the measured amplitude did not change for the first 45 revolutions indicating that additional shearing leading to over mixing did not occur within this time.

The flowability of the particulates was measured to complement vibration measurements and visual observations (30). Figure 3.14 shows that for the sugar spheres, the differences in the flowability as measured by the avalanche time were very small; similar results were obtained for the glass beads. Since the particles are approximately spherical, smooth, and free flowing, the effect of the magnesium stearate on flowability of the particles was not significant. Flowability affects particle motion, and therefore mixing performance, within a tumbling blender. The measured changes in vibrations therefore cannot be attributed to the flowability.

3.5   Conclusions

As particles tumble in a rotating V-blender, they collide with the V-shell. With a collision, some energy is retained by the particles while other energy is dissipated through plastic deformation and stress wave propagation. A sensor attached to the lid of the V-blender measured the vibrations created by the stress waves. These vibrations from collisions of the particles with the lid with the attached sensor provided information about the particles. The measured vibrations increased with particle mass, as varied through size and density, as the kinetic energy upon collision was higher. The vibrations were sensitive to the addition of magnesium stearate. Magnesium stearate flakes adhered to the surface of the primary particles thereby altering the surface and the dissipation of energy upon collision with the V-shell. The measured change in the dissipated vibrations allowed identification of the number of revolutions required to disperse the magnesium stearate into the primary particles. This preliminary study shows potential as an inline method to monitor mixing of magnesium stearate and identify an optimal mixing endpoint**.**

3.6 References

1. Lemieux M, Bertrand F, Chaouki J, Gosselin P. Comparative study of the mixing of free flowing particles in a V-blender and a bin-blender. Chem Eng Sci 2007; 62: 1783-1802.
2. Brone D, Alexander A, Muzzio F. Quantitative characterization of mixing of dry powders in v-blenders. AIChE J 1998; 44: 271-278.
3. Kuo H, Knight P, Parker D, Seville J. Solids circulation and axial dispersion of cohesionless particles in a V-mixer. Powder Technol 2005; 152: 133-140.
4. Lemieux M, Leonard G, Doucet J, Leclaire L, Viens F, Chaouki J, Bertrand F. Large-scale numerical investigation of solids mixing in a V-blender using the discrete element method. Powder Technol 2008; 181: 205-216.
5. Perrault M, Bertrand F, Chaouki J. An investigation of magnesium stearate mixing in a V-blender through gamma-ray detection. Powder Technol 2010; 200(3):234-45.
6. Roblot-Treupel L, Puisieux F. Distribution of magnesium stearate on the surface of lubricated particles. Int J Pharm 1986; 31(1):131-6.
7. Bossert J, Stains A. Effect of mixing on the lubrication of crystalline lactose by magnesium stearate. Drug Dev Ind Pharm 1980; 6(6):573-89.
8. Jarosz PJ, Parrott EL. Effect of lubricants on tensile strengths of tablets. Drug Dev Ind Pharm 1984;10(2):259-73.
9. Kikuta JI, Kitamori N. Effect of mixing time on the lubricating properties of magnesium stearate and the final characteristics of the compressed tablets. Drug Dev Ind Pharm 1994; 20(3):343-55.
10. Deveswaran R, Bharath S, Basavaraj BV, Abraham S, Furtado S, Madhavan V. Concepts and Techniques of Pharmaceutical Powder Mixing Process: A Current Update. J Pharm Technol 2009; 2: 245-249.
11. Garcia T, Wilkinson S, Scott J. The Development of a Blend-Sampling Technique to Assess the Uniformity of a Powder Mixture. Drug Dev Ind Pharm 2001; 27:4, 297-307.
12. Muzzio FJ, Goodridge CL, Alexander A, Arratia P, Yang H, Sudah O, Mergen G. Sampling and characterization of pharmaceutical powders and granular blends. Int J Pharm 2003; 250: 51-64.
13. Bellamy L, Nordon A, Littlejohn D. Non-invasive monitoring of powder mixing with near infrared spectroscopy and acoustics. Spectrosc Eur 2004; 25-27.
14. Blanco M, Gozalez B, Bertran E. Monitoring powder blending in pharmacetical processes by use of near infrared spectroscopy. Talanta 2002; 56: 203-212.
15. Koeller D, Posch A, Hori G, Voura C, Radl S, Urbanetz N, Fraser S, Tritthar W, Reiter F, Schlingmann M, Khinast J. Continuous quantitative monitoring of powder mixing dynamics by near-infrared spectroscopy. Powder Technol 2011; 205: 87-96.
16. De Beer TRM, Bodson C, Dejaegher B, Walczak B, Vercryysse P, Burgraeve A et al. Raman spectroscopy as a process analytical technology (PAT) tool for the in-line monitoring and understanding of a powder blending process. J Pharm Biomed Anal 2008; 48: 772-779.

17. Breintenbach J, Schrof W, Neumann J. Confocal Raman-spectroscopy: analytical approach to solid dispersions and mapping of drugs. Pharm Res 1999; 16: 1109-1113.
18. Vergote G, De Beer T, Vervaet C, Remon J, Baeyens W, Diericx N, Verpoort F. In-line monitoring of a pharmaceutical blending process using FT-Raman spectroscopy. Eur J Pharm Sci 2004; 21: 479-485.
19. Nakagawa M, Altobelli SA, Caprihan A, Fukushima E, Jeong EK. Non-invasive measurements of granular flows by magnetic resonance imaging. Exp Fluids 1993; 16: 54-60.
20. Porion P, Sommier N, Faugere AM, Evesque P. Dynamics of size segregation and mixing of granular materials in a 3D-blender by NMR imaging investigation. Powder Technol 2004; 141: 55-68.
21. Sommier N, Porion P, Evesque P, Leclerc B, Tchoreloff P, Couarraze G. Magnetic resonance imaging investigation of the mixing-segregation process in a pharmaceutical blender. Int J Pharm 2001; 222: 243-258.
22. Broadbent CJ, Bridgewater J, Parker DJ. The effect of fill level on powder mixer performance using a positron camera. Chem Eng J 1995; 56: 119-125.
23. Lai FS, Fan LT. A study on the mixing of flour in a motionless Sulzer (Koch) mixer using a radioactive tracer. Powder Technol 1976; 13: 73-83.
24. Aguiar C, Laudares F. Listening to the Coefficient of Restitution and the Gravitational Accerleration of a Bouncing Ball. Am J Phys 2003; 71: 499-501.
25. Müller P, Böttcher R, Russell A, M Trüe M, Aman S, Tomas J. Contact time at impact of spheres on large thin plates. Adv Powder Technol. 2016; 27(4): 1233-1243.
26. Jackson, R.L., Green I, Marghitu D.B. Predicting the coefficient of restitution of impacting elastic-perfectly plastic spheres. Nonlinear Dyn 2010; 60(3): 217-229.
27. Marinack M, Musgrave R, Higgs C. Experimental Investigations on the Coefficient of Restitution of Single Particles. Tribology Transactions 2013; 56:4, 572-580.
28. Tily P, Porada S, Scruby C, Lidington S. Monitoring of mixing processes using acoustic emission. In: Harnby N, Benkreira H, Carpenter K, Mann R, eds. Fluid Mixing III. Rugby: The Institute of Chemical Engineers 1988; 75-94.
29. Allan P, Bellamy L, Nordon A, Littlejohn D. Non-invasive monitoring of the mixing of pharmaceutical powders by broadband acoustic emission. Analyst 2010; 135: 518-524.
30. Crouter A, Briens L. Passive acoustic emissions from particulates in a V-blender. Drug Dev Ind Pharm 2015; 11: 1809-1818.
31. Crouter A, Briens L. Monitoring lubricant addition using passive acoustic emissions in a V-blender. Powder Technol 2016; 301: 1119-1129.
32. Cameron A, Briens L. An Investigation of Magnesium Stearate Mixing Performance in a V-blender Through Passive Vibration Measurements. AAPS PharmSciTech 2019; 20:199.
33. Sondergaard R, Chaney K, Brennen C. Measurements of Spheres bouncing off flat plates. J Appl Mech 1990; 112.
34. Zener, C. The Intrinsic Inelasticity of Large Plates. Phys Rev 1941; 59, 669–673.

Chapter 4

4 An Investigation of Magnesium Stearate Mixing Performance in a V-blender through Passive Vibration Measurements

Publication status: A version of this chapter was published online in *AAPS PharmSciTech* on May 24, 2019.

4.1 Introduction

The final mixing stage within tablet manufacturing consists of lubricant addition. Lubricants are added to ensure the mixture flows easily into the tablet press and is then cleanly ejected from the tablet die. To monitor this process, many process analytical technologies have been implemented to increase efficiency, product quality, and efficiency to correct issues associated with current off-line sampling methods.

The mixers primarily used within pharmaceutical manufacturing are tumbling mixers, more specifically, the V-blender. Tumbling mixers are mounted on a rotating axis where particles tumble and mix due to gravity. Tumbling mixers can vary in their geometry where V-blenders are composed of two shells connected at angles between 75-90° and can differ in shell size. The V-blender is used since it is well established and provides effective, gentle mixing for fragile granules used in the tablet manufacturing process.

The mixing performance of the V-blender is attributed to the mixing mechanisms that become apparent from revolutions that produce two distinct phases based on the geometry of the mixer itself. One occurs from 0-180° of rotation where the mixer goes from an upright position to that of inverted. Here, mixing is dominated by a convective mechanism of particles being randomly distributed through free fall as they separate to each arm of the shell. The other phase occurs through 180-360° of rotation as the mixer goes from an inverted to an upright position. The particles converge at the bottom and only a fraction of the particles cross the axis of symmetry. That is, mixing is much more effective in each arm of the shell than that between arms, where there is no inherent convective mixing mechanism across the axis of symmetry where the particles rely on axial dispersion due to the geometry of the mixer (1-5). Due to inherent limitations of the

mixing mechanisms of the V-blender, it is critical to optimize process parameters to allow for homogeneity to be achieved faster and increase the mixing performance of the blender. Homogeneity can be largely affected by agitation, rotation rate, fill level, mixing time, and loading profiles. Brone *et al.* (1,2) used a V-blender filled with mono sized red and white coloured spheres to determine the effects of perturbations, rotations rate, fill level, and number of revolutions have on mixing performance through image analysis. Mixing rate is increased as fill decreases, increases with mixing time, and as agitation is introduced or increased. Using positron emission particle tracking technique, Kuo *et al.* (3) found that mixing performance in a V-blender was enhanced with increased rotational speed for 3 mm glass beads. Lemieux *et al.* (4,5) varied loading profiles for mono sized, spherical particles in a V-blender and found that top-bottom loadings are much more effective than that of left-right and right-left. These studies focused on the effect of process parameters for free-flowing particles, which would not be representative of the pharmaceutical mixing applications.

Currently, blend homogeneity is assessed by first taking samples through a thief probe and then analyzed through destructive methods such as high-performance liquid chromatography and UV-spectroscopy. In the manufacturing process, this is laborious and time consuming and contributes significantly to the overall cost. A thief probe has been the primary sampling method for uniformity and researched extensively (6-8) but suffers drawbacks. The insertion of the probe can disturb the powder bed leading to segregation and channeling of the mixture, requiring multiple samples to be taken. It is only at this stage that if the mixture is not homogenous, the entire batch is discarded, and the process must begin again.

In the final mixing stage, a lubricant is added to a mix to allow for easy flow into the tablet press as well as ensuring tablets are ejected out of the dies easily without any breakage. Magnesium stearate is primarily used as it is effective in low amounts (9), inexpensive, and stable. Lubricant dispersal as well as its effectiveness is primarily a function of flowability and shear forces during mixing. It has been proposed that magnesium stearate first fills surface irregularities within particles before forming a semi-continuous layer (5,10). This in turn increases flowability by making particles more

regular in shape and smoother. The contact points between particles and the press are reduced allowing for the tablet to be ejected smoothly. As well, lubricants are more effective for cohesive mixtures than for free-flowing particles (11). Due to its coating mechanism, magnesium stearate can begin to form agglomerates and become more dispersed as mixing continues, negatively affecting tablet strength with increasing mixing time and lubricant concentration (12-14). Shearing during mixing induces delamination of the magnesium stearate particles and impacts the adsorbed film developing on the excipient particles and can therefore have adverse effects the dissolution time (15). The link between the concentration of magnesium stearate and the mixing parameters on tablet properties are therefore difficult to determine as they rely on complex functions of flowability, shear, and lubricant properties. To ensure proper tablet properties, process parameters and the lubricant amount must be optimized and monitored.

To assess uniformity of mixtures and to monitor processes continuously, research has been conducted to further the development of process analytical technologies (PAT) including near infrared spectroscopy (NIR) (16-18), Raman spectroscopy (19-21), magnetic nuclear resonance imaging (MRI) (22-24), and radioactive tracers (10,25,26). These technologies are intrusive as they normally require the insertion of probes or windows to analyze data. Due to the modification and higher cost of equipment, these technologies become expensive. As well, extensive processing capabilities are normally required to analyze data.

Passive acoustic emission or vibration measurements address the issues associated with the other technologies as they are completely non-intrusive, not requiring any modification of existing equipment, and the sensors cost less than other monitoring methods. Acoustic emissions or vibrations within mixers can result from particle-particle and particle equipment collisions. The monitoring can include tracking signal amplitudes from an initial level to another stable level to indicate a mixing endpoint (27). It has been found that acoustic emissions are sensitive to a variety of changes within mixing processes. Bellamy *et al.* (16) mixed cellulose with secondary components in a high shear mixer monitored by both near infrared spectroscopy (NIR) and acoustic sensors. Both measurements were sensitive to particle size and can be used simultaneously to provide

monitoring of mixing processes. Allan et al (28) found that acoustic signals increased with particle size, mass, and impeller speed using a convective mixer to mix aspirin and citric acid with Avicel. Using a V-blender, Crouter and Briens (29) found that increasing particle size, shell size, and moisture, all increased the vibrations using sugar spheres. The applications documented in the literature are primarily confined to monitoring mixing processes in convective mixers with free-flowing particles, which are not always an accurate representation of tablet manufacturing mixing processes.

There have been only a few studies involving lubricant addition monitoring while mixing in a V-blender. Using a radioactive tracer, Perrault *et al.* (10) monitored magnesium stearate addition in a V-blender with lactose. It was found that the pre-blend composition had more effect on mixing performance than the loading profile. Crouter and Briens (30) determined that lubricant monitoring is feasible using vibrations for granule formulations in a V-blender, where the signal changed rapidly until approaching a stable plateau indicating that the lubricant was well dispersed. Due to the lack of research and complexity of lubricant addition, further work is required to optimize and develop a non-intrusive and inline method to monitor the process.

The coefficient of restitution, an intrinsic material property to model collisions and subsequently the vibrations have been well established and investigated (31-33). The coefficient of restitution is a measure of the loss of the kinetic energy from a collision. It is presented as ratio, where a ratio of one represents a completely elastic collision. That is, no energy is dissipated and therefore no vibrations would be initiated within the V-shell to be measured by the sensor. Conversely, a completely inelastic collision has a coefficient of restitution of zero, where the particle has no rebound, and all energy is dissipated.

This study aims to determine the effect of magnesium stearate loading configuration and fill level in a V-blender on mixing performance through non-intrusive, inline monitoring using passive vibration measurements. The results obtained can then further elucidate the mixing dynamics within a V-blender as well as assessing homogeneity in real time,

thereby increasing process efficiency and circumventing the issues associated with current sampling and monitoring methods.

4.2   Materials and Methods

The particles used in the trials consisted of 2 mm, spherical, glass beads with an apparent particle density of 2.5 kg/m^3.

4.2.1   V-blender

An 8 Qt stainless steel Patterson-Kelley V-blender rotating at a fixed speed of 25 rpm was used for all trials (Figure 4.1). The V-blender was run for 1-2 minutes, common within industry trials, corresponding to 25-50 revolutions. The V-shell was filled to 18-45 % of its volume with the glass beads. Magnesium stearate was added corresponding to 2 % by weight in Top-Bottom, Bottom-Top, Middle, Left-Side, and Right-Side loading configurations (Table 4.1), as evenly as possible ensuring uniform thickness between each trial. For radial loading configurations, magnesium stearate was added through the port in each corresponding arm as uniformly ensuring that no magnesium stearate crossed the axis. Trials were conducted in triplicate; however, one trial is shown for each condition as replicates were similar.
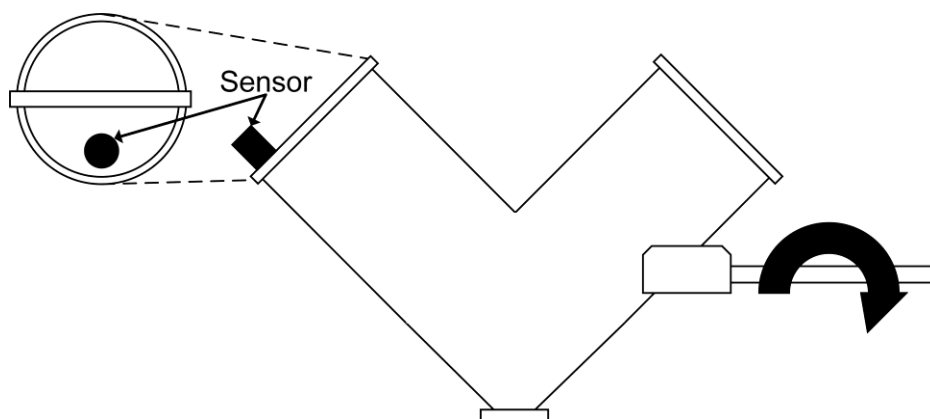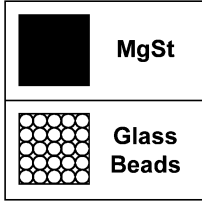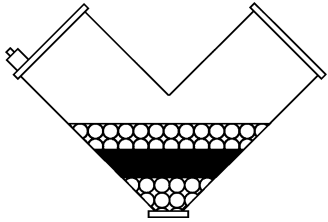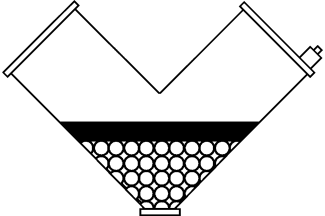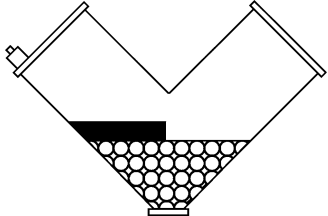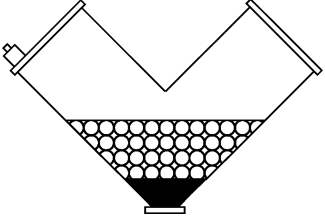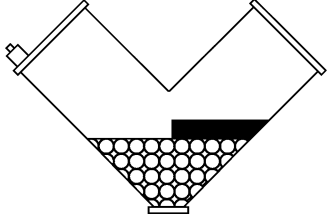

Figure 4.1: V-blender with sensor location and axis of rotation

Table 4.1: Magnesium stearate loading configurations

Configuration	Schematic	Configuration	Schematic
Legend	MgSt / Glass Beads	3) Middle	
1) Top-Bottom		4) Left-Side	
2) Bottom-Top		5) Right-Side	

4.2.2   Sensor and Data Acquisition

Vibrations were measured at an acquisition frequency of 40,000 Hz using a PCB Piezotronics accelerometer (model 353B34) with a frequency range of 0.35-12,000 Hz, combined with an ICP signal conditioner (model 480E09). The accelerometer was securely attached to V-shell lid at a radial position of r/R = 0.74 using adhesive wax (Figure 4.1). Signals were captured using Labview 8.5 with a National Instruments DAQ-6036E card. A multilevel wavelet decomposition filter was used to focus on vibrations from the particle interactions within the shell (29) to remove frequencies under 3 Hz without affecting the time or frequency coded information of the system. Code for a high-pass, 6 tap Daubechies wavelet decomposition was based on Daubechies (34). Data was analyzed in MATLAB, where representative Feature 1 signals were obtained through averaging the three largest amplitudes per revolution.

4.2.3   Coefficient of Restitution (COR)

Drop tests were used to estimate the COR. Glass beads were dropped onto the supported V-blender lid with the acoustic sensor attached. Beads were dropped past the critical distance from the support to ensure accurate measurements (35). The beads were dropped from heights of 11.1, 5.6, and 2.8 cm onto the lid (3.1 mm in thickness) (Figure 4.2). The time between successive peak amplitudes as particles rebounded were used to determine the COR (36), repeated for a total of 15 times.
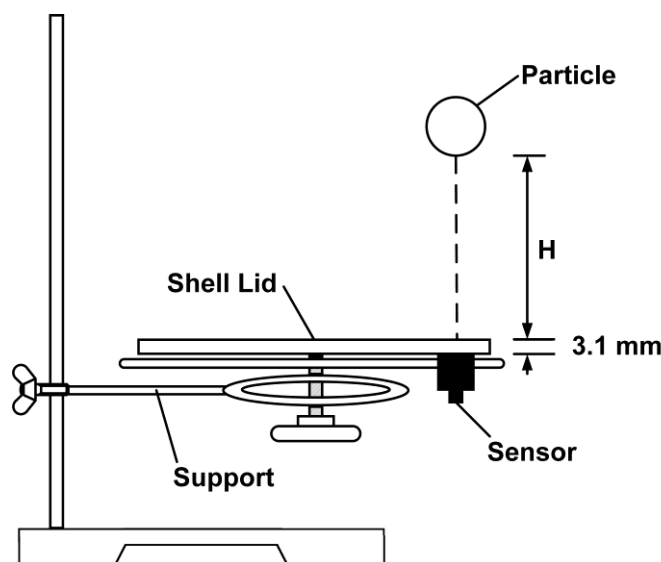
Figure 4.2: Schematic of apparatus used to measure the coefficient of restitution

4.2.4   Flowability

The avalanche time was used as a flowability indicator and was measured using a Mercury Scientific Revolution Powder Analyzer. Sample sizes were 59, 88.5, 118, and 147.5 cm^3 corresponding to 5.5, 8.2, 10.9, and 13.6 % of the drum volume, or ranging from 50 to 125 % of the manufacturer's recommended sample size. Samples were loaded into the sampling drum of 11 cm in diameter and a width of 3.5 cm. The drum was rotated at 0.3 rpm for a total of 50 avalanches occurred. An avalanche was defined as a rearrangement of more than 0.65 % by volume of the sample in the drum. Optical measurements of the powder surface were taken at a resolution of 648 x 488 at 60 frames

per second. Software calculated the avalanche time from the optical measurements. Samples were measured in triplicate.

4.3 Results

For particulates tumbling in a V-blender, three features have been observed during each revolution for the filtered vibration measurements: Feature 1 corresponds to vibrations created from particles impacting the lid of the V-shell, Feature 2 to particles flowing along the sides of the V-shell, and Feature 3 to particles impacting the bottom plate (Figure 4.3). Feature 1 showed the most information about particle properties and behaviour (29). Therefore, only Feature 1 vibrations will be shown in the results. To investigate the effect of fill level on particle behaviour within the V-shell, the glass beads were loaded into the V-shell at fill levels ranging from 18-45 % by volume. Figure 4.4 shows the measured amplitudes of the vibrations of Feature 1 at the various fill levels. The amplitudes increased to a maximum at a fill level of about 21-23 % by volume and then decreased at higher fill levels.
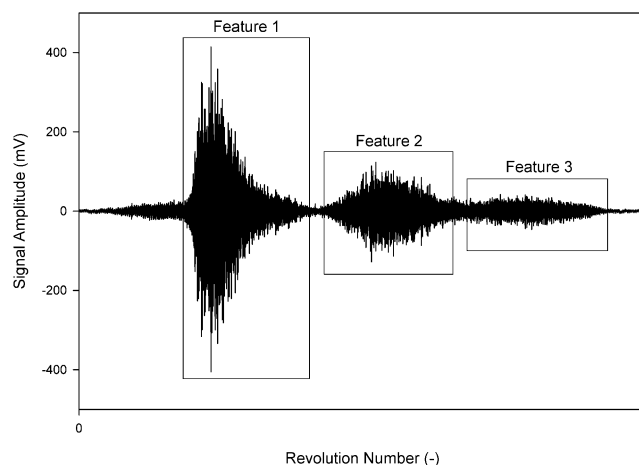
Figure 4.3: Filtered signal of 2 mm glass beads related to particle motion
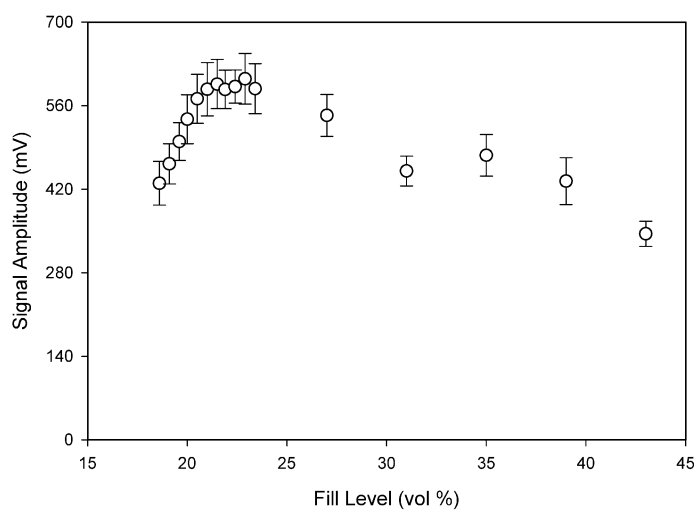
Figure 4.4: Feature 1 signal amplitudes with increasing fill level; averages shown with ± 1 standard deviation

Figure 4.5 shows both the coefficient of restitution and the signal amplitude measured from the drop experiments with increasing drop height. With increasing drop height, the coefficient of restitution decreased slightly while the signal amplitudes significantly increased.
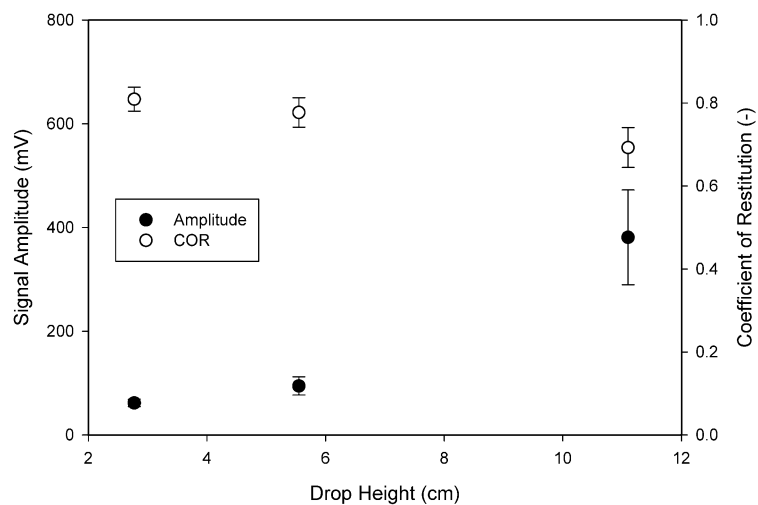
Figure 4.5: Coefficient of restitution for 2 mm glass beads at various drop heights; averages shown with ± 1 standard deviation

The avalanche time was measured using the Revolution Powder Analyzer to estimate flowability. The recommended sample size is 118 cm^3 in the sampling drum of 1082 cm^3 or a fill level of approximately 11 % by volume. To simulate particulate tumbling and flow in the V-shell at various fill levels, the sampling drum was filled to different levels. Figure 4.6 shows that as the fill level increased, the avalanche time also increased indicating a decline in flow.
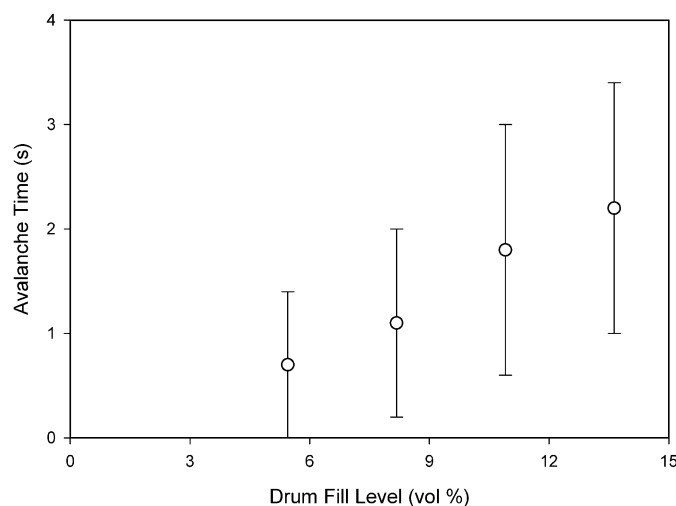
Figure 4.6: Avalanche time for 2 mm glass beads with increasing sampling drum fill levels; averages shown with ± 1 standard deviation

Magnesium stearate at 2 wt % was added in different loading configurations within the V-blender at a fixed total fill level of 23 % by volume (Figure 4.7). The measured amplitudes of Feature 1 of the signals was initially high and then decreased from 380 to about 20 mV with the addition and incorporation of the magnesium stearate into the mixture. As shown in Figure 4.7, the revolutions required to obtain a low and stable amplitude varied with loading configuration, from about 2 to 9 revolutions.
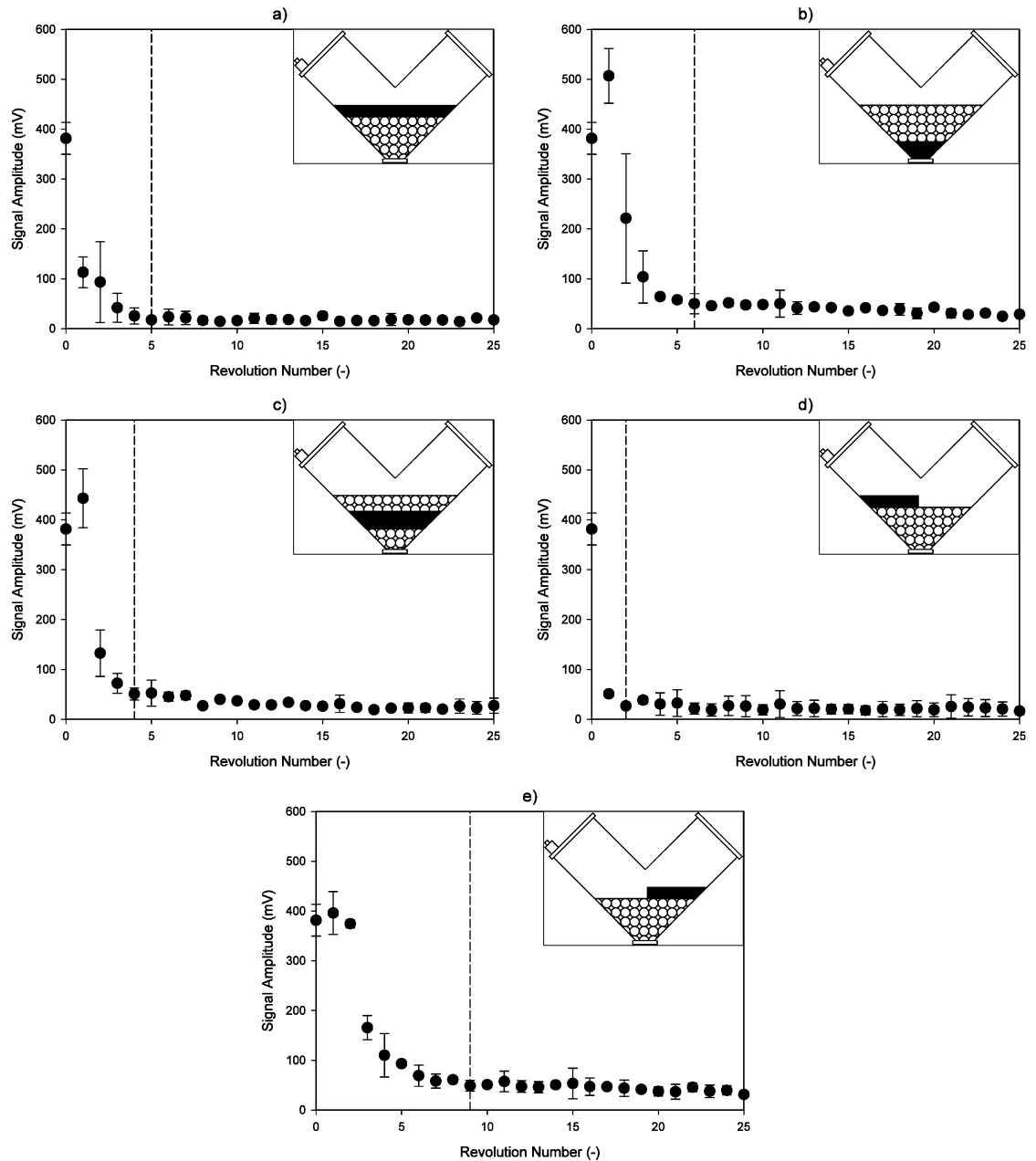
Figure 4.7: Mixing profiles of 2 mm glass beads mixed with 2 wt % MgSt in a) Top-Bottom, b) Bottom-Top, c) Middle, d) Left-Side, and e) Right-side loading configurations; 23 vol % fill level, mixing end-points shown by dashed lines

The effect of fill level for various loading configurations was also investigated. Figures 4.8 and 4.9 show example results for the Right-Side loading and Top-Bottom loading configurations. For all configurations, as the fill level increased, the number of revolutions to achieve a low and approximately constant signal amplitude increased.

The effect of fill was largest when magnesium stearate was added in a Right-side configuration.
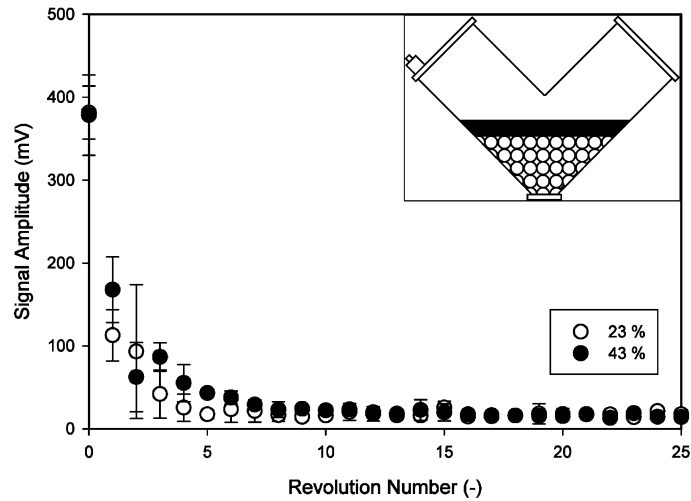
Figure 4.8: Feature 1 amplitudes with increase fill level for 2 mm glass beads with 2 wt % MgSt; Top-Bottom loading
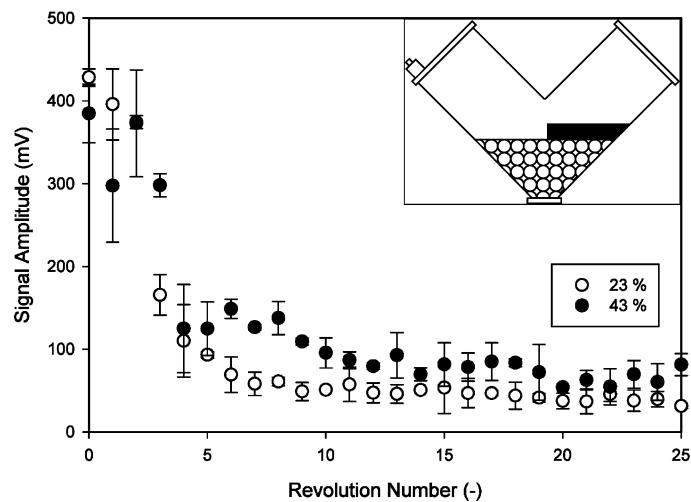
Figure 4.9: Feature 1 signal amplitudes with increase of fill level of 2 mm glass beads with 2 wt % MgSt; Right-Side loading configuration

Figure 4.10 compares the Right-side and Top-Bottom loading configurations at a fill level of 43 % by volume. For the Top-Bottom loading, the signal amplitude reached a

low and approximately constant value by 8 revolutions, while more than 25 revolutions were required for the Right- side loading configuration.
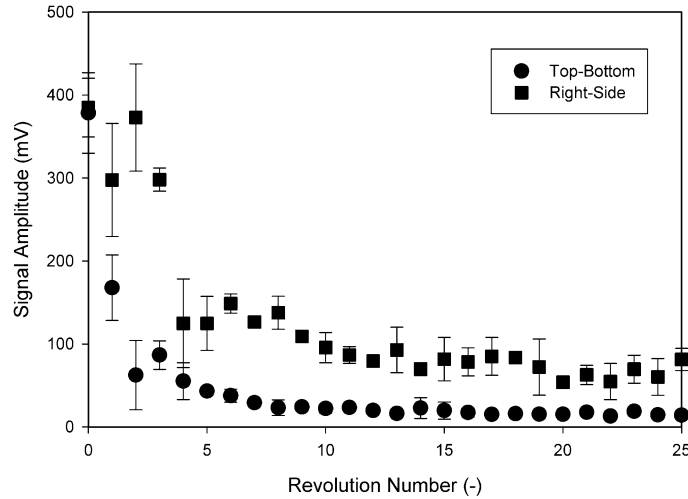
Figure 4.10: Feature 1 signal amplitudes for 2 mm glass beads with 2 wt % MgSt for Top-Bottom and Right-Side loading configurations; 43 % fill level

4.4 Discussion

The filtered signals presented in the results correspond to vibrations measured by the sensor as the particles impact the lid of the V-shell to which the sensor is attached (Feature 1 vibrations). As the V-shell rotates, the particles tumble within. As the V-shell is inverted, the particles move away from the wall and free fall the height of the V-shell and then collide with the lid, now at the bottom of the revolution path.

The coefficient of restitution and the vibrations were measured with drop experiments. The beads were dropped from heights of 2.8, 5.6, and 11.1 cm. As these heights were lower than a critical height to reach terminal velocity, the beads had different velocities and therefore different kinetic energies upon collision with the lid. The theoretical velocities and kinetic energies were calculated to be 74, 100, and 150 cm/s and 3.3, 6.6, and 13.1 mJ. Upon collision, some of the energy remains with the bead, allowing it to rebound to a certain height; the retention of the energy by the bead is indicated by the coefficient of restitution. As shown in Figure 4.5, the measured coefficient of restitution

decreased with increasing kinetic energy. As the kinetic energy increases, more energy is dissipated through plastic deformation and stress wave propagation with less energy retained by the bead to rebound following the collision. Plastic deformation was minimal for clean glass beads within the test conditions. The stress waves are propagated through the lid and their amplitudes are measured by the sensor. Figure 4.5 indicated that as the drop height or kinetic energy of a bead increased, more energy became dissipated into stress wave propagation as indicated by the significant increase in their measured amplitudes from 62 mV to about 380 mV.

Figure 4.4 shows that the measured amplitudes increased to a maximum fill level of about 21-23 % by volume and then decreased at higher fill levels. At low fill levels, there is a high probability that a glass bead will fall unimpeded the height of the V-shell as it is inverted before collision with the lid with the sensor attached; a relatively high kinetic energy is reached and dissipated into stress waves with measured high amplitudes. As the fill level is increased, the total number or mass of beads colliding with the lid increased, further increasing dissipated energy and measured amplitudes. There is a critical fill level of about 21- 23 % by volume. At this critical fill level, the number of beads within the V-shell has increased such that a bead will now likely collide with another bead as it tumbles and falls, before colliding with the lid. The kinetic energy of a bead upon collision with the lid begins to decrease with corresponding lower dissipated, measured stress wave energy. With further increases in fill level, a bead will collide with many other beads before collision with the lid and therefore the kinetic energy at collision and the amplitudes of stress waves measured by the sensor continue to decrease.

Effective convective mixing relies on particles free falling within the V-shell to promote distribution. The results from Figure 4.4 indicated that an optimal fill level for convective mixing would be 21-23 % by volume. Lower fill levels would not be process efficient while higher fill levels start to impede the required particle motion for effective mixing.

The movement or flowability of particles was further investigated by measuring the avalanche time using the Revolution Powder Analyzer. High avalanche times indicate poor flowability. As the fill volume of the sampling drum increased, the avalanche time

increased indicating a decline in flow. At high fill volumes, particles inhibit other particle flow as an individual particle does not free fall for long distances before collision with another particle. These independent measurements within the Revolution Analyzer support the conclusions from Figure 4.4.

Figure 4.7 shows that the measured vibrations decreased when 2 wt % magnesium stearate was added. The magnesium stearate flakes adhere to the surface of the glass beads creating a layer. When a bead with magnesium stearate collides with the V-shell lid, some energy is dissipated into the deformation of the magnesium stearate layer. As a result, less energy is retained by the bead and less energy is dissipated through stress wave propagation resulting in lower amplitude vibrations measured by the sensor.

The number of revolutions of the V-shell required to obtain approximately a low and stable measured amplitude varied with loading configuration of the magnesium stearate. For the three axial loading configurations, the required revolutions ranged from 4 to 6 indicating very rapid mixing of the magnesium stearate. This rapid mixing is attributed to the convective mechanism of mixing. In contrast, when the magnesium stearate was added through the Right-Side loading configuration, the number of revolutions required for mixing was longer. With the initial revolutions, a significant amount of magnesium stearate will remain within the right arm of the V-shell as the particle motion is mostly vertical with only a small fraction moving across the axis of symmetry into the other arm of the V-shell. With each revolution, more magnesium stearate is transferred between the arms and then combined with axial convective mixing is approximately uniformly distributed by 9 revolutions. The very low value of 2 revolutions for the Left-Side loading configuration was misleading. With the first revolution, all the magnesium stearate contacts the surface of the lid, creating a layer on the lid that affects subsequent measurements. This can occur with the other configurations but would not have as large of an impact. To minimize signal error associated with magnesium stearate coating the lid of the mixer, it is recommended to utilize the middle loading configuration as it provides the axial configuration for effective mixing while preventing the magnesium stearate from directly impacting and coating the shell lid. Measured vibrations were supported through visual observation by using a clear, acrylic V-shell.

The trials with the different fill levels of glass beads indicated that fill level affects the free fall motion of the particles which in turn would affect convective mixing. This was confirmed with the trials adding magnesium stearate in different loading configurations for different fill levels. For example, with a Top-Bottom loading configuration, the number of revolutions required for mixing increased from about 4 to 8 (Figure 4.8). The effect of fill was even more pronounced for the Right-Side loading configuration (Figure 4.9). With increasing fill level, particle motion across the axis of symmetry becomes restricted. When increasing the fill level from 23-43 % fill by volume, the particle bed was raised from approximately 19 cm to 14 cm to where the two arms of the V-shell are joined and determines the space at which particles can cross the axis of symmetry and the height at which particles fall to collide with the lid (Figure 4.11). This restriction in space can have adverse effects by limiting axial dispersion (axial loading configurations rely on) and convection (radial loadings rely on) within each arm of the V-shell corresponding to longer mixing times or revolution number and smaller signal amplitudes measured by the sensor.
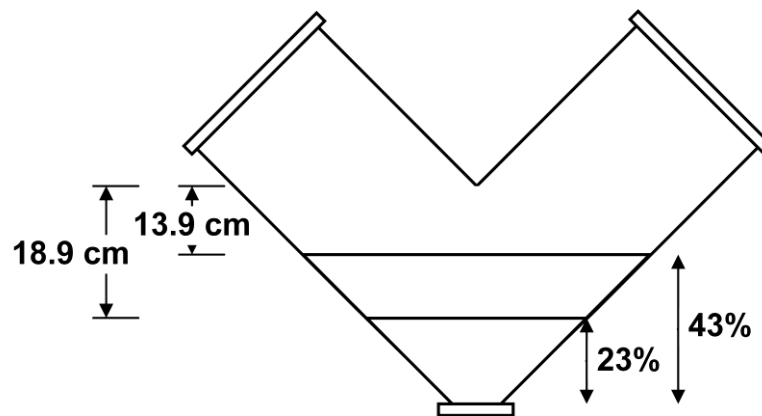
Figure 4.11: V-blender schematic of increased powder bed height from 23 to 43 % by volume

A comparison of an axial versus a radial loading configuration in Figure 4.10 confirms the significant effect of loading configuration on mixing time (or number of revolutions). Mixing occurs faster for axial than for radial loading configurations.

4.5 Conclusions

Passive measurements of vibrations created by particle movement in a V-blender were measured using an accelerometer attached to the lid of the V-shell. The measured vibrations showed that the optimum fill level to promote effective convective mixing was 21-23 % by volume. The measurements also showed that axial loading configurations required less mixing time or number of revolutions compared to radial loading configurations. Magnesium stearate flakes adhere to the surface of the particles during mixing, altering the properties of the particles and making collisions less elastic. This alteration allows vibration measurements the potential for monitoring mixing of magnesium stearate and identification of a mixing end-point. Ideally, magnesium stearate should be mixed just until a desired uniformity is reached as overmixing has many negative effects. Inline monitoring of magnesium stearate mixing would lead to improved control of the mixing process.

4.6 References

1. Brone D, Wightman C, Connor K, Alexander A, Muzzio FJ, Robinson P. Using flow perturbations to enhance mixing of dry powders in V-blenders. Powder Technol 1997; 91: 165-172.
2. Brone D, Alexander A, Muzzio FJ. Quantitative Characterization of mixing of dry powders in v-blenders. AIChE J 1998; 44:271-278.
3. Kuo H, Knight P, Parker D, Seville J. Solids circulation and axial dispersion of cohesionless particles in a V-mixer. Powder Technol 2005; 152: 133-140.
4. Lemieux M, Bertrand F, Chaouki J, Gosselin P. Comparative study of the mixing of free-flowing particles in a V-blender and a bin-blender. Chem Eng Sci 2007; 62: 1783-1802.
5. Lemieux M, Leonard G, Doucet J, Leclaire L, Viens F, Chaouki J, Bertrand F. Large-scale numerical investigation of solids mixing in a V-blender using the discrete element method. Powder Technol 2008; 181:205-216.
6. Deveswaran R, Bharath S, Basavaraj BV, Abraham S, Furtado S, Madhavan V. Concepts and techniques of pharmaceutical powder mixing process: A current update. J Pharm Tech 2009; 2: 245-249.
7. Garcia T, Wilkinson S, Scott J. The development of a blend-sampling technique to assess the uniformity of a powder mixture. Drug Dev Ind Pharm 2001; 27(4), 297-307.
8. Muzzio FJ, Goodridge CL, Alexander A, Arratia P, Yang H, Sudah O, Mergen G. Sampling and characterization of pharmaceutical powders and granular blends. Int J Pharm 2003; 250: 51-64.
9. Morin G, Briens L. The effect of lubricants on powder flowability for pharmaceutical application. AAPS PharmSciTech 2013; 14(3): 1158-1168.
10. Perrault M, Bertrand F, Chaouki J. An investigation of magnesium stearate mixing in a V-blender through gamma-ray detection. Powder Technol 2010; 200(3): 234-245.
11. Faqih AM, Mehrotra A, Hammond SV, Muzzio FJ. Effect of moisture and magnesium stearate concentration on flow properties of cohesive granular materials. Int J of Pharm 2007; 336(2): 338-345.
12. Bossert J, Stains A. Effect of mixing on the lubrication of crystalline lactose by magnesium stearate. Drug Dev Ind Pharm 1980; 6(6):573-89.
13. Jarosz PJ, Parrott EL. Effect of lubricants on tensile strengths of tablets. Drug Dev Ind Pharm 1984;10(2):259-73.
14. Kikuta JI, Kitamori N. Effect of mixing time on the lubricating properties of magnesium stearate and the final characteristics of the compressed Fts. Drug Dev Ind Pharm 1994;20(3):343-55.
15. Murthy, J Samyn. Effect of shear mixing on in vitro drug release of capsule formations containing lubricants. J Pharm Sci 1977; 66(99): 1215-1219.
16. Bellamy L, Nordon A, Littlejohn D. Non-invasive monitoring of powder mixing with near infrared spectroscopy and acoustics. Spectrosc Eur 2004: 25-27.

17. Blanco M, Gozalez B, Bertran E. Monitoring powder blending in pharmaceutical processes by use of near infrared spectroscopy. Talanta 2002; 56: 203-212.
18. Koeller D, Posch A, Hori G, Voura C, Radl S, Urbanetz N, Fraser S, Tritthar W, Reiter F, Schlingmann M, Khinast J. Continuous quantitative monitoring of powder mixing dynamics by near-infrared spectroscopy. Powder Technol 2011; 205: 87-96.
19. De Beer TRM, Bodson C, Dejaegher B, Walczak B, Vercryysse P, Burgraeve A et al. Raman spectroscopy as a process analytical technology (PAT) tool for the in-line monitoring and understanding of a powder blending process. J Pharm Biomed Anal 2008; 48: 772-779.
20. Breintenbach J, Schrof W, Neumann J. Confocal Raman-spectroscopy: analytical approach to solid dispersions and mapping of drugs. Pharm Res 1999; 16: 1109-1113.
21. Vergote G, De Beer T, Vervaet C, Remon J, Baeyens W, Diericx N, Verpoort F. In-line monitoring of a pharmaceutical blending process using FT-Raman spectroscopy. Eur J Pharm Sci 2004; 21: 479-485.
22. Nakagawa M, Altobelli SA, Caprihan A, Fukushima E, Jeong EK. Non-invasive measurements of granular flows by magnetic resonance imaging. Exp Fluids 1993; 16: 54-60.
23. Sommier N, Porion P, Evesque P, Leclerc B, Tchoreloff P, Couarraze G. Magnetic resonance imaging investigation of the mixing-segregation process in a pharmaceutical blender. Int J Pharm 2001; 222: 243-258.
24. Porion P, Sommier N, Faugere AM, Evesque P. Dynamics of size segregation and mixing of granular materials in a 3D-blender by NMR imaging investigation. Powder Technol 2004; 141: 55-68.
25. Broadbent CJ, Bridgewater J, Parker DJ. The effect of fill level on powder mixer performance using a positron camera. Chem Eng J 1995; 56: 119-125.
26. Lai FS, Fan LT. A study on the mixing of flour in a motionless Sulzer (Koch) mixer using a radioactive tracer. Powder Technol 1976; 13: 73-83.
27. Tily P, Porada S, Scruby C, Lidington S. Monitoring of mixing processes using acoustic emission. In: Harnby N, Benkreira H, Carpenter K, Mann R, eds. Fluid Mixing III Rugby: The Institute of Chemical Engineers 1988; 75-94.
28. Allan P, Bellamy L, Nordon A, Littlejohn D. Non-invasive monitoring of the mixing of pharmaceutical powders by broadband acoustic emission. Analyst 2010; 135: 518-524.
29. Crouter A, Briens L. Passive acoustic emissions from particulates in a V-blender. Drug Dev Ind Pharm 2015; 11: 1809-1818.
30. Crouter A, Briens L. Monitoring lubricant addition using passive acoustic emissions in a V-blender. Powder Technol 2016; 301: 1119-1129.
31. Müller P, Böttcher R, Russell A, M Trüe M, Aman S, Tomas J. Contact time at impact of spheres on large thin plates. Adv Powder Technol 2016; 27(4):1233-1243.

32. Jackson, R.L., Green I, Marghitu D.B. Predicting the coefficient of restitution of impacting elastic-perfectly plastic spheres. Nonlinear Dyn 2010; 60: 217.

33. Marinack M, Musgrave R, Higgs C. Experimental investigations on the coefficient of restitution of single particles. Tribology Transactions 2013; 56(4), 572-580.

34. Daubechies I. The wavelet transform, time-frequency localization and signal analysis. IEEE Trans Inf Theory 1990; 36: 961-1005.

35. Sondergaard R, Chaney K, Brennen C. Measurements of spheres bouncing off flat plates. J Appl Mech 1990; 112(3): 694-699.

36. Aguiar C, Laudares F. listening to the coefficient of restitution and the gravitational accerleration of a bouncing ball. Am J Phys 2003; 71: 499-501.

Chapter 5

5   Monitoring Lubricant Addition in Pharmaceutical Tablet Manufacturing through Passive Vibration Measurements in a V-blender

Publication status: A version of this chapter is to be submitted for publication in *Powder Technology*.

5.1   Introduction

Oral solid dosage pharmaceuticals, particularly tablets are the preferred dosage method due to convenience for consumers and ease of manufacturing. In solid dosage manufacturing, particle properties are determined within and between each stage of the manufacturing process. Differences in particle size, density, shape, and surface morphology of the ingredients can ultimately affect the final tablet properties and must be monitored and controlled to ensure production of tablets with uniform weight and consistent, reproducible properties.

The final mixing step is critical to ensure specified tablet properties. A lubricant is added prior to tablet compression to ensure the tablet is ejected from the press smoothly without sticking or breakage. The lubricant decreases friction between the tablet surface and the die wall. This is achieved most commonly through a boundary lubrication mechanism (1). In boundary lubrication, lubricant particles form layers between surfaces and interfaces of the excipients and the tablet die. Magnesium stearate is the most common boundary lubricant and is used since it has a high lubricant efficiency, is inexpensive, and chemically stable (2). It has been proposed that magnesium stearate first fills cavities in surface irregularities of granules before forming a semi-continuous layer on the surface of the granules (2,3). This in turn makes granules smoother and more regular shaped decreasing contact area. The reduction in contact points of granules and the tablet press die allow for tablets to be ejected smoothly.

Lubricants are usually added using a tumbling mixer such as the V-blender. A V-blender is composed of a shell with two arms connected at angles ranging from 75-90° and mounted on a rotating axle. The V-blender relies on gravity to provide effective

incorporation of the magnesium stearate, while preventing attrition and breakage of granules. Gravity driven mixing can cause trajectory segregation which can lead to variation within tablet weight uniformity (4-6). Large differences in particle size, density, and distribution width from the granulation stage cause heavier, more dense particles to fall faster within the mixer and separate from their smaller or lighter counterparts. Material flow into the tablet press is then preferential to larger particles resulting in differences in tablet weight and content uniformity. Segregation is also experienced in the primary sampling methods through thief probes leading to non-representative samples and misleading results (7-10). Segregation is more likely to occur with free-flowing particles, a primary function of particle size and shape (11,12). As lubricants improve flowability (3,13,14), mixtures are more susceptible to segregate during lubricant addition. In addition to contributing to segregation, particle size also affects tablet hardness. Larger particles have a smaller surface area compared to smaller particles resulting in less contact points and friction between particles, effectively decreasing tablet compressibility and hardness (15). Particle size and distribution should then be optimized to ensure proper lubricant dispersal, minimize segregation effects, and obtain tablets with desirable final properties.

Final tablet properties are affected by lubricant dispersal. Due to its hydrophobic nature, magnesium stearate negatively affects dissolution and disintegration time as a function of mixing time and concentration (16,17). With increases in concentration and mixing time, particles have a more complete coverage of magnesium stearate, increasing particle hydrophobicity. In addition, tablet hardness is negatively affected with mixing time and magnesium stearate concentration (18-20); due to its ability to reduce contact area, particle-particle bonding is decreased with magnesium stearate resulting in brittle tablets. It is then critical to optimize lubricant concentration and mixing time, as magnesium stearate is only effective in small amounts and magnesium stearate layers are difficult to disrupt once formed (13,19).

To monitor, control, and optimize pharmaceutical mixing processes, process analytical techniques (PAT) are being developed. PAT include systems that implement sensors to monitor and detect changes real time in manufacturing processes with the aim of

increasing product quality and efficiency while removing issues associated with extractive sampling (21). PAT to determine uniformity and homogeneity within mixing include near infrared spectroscopy (NIR) (22-24), Raman spectroscopy (25-27), magnetic nuclear resonance imaging (MRI) (28-30), and radioactive tracers (31-33). More recently, passive acoustic emissions or passive vibration measurements have been developed and investigated as they are completely non-invasive, non-destructive, and have a lower capital cost compared to other methods (34).

Vibrations from acoustic emissions within mixers are created due to particle-equipment and particle-particle collisions and are responsive to a variety of process changes. Crouter and Briens characterized acoustic vibrations in a V-blender filled with sugar spheres. Particle size, mixer scale, and mixer fill level all affected measured vibrations due to changes in momentum and mass (35). In addition, it was determined that moisture affects signals directly through changes in mass, and indirectly through changes in flow behaviour as shown with wooden beads and granule formulations (36). The differences in produced vibrations due to differences in particle properties can allow for the direct monitoring of mixing processes. Allan *et al.* recorded acoustic vibrations in a convective blender when mixing aspirin into Avicel. The impeller speed and particle mass affected measured signals. It was found that the signal increased and approached a plateau as the mixture became more homogenous (37).

Preliminary research has been conducted to monitor lubricant addition using acoustic vibrations. Crouter and Briens monitored magnesium stearate dispersal in sugar spheres and granule formulations in a tumbling V-blender (38). Measured vibrations decreased as the magnesium stearate became incorporated into the sugar spheres. Lubricant dispersal was more difficult to monitor with the granule formulations, but became more distinct with increasing amounts of magnesium stearate. Cameron and Briens monitored and assessed mixing performance of magnesium stearate into glass beads in a V-blender (39). It was found that axial loading configurations and increased fill levels inhibited mixing performance. Lubricant addition is a complex function of V-blender mixing mechanisms, particle properties, flow, and lubricant properties as outlined by the literature. Due to lack

of research and complexity, further process knowledge and optimization of monitoring methods is required.

This study aims to further evaluate passive vibration measurements as an inline monitoring method for lubricant addition to pharmaceutical granules varying in size and distribution properties. The results obtained can then detect particle properties and changes in mixing in real time and, with incorporation into a process control system, shows that the method has the potential to increase manufacturing efficiency.

5.2   Materials and Methods

5.2.1   Particles

Glass beads (Propper) with diameters of 1, 2, and 3 mm were used as model particles in selected comparison trials.

Granules were prepared using a Niro Pharma Systems PMA high shear granulator in 1.5 kg batches. The impeller and chopper speed were constant at 700 and 1000 rpm during 2 minutes of dry mixing of excipients, 8-10 minutes of water addition (12 mL/min), and 2-3 minutes of wet massing. The formulation composition is listed in Table 5.1. Granules were tray dried at 24 °C for 24 hours to ensure that the moisture content was below 2 wt % as measured by a Mettler-Toledo HG63 halogen moisture analyzer.

Table 5.1: Granule formulation composition

Supplier	Particle	Quantity (wt %)
Alfa Aesar	Mannitol	57
FMC Biopolymer	Avicel (MCC)	36
Shin-Etsu Chemical Co.	Pharmacoat 603 (HPMC)	5
Alfa Aesar	Croscarmellose Sodium	2

Granules were intentionally under and over granulated to obtain batches that were categorized as small, medium, and large relative to one another in size. The size distributions of the granules were determined by sieving using standard sieve sizes ranging from 300 µm to 6.3 mm. To investigate the effect of large particles within a

distribution on the measured vibration amplitudes, particles were combined to make composite batches with asymmetrical particle size distributions. The asymmetry was characterized through the skewness, defined as:

$$sk = \frac{n}{(n-1)(n-2)} \Sigma \left(\frac{x_i - \bar{x}}{s}\right)^3 \qquad \text{(eq. 5.1)}$$

where n is the number of sieved fractions in a particle batch, $\bar{x}$ is the average particle batch diameter, and s is the particle batch standard deviation (40). The properties of the particles are summarized in Table 5.2. The particle size distributions are provided in Figures 5.1-5.4.

Table 5.2: Particle properties

Batch Label	Particle Type	Particle Density (g/cm^3)	Particle Sphericity (-)	dp$_{50}$ (mm)	sk (-)
GR1	Under granulated	0.7		0.84	1.0
GR2	Optimal Granules	1.5		1.13	0.7
GR3	Over Granulated	1.3	~ 0.7	3.42	0.5
GR4	Granule composite 1	1.6		1.28	1.5
GR5	Granule composite 2	1.0		1.9	1.7
GS1	Small glass beads	2.5		1	0
GS2	Medium glass beads	2.5		2	0
GS3	Large glass beads	2.5	~ 1	3	0
GS4	Glass composite 1	2.5		1.75	-5.1
GS5	Glass composite 2	2.5		2.25	5.1
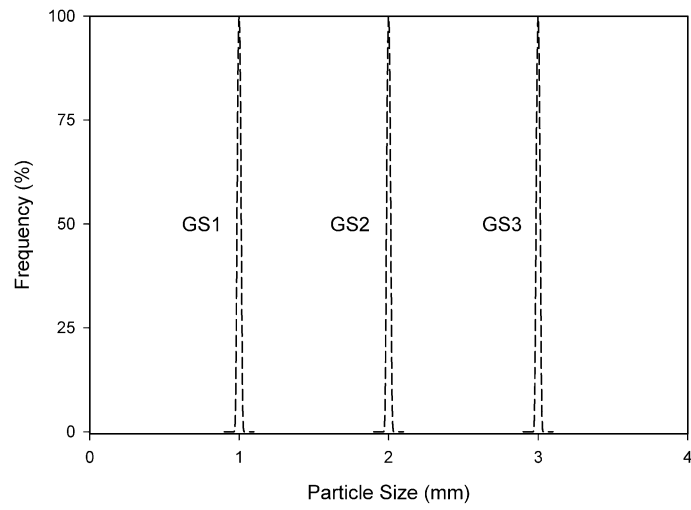
Figure 5.1: Glass beads size distribution
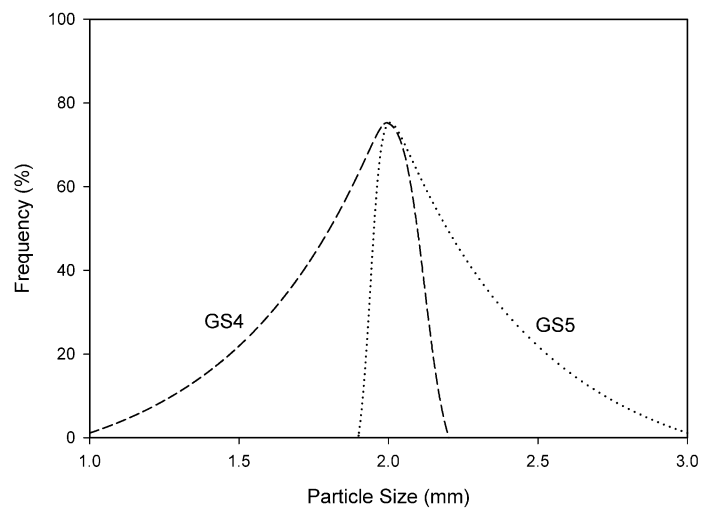
Figure 5.2: Composite glass beads size distribution
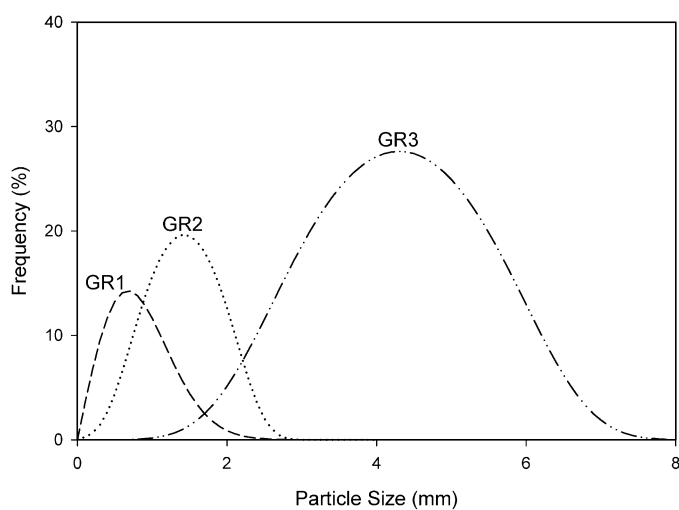
Figure 5.3: Granules size distribution
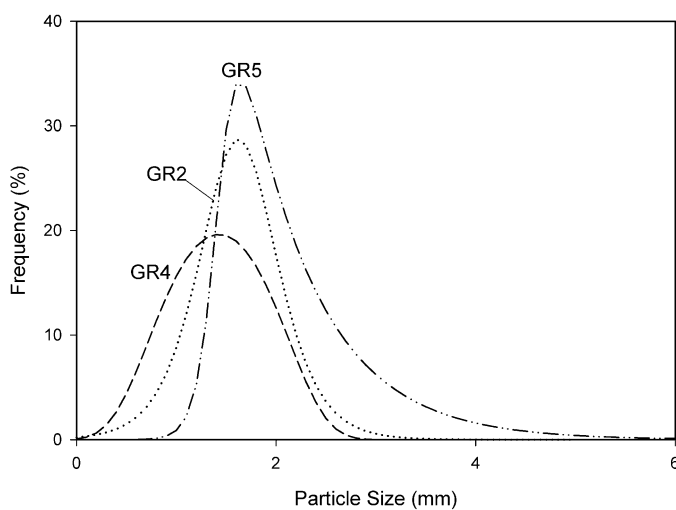
Figure 5.4: Composite granules size distribution

5.2.2   V-blender and Mixing

Trials were conducted in an 8 Qt (7.6 L) stainless steel Patterson-Kelly V-blender rotating at a fixed speed of 25 rpm. The V-blender was filled to 25 % of its working volume with granules or glass beads. Magnesium stearate (Alfa Aesar) was loaded in a uniform layer on top of the granule bed, for the specified amount of 1, 2, 5, or 10 wt %. Solids were mixed for 125 revolutions (5 minutes) within the V-blender.

5.2.3   Sensor and Data Acquisition

Vibrations were measured and recorded using a PCB Piezotronics accelerometer (model 353B34) with a frequency range of 0.35-12,000 Hz combined with an ICP signal conditioner (model 480E09). The accelerometer was securely attached to the left V-blender lid using adhesive wax at a radial position of r/R = 0.74 (Figure 5.5). Signals were captured at an acquisition frequency of 40,000 Hz using Labview 8.5 with a National Instruments DAQ-6036E card. To focus on particle-lid collisional vibrations, background oscillations resulting from the motion of the shell were removed using a multilevel wavelet filter based on a 6 tap, high pass, Daubechies wavelet decomposition filter (41). Data analysis was performed in MATLAB.
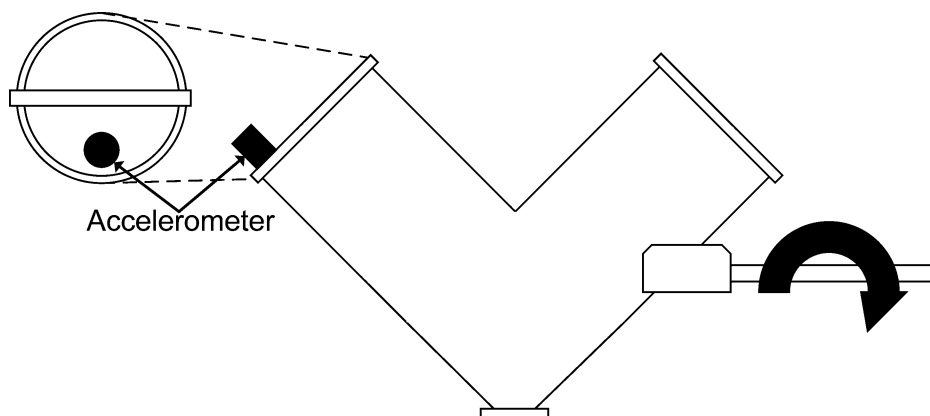
Accelerometer

Figure 5.5: V-blender with accelerometer location and axis of rotation

5.2.4   Coefficient of Restitution

The coefficient of restitution was estimated using individual glass bead and granule drop tests. Glass beads and granules were dropped onto the supported V-blender lid (3.1 mm in thickness) from a height of 11.1 cm. The accelerometer was attached to the V-shell lid and vibrational amplitudes recorded. Trajectories of granule drops were recorded using a high-speed camera. Each trial was repeated for a total of 15 times. The coefficient of restitution was determined using the time between successive peak amplitudes as particles rebounded as measured by the accelerometer and the particle rebound height as measured by the high-speed camera.

5.2.5   Particle Surface Morphology

Scanning electron microscope (SEM) images of granules and glass beads were taken using a Hitachi SU8230 Regulus Ultra-High-Resolution Field Emission scanning electron microscope. Particles were mounted on a plate using carbon adhesive discs before analysis. For particles with excessive amounts of magnesium stearate, conductive carbon paint was used for mounting. Images allowed for surface morphology of the particles to be examined to determine differences before and after mixing with increasing amounts of magnesium stearate.

5.3   Results

As the V-blender shell rotates, solids motion within the shell results in particle-particle and particle-equipment collisions producing vibrations which are measured by the sensor. Related to solids motion within the V-blender, three features were observed: Feature 1 corresponds to vibrations created by particles colliding with the V-shell lid upon inversion of the shell, Feature 2 is related to vibrations due to particles sliding along the shell wall, and Feature 3 is produced when particles recombine and impact the bottom plate (Figure 5.6). Since Feature 1 is the most distinctive and revealed the most process information (36,38,39), only Feature 1 vibrations were reported.
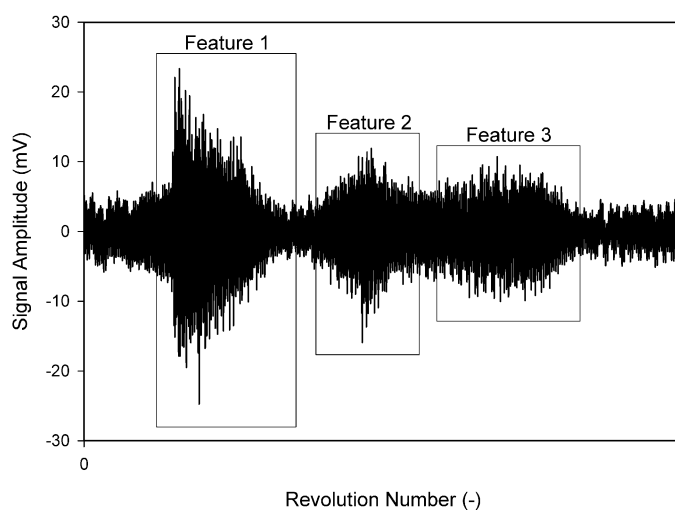
Figure 5.6: Filtered signal of medium granules (GR2) related to particle motion

Particles were added to the V-blender at a fixed working volume of 25 %. Unmixed particles were tumbled in the V-blender for 20 revolutions and vibrational amplitudes recorded to create a baseline mean with a corresponding standard deviation of Feature 1 amplitudes. Magnesium stearate at 1 wt % was then added and mixed with the granules or the glass beads. Vibrational measurements were recorded for the duration of mixing (Figure 5.7). Feature 1 signal amplitudes were initially high at the baseline mean and then began to decrease as the magnesium stearate was incorporated into the bed of particles. The measured vibrational amplitudes continued to decrease until the amplitudes approached a relatively stable plateau indicating a mixing end-point at approximately 5 revolutions for the 2 mm glass beads (GS2) and 25 revolutions for the medium granules (GR2).
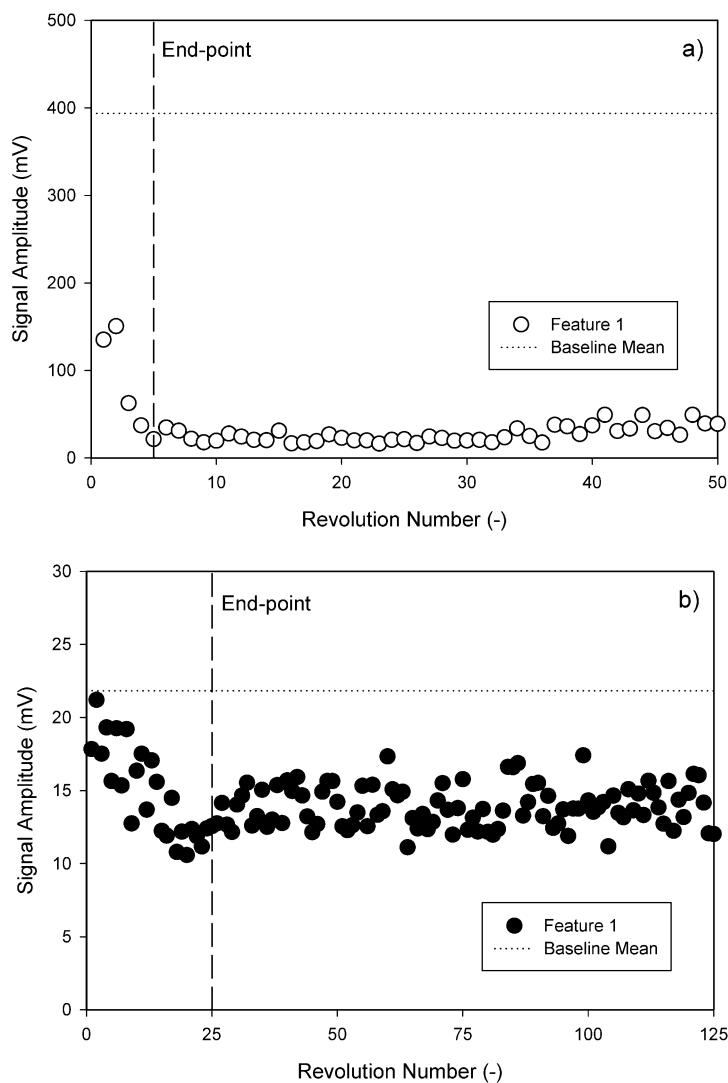
Figure 5.7: Feature 1 amplitudes of a) 2 mm glass beads (GS2) and b) medium granules (GR2) mixed with 1 wt % MgSt

The glass beads and the granules were then mixed with increasing amounts of magnesium stearate. The results were similar to the mixing profiles obtained with 1 wt % magnesium stearate: the vibration measurements decreased to an approximately stable plateau that allowed a mixing end-point to be identified. With increasing magnesium stearate amounts, the magnitude of the end-point vibrational amplitudes decreased. Although the vibrational amplitudes of the unmixed glass beads and granules were very different, when mixed with more than 2 wt % magnesium stearate, the measured amplitudes became very similar as shown in Figure 5.8.
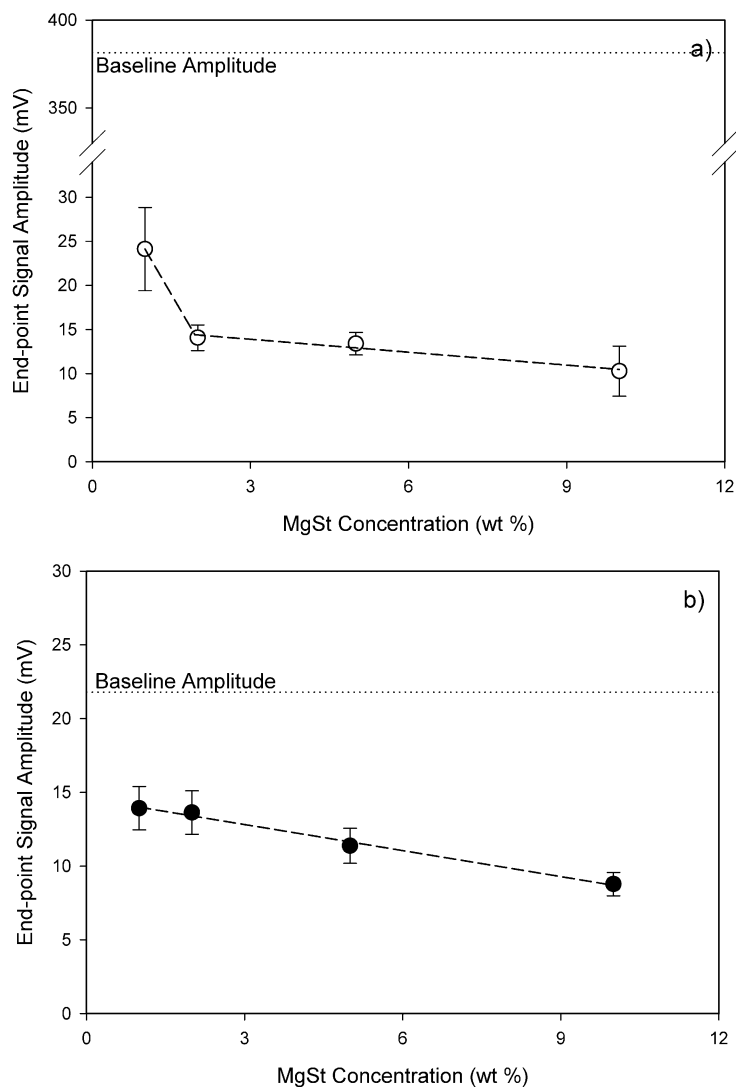
Figure 5.8: Feature 1 end-point signal amplitudes of a) 2 mm glass beads (GS2) and b) medium granules (GR2) mixed with 1 - 10 wt % MgSt; ± 1 standard deviation

SEM images were taken to visualize the interactions of the magnesium stearate with the particles (Figure 5.9). The uncoated granules were irregularly shaped with many surface asperities. Magnesium stearate particles began to fill surface irregularities before adhering to the other surfaces of the granule thereby creating a particle with an overall more uniform and smoother surface with increasing amounts of magnesium stearate. Glass beads were smooth and spherical. With the introduction of magnesium stearate, magnesium stearate particles adhered to the surface of the glass beads. With increasing amounts of magnesium stearate, the magnesium stearate layer become more uniform and

complete, forming a near continuous layer between 2 and 5 wt %. Beyond 5 wt %, the magnesium stearate layer was complete and began to increase in thickness.

MgSt (wt %)	Glass Bead (GS2)	Granule (GR2)
0		
1		
2		
5		
10		
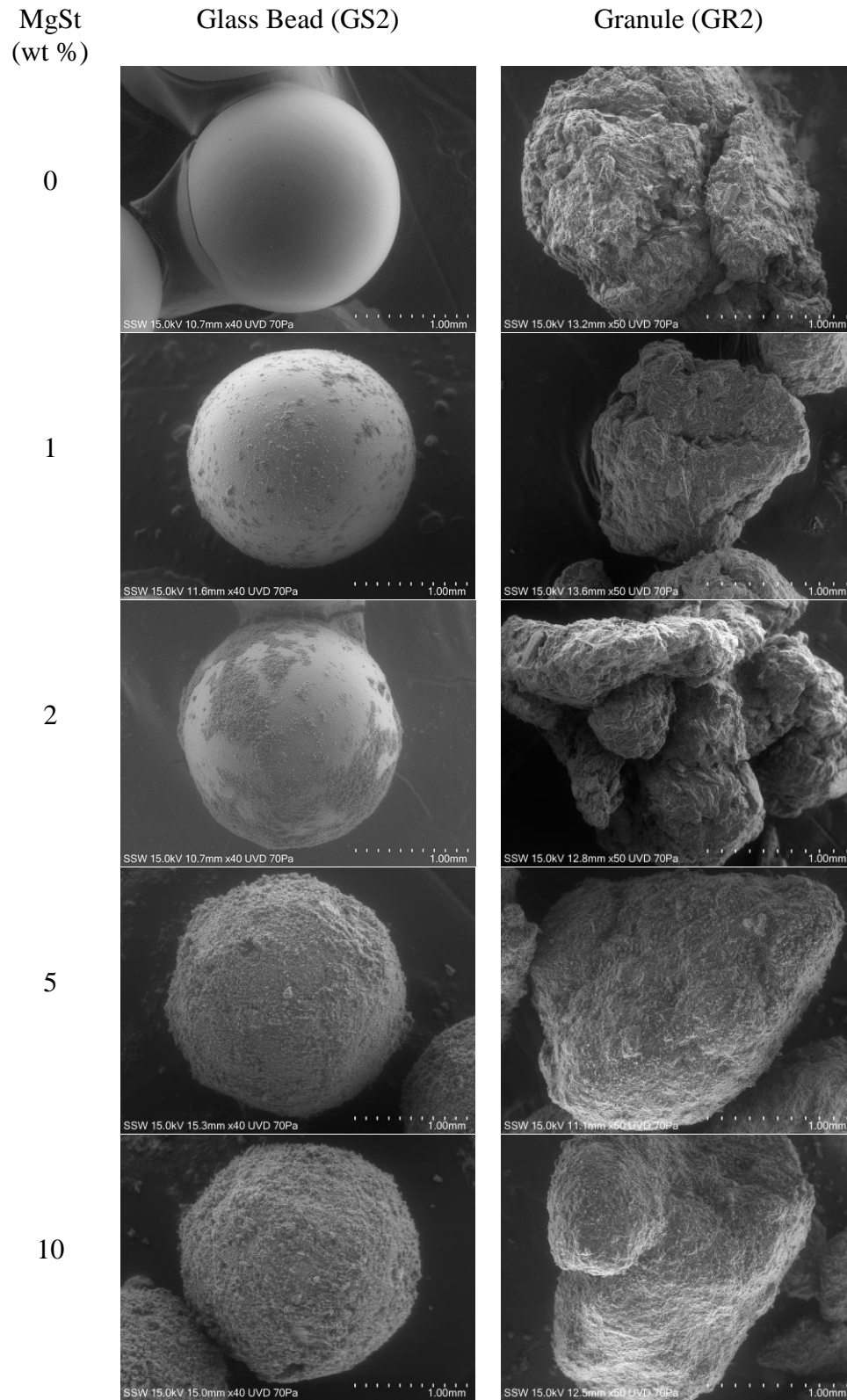
Figure 5.9: SEM images of glass beads and granules mixed with increasing amounts of MgSt

Glass beads of 1, 2, and 3 mm diameters (Figure 5.1, Table 5.2) were mixed with 2 wt % magnesium stearate. As shown in Figure 5.10, the measured signal amplitude and its variation increased with particle size. In addition, the mixing end-point also increased with particle size from about 2 revolutions for the 1 mm glass beads to about 6 revolutions for the 3 mm glass beads.

Granules were under and over granulated to vary the average particle diameters as shown in Figure 5.3 and summarized in Table 5.2. These granule batches were then mixed with 2 wt % magnesium stearate and their vibration measurements recorded (Figure 5.10). As with the glass beads, the measured amplitude and its variation along with mixing end-point increased with increasing particle size for granule batches. For the batch of large granules (GR3), the variation in the measured amplitudes was large enough that a mixing end-point could not be easily and reliably identified.
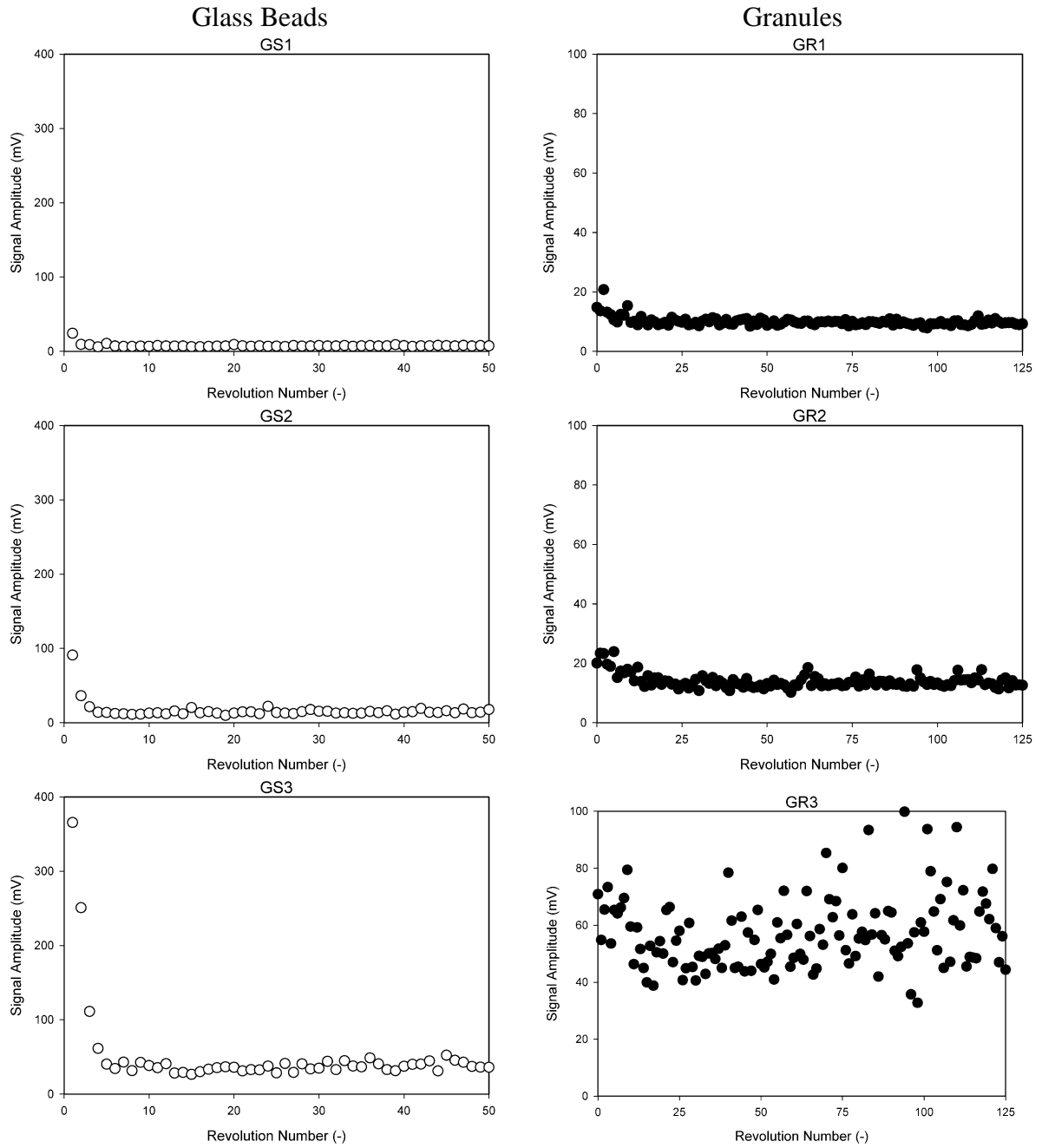
Figure 5.10: Effect of increasing average particle diameter on granule and glass beads mixed with 2 wt % MgSt

The size distribution was varied by creating composite batches of particles. These composite batches are shown in Figures 5.2 and 5.4 and summarized in Table 5.2. The composite batches were mixed with 2 wt % magnesium stearate and the measured vibration profiles compared to either the 2 mm glass beads or the medium sized granules (Figures 5.11 and 5.12). Signal amplitudes and variations increased as the fraction of larger particles in the distribution was increased as indicated by positive large skewness numbers. For a granule distribution containing a large fraction of large granules (GR5 with sk = 1.7), the scatter in the measured vibration amplitudes made it difficult to reliably and easily identify a mixing end-point.
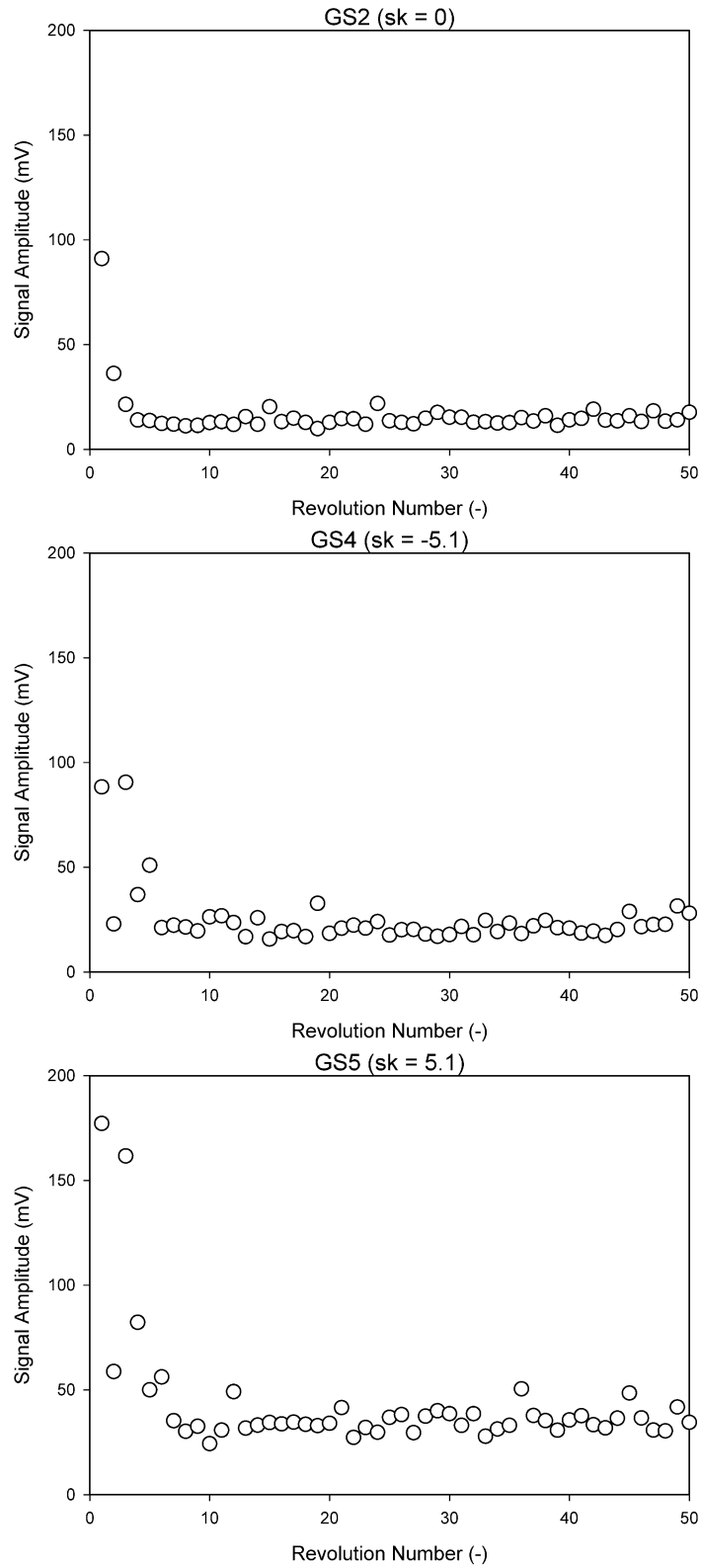
Figure 5.11: Effect of size distribution properties on glass beads mixed with 2 wt % MgSt
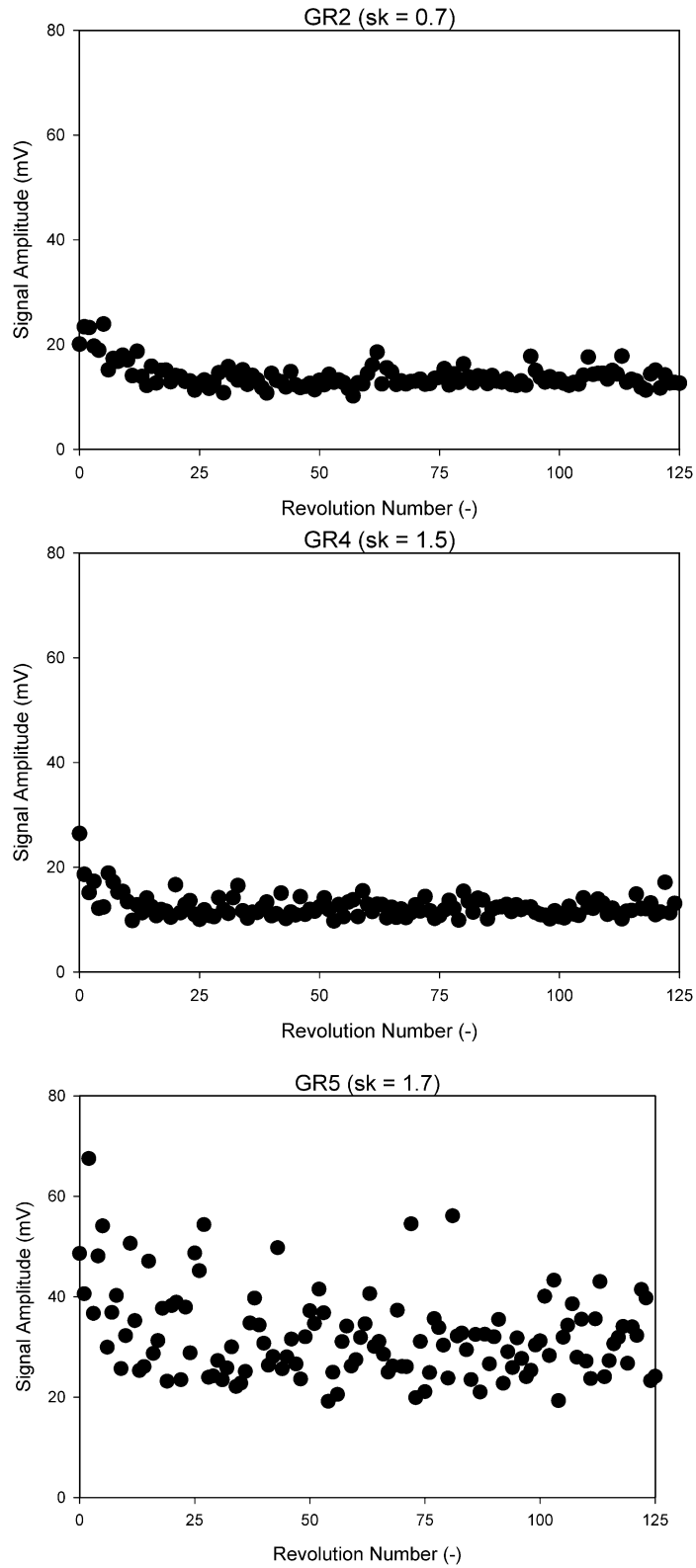
Figure 5.12: Effect of size distribution properties on granules mixed with 2 wt %

MgSt

Average end-point signal amplitude values and standard deviation of each mixing trial were compared (Figure 5.13). For glass beads, the average amplitudes and standard deviation were assessed for the last 25 revolutions (1 min) of 50 revolutions (2 min) mixing trials. For granules, the average amplitudes and standard deviation were assessed for the last 50 revolutions (2 minutes) of 125 revolutions (5 min) mixing trials. The signal amplitudes and corresponding standard deviations both increased with average particle size. The composite batches were influenced by the large particles within their distribution, but the large particles did not completely dominate the measured signal as the measured amplitudes of the composite batches did not equal those of the large particle batches (GS5 vs. GS3 and GR5 vs. GR3).
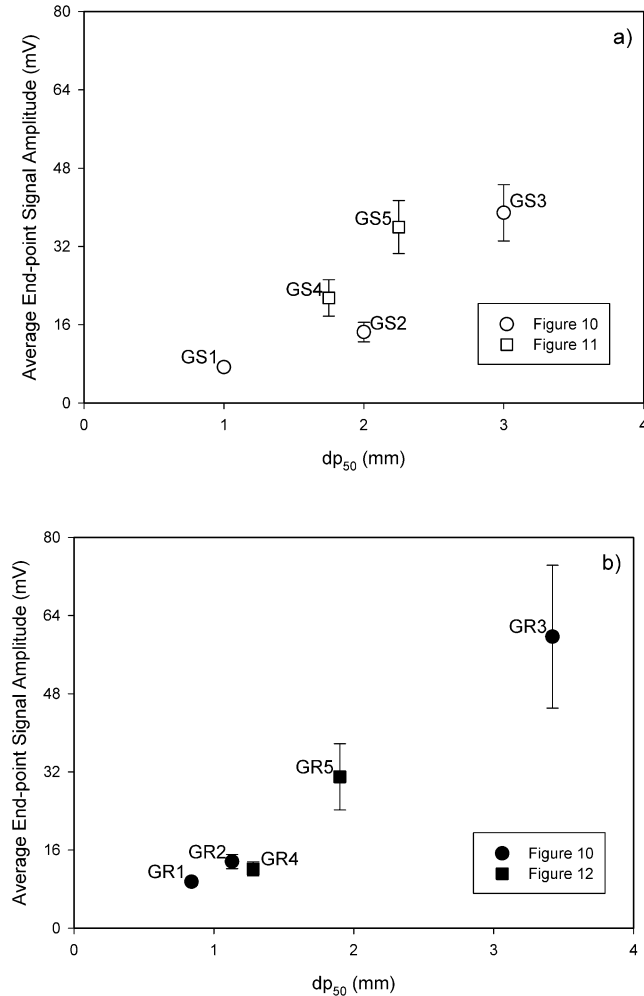
Figure 5.13: Average end-point signal amplitude of glass beads and granules; ± 1 standard deviation

The coefficient of restitution was measured for the 2 mm glass beads (GS2) and medium sized granules (GR2) before and after mixing with 1 wt % magnesium stearate. The coefficient of restitution decreased with the introduction of magnesium stearate for the glass beads but was difficult to measure for the granules as shown in Table 5.3.

Table 5.3: Coefficient of restitution of glass beads and granules

MgSt Concentration (wt %)	Particle Type	
	Glass (GS2)	Granule (GR2)
0	0.69 ± 0.048	< 0.2
1	0.57 ± 0.085	< 0.2

5.4 Discussion

Due to the inherent geometry of the V-blender, particle motion can be separated into two distinct phases: the separation phase as the V-blender inverts from 0 - 180°, and the recombination phase from 180 - 360° in motion. As particles collide with one another and the V-shell itself at each phase of motion, kinetic energy is transferred through propagating vibrations which are recorded by the accelerometer, producing three distinct features, as shown in Figure 5.6.

Feature 1 arises when the V-blender is completely inverted, forcing particles to separate into both arms of the V-shell, impacting each lid of the V-shell. Here, particles fall long distances impacting the lids at high velocities and high kinetic energies. Upon impact, stress waves propagate through the lids creating vibrations measured by the accelerometer that is attached to the one lid. Attenuation is minimized as the transmission distance from impact to the accelerometer is short resulting in large measured vibrational signal amplitudes.

Feature 2 vibrations are created in the intermediate phase of motion between the upright and inverted positions of the V-shell, due to the sliding and rolling motion along the side of the V-shell wall. Particles still impact the V-shell, however, at low velocities as particle motion is impeded by the bulk mass. In addition, vibrations are significantly

attenuated as vibrations must travel up the shell wall before reaching the accelerometer attached to the lid resulting in low measured amplitudes.

Feature 3 vibrations occur when the V-shell is fully upright, where particles recombine and collect at the bottom of the V-blender, impacting the bottom of the V-shell. Similar to Feature 1, the particles fall at large trajectories and high velocities; the corresponding measured signal should be large; however, the signals are significantly attenuated. The vibrations must propagate first through a rubber gasket attached to the bottom of the V-shell, up the sides of the shell before reaching the lid. In addition, due to the geometry of the V-shell, the bulk mass of particles impacts the shell wall rather than the bottom plate, resulting in additional energy loss due to the non-normal component at the inclined surface into the V-shell wall. As Feature 1 vibrations were most distinctive and revealed the most information about particle behaviour (Figure 5.6), only Feature 1 was considered for further analysis.

The measured Feature 1 vibrations are significantly dependent on the mechanisms of energy dissipation to the accelerometer. When a particle impacts the lid of the V-shell, it elastic-plastically deforms. As no fractures or breaks were visible after drop tests, it was assumed that impact velocities did not exceed the critical yield stress of the particles. Upon impact, most of the kinetic energy of a particle was dissipated through stress wave propagation in the form of vibrations which were directly measured by the accelerometer. A portion of the energy was retained by the particle which can be estimated by the coefficient of restitution.

Conventionally, the coefficient of restitution is measured through individual particle drop tests and recording the height of rebound and energy upon impact to model energy loss. The coefficient of restitution of the glass beads was relatively easily measured using this method, approximately 0.7 for unmixed glass beads. However, for non-spherical granules, based on visual observations, upon impact they rotated and rolled, and the coefficient of restitution was difficult to measure (42). As well, due to their relatively low density and mass, the recorded dissipated energy of individual granules was small. This implies that the rotational energy of the granules was much greater than the stored elastic

energy resulting in a very low coefficient of restitution (< 0.2). Since glass beads have a much higher coefficient of restitution, collisions with glass beads are much more elastic than granules, with glass beads retaining most of their energy after impact with the V-shell lid. In addition, as glass beads have a higher density than granules, the measured vibrations for glass beads are also much higher.

With the addition of magnesium stearate, the magnesium stearate particles began to adhere to the glass beads or granules. For the smooth glass beads, the magnesium stearate particles immediately started to form a layer that became more uniform and complete, becoming thicker with the addition of even more magnesium stearate (Figure 5.9). For the granules, the magnesium stearate first began filling nay surface irregularities before starting to form a layer around the granule. The layer of magnesium stearate around the particles for both glass beads and granules altered the particle surface properties, making collisions more inelastic, where energy was dissipated into the magnesium stearate layer. This is reflected in the coefficient of restitution of unmixed and lubricated glass beads, where the coefficient of restitution decreased from approximately 0.7 to 0.6. The energy available and dissipated as vibrations was lower with corresponding lower measured vibrational amplitudes (Figure 5.7).

With mixing, the magnesium stearate particles become dispersed into the bed of glass beads or granules and the layer of magnesium stearate on a given individual particle becomes more complete and uniform. More energy is dissipated into this magnesium stearate layer upon collision and the measured vibrational amplitudes continue to decrease. The measured vibrational amplitudes reached approximately stable values when the magnesium stearate was completely dispersed into the particle bed and formed a layer around particles. The mixing time or shell revolution number at which the measured vibrational amplitude becomes approximately stable is therefore considered an optimal mixing end-point and can be identified through passive vibrations (Figure 5.7).

Figure 5.7 shows some differences in the amplitude profiles for the glass beads and granules. The optimal mixing time for the glass beads was significantly lower than the time for the granules. The magnesium stearate particles first start to fill any surface

irregularities before forming a layer around the granules (Figure 5.9). This dispersion takes a significant amount of mixing time to allow for the magnesium stearate particles to transfer between particles. In contrast, for the glass beads, the magnesium stearate layer begins to form on the particles immediately and dispersion happens readily through particle-particle contact (Figure 5.9). As shown in Figure5. 7, the optimal mixing time with 1 wt % magnesium stearate for medium sized granules (GR2) was about 25 revolutions compared to 5 revolutions for the glass beads (GS2).

Figures 5.7, 5.8, and 5.10 also indicate that the measured amplitudes of the unmixed glass beads were much higher than the amplitudes of the unmixed granules. This difference reflects the higher density of the glass beads. The kinetic energy of a glass bead just before collision with the V-shell lid was higher than a granule resulting in more energy dissipated as vibration (35) and therefore higher measured amplitudes.

Figure 5.8 indicates that the measured vibration amplitudes of the glass beads and granules completely mixed with magnesium stearate were similar for magnesium stearate concentrations above 2 wt %. This indicates, that upon collision, a significant amount of energy is dissipated into the magnesium stearate layer, having only small amounts retained by the particles and dissipated as vibrations. The relative amount dissipated into the magnesium stearate layer of the glass beads is larger than for granules as the layer would be more complete, uniform, and thicker as all magnesium stearate particles would contribute to the layer formation without a need for first filling surface asperities (Figure 5.9). The decrease in measured amplitudes from unmixed to completely mixed with magnesium stearate was therefore larger for glass beads than granules.

Figures 5.7, 5.8, and 5.10 indicate that measured vibrational amplitudes are significantly affected by particle size. Figure 5.10 indicates further differences between the glass beads and granules, which were attributed to particle size and property distributions. The glass beads were almost spherical and mono size (Figure 5.1) with a constant particle density of 2.5 g/cm^3. The low signal amplitude plateau indicating adequate mixing of the magnesium stearate into the bed of glass beads was almost constant and with little deviation thereby allowing the optimal mixing end-point to be easily identified. As

shown in Figure 5.3 and summarized in Table 5.2, for the granules, there was always a distribution of sizes and properties.

The small, medium, and large sized granule batches were created by granulating for different times. In high shear granulation, granule growth and development relies on coalescence through collisions, attrition, and further collisions also promoting consolidation and densification. Stopping the granulation early resulted in small sized granules that had relatively low densities due to shorter times for consolidation and densification. Stopping the granulation at the expected end-point produced granules with a mean diameter of about 1 mm and larger density of 1.5 g/cm^3. Overgranulation produced larger granules with a density of about 1.3 g/cm^3, very close to the density of the medium sized granules. Figure 5.10 shows significant differences in measured vibrational amplitudes for the small, medium, and large granules. For the small and medium sized granules, the measured amplitudes were initially high and then decreased with the introduction of the magnesium stearate. Mixing end-points could be identified at about 17 and 22 revolutions for the small and medium granules, respectively. The overgranulated batch had a wide distribution of sizes and with many large granules over 3 mm (Figure 5.3). The measured signal amplitudes were high, as expected. However, identification of a mixing end-point was almost impossible as the scatter in the amplitudes was significant.

Figure 5.10 also indicates that the mixing time increased with particle size. For the glass beads, it increased from 2 to 4 to 6 revolutions as the size increased from 1 mm to 2 mm to 3 mm in diameter. For the granules, it increased from 17 for the small sized batch (GR1) revolutions to 22 revolutions for the medium sized batch (GR2). Small particles have a large surface area which provide more contact opportunities that allow the magnesium stearate flakes to adhere to the particles and transfer between particles for dispersion (39), resulting in lower required mixing times.

To further investigate the effect of large particles within a distribution on the measured vibration amplitudes, batches were combined to make composite batches with asymmetrical particle size distributions. The composite batches are shown in Figures 5.2

and 5.4 and are summarized in Table 5.2 including estimates of the skewness. Larger positive skewness values indicate the greater the fraction of large particles in the batch. Figure 5.11 shows the effect for glass beads of incorporating more 3 mm beads into the batch on the measured signal amplitude. The measured amplitude, the optimal mixing time, and the scatter in amplitudes of the composite batches increased. The effect of the addition of large particles was even more pronounced for the granules, as shown in Figure 5.12. For the granule batch with a skewness of 1.7, a significant fraction of granules were larger than 2 mm. The measured signal amplitudes decreased with the introduction of magnesium stearate, but low and stable amplitudes were not observed even after mixing for extended times and an optimal mixing end-point could not be reliably identified.

Particle segregation based on size can occur as particles tumble in the rotating V-shell due to a trajectory segregation mechanism. Air drag during free fall has a larger effect on small particles compared to large particles (6). The large particles will therefore reach and impact the lid first and with high velocities and kinetic energies resulting in dissipation of large vibrations leading to large measured amplitudes by the accelerometer attached to the lid. Small particles fall with lower velocities and may not impact the lid directly, but the layer of large particles now resting on top of the lid. The measured vibration amplitudes from these smaller particle collisions will be low due to the lower energy available for dissipation and attenuation through the particle layer to the lid with attached accelerometer. As shown in Figure 5.6, there is a window with fluctuations in the signal amplitudes that contribute to Feature 1. The information extracted from Feature 1 was the average of three largest amplitudes. This information has been shown to provide information about particle movement with respect to radial versus axial mixing, optimal shell loading capacity, fill level, particle size, particle density, moisture, and the effect of increasing magnesium stearate amounts on mixing (35, 36, 38, 39). Particles with wide size distributions containing significant fractions of large particles may benefit from alternative signal analysis to extract more process information from passive vibrations of a V-blender. It is noted, however, in practice these size distributions are unlikely to be encountered.

5.5 Conclusions

Passive measurements of vibrations created by particle movement in a V-blender were measured using an accelerometer attached to the lid of the V-shell for glass beads and granule formulations. The measurements showed that glass beads required less mixing time compared to granules due to differences in magnesium stearate interactions with the surface of the particles. Magnesium stearate alters the properties of particles making collisions more inelastic. This alteration allows for the potential of using vibration measurements to monitor mixing of magnesium stearate and identification of a mixing end-point with changes in particle type, size and distribution, and lubricant concentration. Ideally, particles should have an optimal size range and distribution width as segregation and particle size can lead to negative effects on tablet strength and weight uniformity. In addition, magnesium stearate should be mixed just until a desired uniformity is reached as overmixing has negative effects on final tablet properties. Inline monitoring of lubricant dispersal would then lead to improved control of the mixing process.

5.6 References

1. Wang J, Wen H, Desai D. Lubrication in tablet formulations. Eur J Pharm Biopharm 2010; 75: 1–15.
2. Perrault M, Bertrand F, Chaouki J. An investigation of magnesium stearate mixing in a V-blender through gamma-ray detection. Powder Technol 2010; 200(3):234–45.
3. Morin G, Briens L. The effect of lubricants on powder flowability for pharmaceutical application. AAPS PharmSciTech 2013;14(3): 1158-1168.
4. Arratia PE, Duong N, Muzzio FJ, Godbole P, Reynolds S. A study of the mixing and segregation mechanisms in the Bohle Tote blender via DEM simulations. Powder Technol 2006; 164(1): 50-57.
5. Alexander A, Shinbrot T, Johnson B, Muzzio FJ. V-blender segregation patterns for free-flowing materials: effects of blender capacity and fill level. Int J Pharm 2004; 269(1): 19-28.
6. Alexander A, Muzzio FJ, Shinbrot T. Segregation patterns in V-blenders. Chem Eng Sci 2003; 58(2): 487-496.
7. Deveswaran R, Bharath S, Basavaraj BV, Abraham S, Furtado S, Madhavan V. Concepts and techniques of pharmaceutical powder mixing process: A current update. Research J Pharm Tech 2009; 2: 245-249.
8. Muzzio FJ, Goodridge CL, Alexander A, Arratia P, Yang H, Sudah O, Mergen G. Sampling and characterization of pharmaceutical powders and granular blends. Int J Pharm 2003; 250: 51-64.
9. Garcia T, Wilkinson S, Scott J. The development of a blend-sampling technique to assess the uniformity of a powder mixture. Drug Dev Ind Pharm 2001; 27(4), 297-307.
10. Muzzio FJ, Robinson P, Wightman C, Brone D. Sampling practices in powder blending. Int J Pharm 1997; 155(2): 153-178.
11. Ottino JM, Khakhar DV. Mixing and segregation of granular materials. Annu Rev Fluid Mech 2000; 32: 55-91.
12. Bridgewater J. Mixing and segregation mechanisms in particle flow. Granular Matter. 1994; 161-193.
13. Pingali KC, Saranteas K, Foroughi R, Muzzio FJ. Practical methods for improving flow properties of active pharmaceutical ingredients. Drug Dev Ind Pharm 2009; 35(12): 1460-1469.
14. Faqih AM, Mehrotra A, Hammond SV, Muzzio FJ. Effect of moisture and magnesium stearate concentration on flow properties of cohesive granular materials. Int J Pharm. 2007; 336(2): 338-345.
15. Yajima T, Shigeru ITAI, Hayashi H, Takayama K, Nagai T. Optimization of Size Distribution of Granules for Tablet Compression. Chem Pharm Bull 1996; 44(5): 1056-1060.

16. Kikuta JL, Kitamori N. Effect of mixing time on the lubricating properties of magnesium stearate and the final characteristics of the compressed tablets. Drug Dev Ind Pharm 1994; 20: 343-355.
17. Abe H, Otsuka M. Effects of lubricant-mixing time on prolongation of dissolution time and its prediction by measuring near infrared spectra from tablets. Drug Dev and Ind Pharm 2012; 38: 412-419.
18. Jarosz PJ, Parrott EL. Effect of lubricants on tensile strengths of tablets. Drug Dev and Ind Pharm. 1984; 10: 259-273.
19. Johansson ME. Influence of the granulation technique and starting material properties on the lubricating effect of granular magnesium stearate. J Pharm Pharmacol 1985; 37: 681-685.
20. Perrault M, Bertrand F, Chaouki, J. An experimental investigation of the effect of the amount of lubricant on tablet properties. Drug Dev Ind Pharm 2011; 37(2): 234-242.
21. Bakeev K. Overview of Process Analysis and PAT. *Process Analytical Technology: Spectroscopic Tools and Implementation Strategies for the Chemical and Pharmaceutical Industries*. Wiley 2010; 1–14.
22. Koeller D, Posch A, Hori G, Voura C, Radl S, Urbanetz N, *et al*. Continuous quantitative monitoring of powder mixing dynamics by near-infrared spectroscopy. Powder Technol 2011; 205: 87-96.
23. Bellamy L, Nordon A, Littlejohn D. Real-time monitoring of powder mixing in a convective blender using non-invasive reflectance NIR spectrometry. Analyst 2008; 133: 58-64.
24. Blanco M, Gozalez B, Bertran E. Monitoring powder blending in pharmaceutical processes by use of near infrared spectroscopy. Talanta 2002; 56: 203-212.
25. De Beer T, Bodson C, Dejaegher B, Walczak B, Vercryysse P, Burgraeve A, *et al*. Raman spectroscopy as a process analytical technology (PAT) tool for the in-line monitoring and understanding of a powder blending process. J Pharma Biomed Anal 2008; 48: 772-779.
26. Vergote G, De Beer T, Vervaet C, Remon J, Baeyens W, Diericx N, *et al*. In-line monitoring of a pharmaceutical blending process using FT-Raman spectroscopy. Eur J Pharm Sci 2004; 21(4): 479-485.
27. Breintenbach J, Schrof W, Neumann J. Confocal raman-spectroscopy: analytical approach to solid dispersions and mapping of drugs. Pharm Research 1999; 16(7): 1109-1113.
28. Porion P, Sommier N, Faugere AM, Evesque P. Dynamics of size segregation and mixing of granular materials in a 3D-blender by NMR imaging investigation. Powder Technol 2004; 141: 55-68.
29. Sommier N, Porion P, Evesque P, Leclerc B, Tchoreloff P, Couarraze G. Magnetic resonance imaging investigation of the mixing-segregation process in a pharmaceutical blender. Int J Pharm 2001; 222(2): 243-258.

30. Nakagawa M, Altobelli SA, Caprihan A, Fukushima E, Jeong EK. Non-invasive measurements of granular flows by magnetic resonance imaging. Exp Fluids 1993; 16(1): 54-60.
31. Perrault M, Bertrand F, Chaouki J. An investigation of magnesium stearate mixing in a V-blender through gamma-ray detection. Powder Technol 2010; 200(3): 234-245.
32. Broadbent CJ, Bridgewater J, Parker DJ. The effect of fill level on powder mixing performance using a positron camera. Chem Biochem Eng 1995; 56(3): 119-125.
33. Lai FS, Fan LT. A study on the mixing of flour in a motionless Sulzer (Koch) mixer using a radioactive tracer. Powder Technol 1976; 13: 73-83.
34. Crouter A, Briens L. Methods to assess mixing of pharmaceutical powders. AAPS PharmSciTech. 2019; 20:84.
35. Crouter A, Briens L. Passive acoustic emissions from particulates in a V-blender. Drug Dev Ind Pharm 2015; 41: 1809-1818.
36. Crouter A, Briens L. The effect of moisture on passive acoustic emissions in a V-blender. Powder Technol 2016; 299: 226-234.
37. Allan P, Bellamy L, Nordon A, Littlejohn D. Non-invasive monitoring of the mixing of pharmaceutical powders by broadband acoustic emission. Analyst 2010; 135(3): 518-524.
38. Crouter A, Briens L. Monitoring lubricant addition using passive acoustic emissions in a V-blender. Powder Technol 2016; 301: 1119 – 1129.
39. Cameron A, Briens L. An investigation of magnesium stearate mixing performance in a V-blender through passive vibration measurements. AAPS PharmSciTech 2019; 20: 199.
40. Weingberg S, Abramowitz S. Measure of Location, Spread, and Skewness. *Statistics using SPSS an integrative approach*. Cambridge University Press 2008.
41. Daubechies I. The wavelet transform, time-frequency localization and signal analysis. IEEE Trans Inf Theory 1990; 36: 961-1005.
42. Fu J, Adams MJ, Reynolds GK, Salman AD, Hounslow MJ. Impact deformation and rebound of wet granules. Powder Technol 2004; 140: 248-257.

Chapter 6

6 General Discussion and Conclusions

The final lubricant mixing stage in tablet manufacturing is crucial as it is the last step before tablet compression which can directly affect final product quality. A lubricant is added to ensure smooth ejection of the tablet following compression. Lubricants are mixed typically in a tumbling V-blender in batch stages which are sampled and tested offline resulting in a reduction in process efficiency and an increase in manufacturing costs. Lubricant addition should be monitored and controlled as overmixing and increased concentrations can degrade final tablet quality. To ensure product quality and control, process analytical technologies (PAT) can be implemented to increase process efficiency, product quality and consistency. However, most of these methods require extensive signal analysis or require insertion of probes or windows which disrupt the system. Passive vibration measurements can then be used to monitor lubricant addition without the limitations of other techniques

The objective of this work was to evaluate and optimize passive vibration measurements monitoring as a PAT for tablet lubricant addition. Previous work has established that vibration measurements from unlubricated particles are responsive to a variety of process changes and assessed the potential of vibration measurements to monitor lubricant dispersal. However, further work was required to understand how process parameters affect lubricant mixing performance by i) relating parameters including particle size, density, and lubricant concentration to energy dissipation and lubricant coating morphology, ii) investigating the effect of lubricant loading configuration and V-blender fill level on mixing performance, and iii) investigating the effect of lubricant concentration and segregation effects of varying sized granules on lubricant mixing profiles.

Various sized sugar spheres and glass beads were loaded into a V-blender and vibration measurements recorded. Three features were identified with one revolution attributed to particle motion. Feature 1 produced the most distinctive signals which responded to expected trends in process parameters and was chosen for future studies. Magnesium

stearate was mixed with particles and monitored. The introduction of magnesium stearate made collisions more inelastic decreasing the signal amplitude and the coefficient of restitution. With mixing, the signal amplitude decreased with further mixing until a stable value was reached indicating a mixing end-point. These findings were congruent with SEM images of lubricant dispersal progression. Further increases in lubricant concentration reduced required mixing time and lowered mixing end-point signal amplitudes as collisions were more inelastic and shearing and delamination of the lubricant particles occurred faster. Similarly, changes in particle type resulted in changes in mixing profiles. This study gained process knowledge of the mechanisms behind lubricant addition in coating morphology and energy dissipation as measured by the accelerometer. It also demonstrated the potential of vibration measurements to monitor lubricant addition for a variety of process parameters.

Since V-blenders possess inherent mixing mechanisms that can affect mixing performance, the effect of lubricant loading configuration and blender fill level on mixing performance was investigated to optimize lubricant addition. Glass beads were loaded into a V-blender at various fill levels and mixed with magnesium stearate loaded in various axial and radial loading configurations. Vibration measurements were recorded throughout the duration of mixing to monitor the process. Mixing time was reduced for axial loading configurations as the V-blender has a dominant convective mixing mechanism. Vibration measurements increased at lower fill levels, and decreased at higher fill levels, indicating an optimal fill level at $21 - 23$ vol %. The results demonstrated that lubricant addition can be monitored and optimized with axial loading configurations and $21 - 23$ vol % fill level as measured through passive vibrations.

Knowledge from previous studies was applied to monitor lubricant addition with granule formulations to simulate industrial conditions. Vibration measurements were used to monitor lubricant dispersal to investigate the effect of particle size, particle size distribution, and lubricant concentration on mixing. Signal amplitude increased with particle size due to changes in momentum. An increase in particle size resulted in a longer required mixing time due to an increased surface area to volume ratio. An increase in lubricant concentration effectively lowered the mixing end-point signal amplitude.

Changes in particle size distribution were reflected in changes in both signal amplitude and variation. In segregated mixtures, the signal was more responsive to larger particles due to trajectory segregation. These findings were supported by trials with glass beads. This study demonstrated the potential for passive vibration measurements to be implemented to monitor lubricant addition for common process parameters involved in granule formulations.

The research conducted indicated that passive vibration measurements can be used as a potential PAT for lubricant monitoring in tablet manufacturing. This allows for better process understanding, control, and optimization. Real-time measurements from the sensor would make it possible to monitor, control, and adjust operations accordingly in real-time reducing the dependence on offline sampling and testing. Vibration measurements monitoring would also allow for detection of mixtures out of specification including: segregated mixtures, larger particle sizes, and excessive lubricant concentrations. A secondary check would then be in place allowing for further processing to meet specifications before tableting resulting in fewer discarded batches. Furthermore, vibration measurement monitoring could allow for identification of factors that optimize lubricant addition including loading configuration and fill level which would reduce time in development and reduce mixing times.

6.1 Future Work

The research focused on ideal particles to easily identify and monitor solids flow and lubricant coating morphology. The ideal particles were chosen as they were uniform in shape and composition. Placebo granules were then used for their similarity to what is done commercially. Granules of different sizes were made by different granulation times and changes were easily visible resulting in granule sizes that are much larger than industry. As demonstrated in the research, smaller particle sizes can be detected by vibration measurements, however, further work involving commercially sized granules should be conducted to better simulate industry conditions.

In this research, mixing end-points of mixing profiles of trials susceptible to segregation containing large particles were more difficult to identify due to large variations in the

signal. The signal analysis method could then be adjusted to incorporate the entire power spectrum of the feature rather than the average amplitude of a specified number of peaks to reduce signal variation.

Furthermore, this research should be validated through relating obtained vibrational measurements to final tablet properties as lubricant dispersal has a direct impact on final tablet quality. Tablets are often characterized by their hardness which can be linked to friability and attrition resistance, and dissolution or disintegration time. Both characteristics must meet strict regulations and can be affected by particle size and lubricant concentration. In addition, traditional spectroscopic techniques should be implemented to assess lubricant content uniformity to validate mixing end-points. This would further reduce the dependence on offline measurements supporting the commercial implementation of vibration measurements monitoring for lubricant addition.

A preliminary study was conducted and indicated that the vibrational measurements and tablet properties were correlated.

6.1.1 Preliminary Study

6.1.1.1 Materials and Methods

6.1.1.1.1 Pellets

Pellets were made using samples of granules (Chapter 5, GR2) mixed with 1 – 10 wt % magnesium stearate. Samples of 350 mg were pelletized using a 2811 Parr Pellet Press with a die 6 mm in diameter and 25 mm in length with a compressive force upwards of 1000 lbs. Pellets were uniform with a diameter of 6 mm and a length of 11 mm.

6.1.1.1.2 Attrition Resistance

The method for testing attrition resistance was adapted from the United States Pharmacopeia (1). A sample of pellets corresponding to 6.5 g was placed inside a drum of 283 mm in diameter. The drum was rotated at a speed of 25 RPM and the tablets were tumbled by a curved projection of 76 mm in diameter. The drum was rotated for 100 revolutions where the pellets were susceptible to collisions with the drum wall or the

pellets themselves causing attrition. The samples were then dedusted and reweighed. The attrition resistance was expressed as the percent of the mass of pellets after and before testing. Trials were conducted in triplicate.

6.1.1.1.3   Disintegration Time

The method for the determination of disintegration time was adapted from the Ministry of Health of Canada (2). Six pellets were placed inside of a basket assembly consisting of six tubes. Perforated plates were found at each end of the tubes with holes 1.7 mm in diameter to retain larger pellet material. Plungers attached to the tubes submerged and raised pellets in 37 °C water in a repeated motion until no more pellet material was retained. The disintegration time was measured from the start of the test to the moment that all pellet material passed through the perforated plates. Trials were conducted in triplicate.

6.1.1.2   Results and Discussion

Vibration measurements amplitudes of granules mixed with 1 – 10 wt % magnesium stearate were obtained from Chapter 5 (Figure 5.8 b). These measurements were then compared to the attrition resistance and disintegration time of pellets made from the same granules as shown in Figure 6.1 and 6.2.
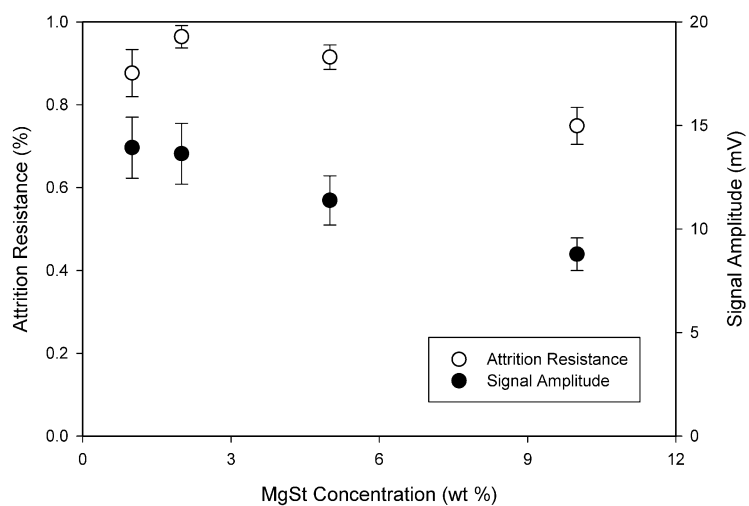
Figure 6.1: Vibration measurements and attrition resistance of granules and pellets with increasing magnesium stearate
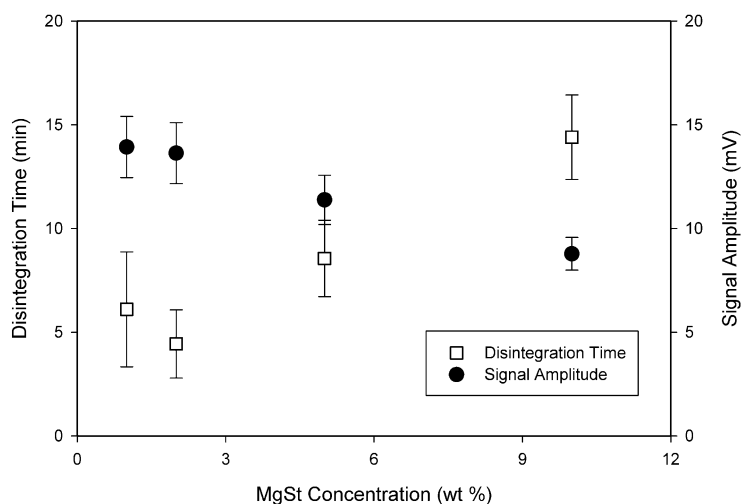
Figure 6.2: Vibration measurements and disintegration time of granules and pellets with increasing magnesium stearate

Both vibration measurements and attrition resistance decreased with increasing amounts of magnesium stearate. With the introduction of magnesium stearate to granules, magnesium stearate particles fill surface irregularities before adhering to the surface of the granules. The magnesium stearate particles alter the surface properties of the granules

making collisions more inelastic resulting in less energy being dissipated and transmitted into the accelerometer. With increasing amounts of magnesium stearate, the magnesium stearate layer on the surface of the particle becomes more complete and uniform, making collisions even more elastic resulting in a further decrease in measured vibrational amplitudes. Due to its lubricating ability, magnesium stearate reduces contact points and friction between granules and the pellet die during compression. Magnesium stearate interferes with the compression as it forms a layer so that granules do not bond together as well in the tablet resulting in weaker, more friable pellets (3) as measured by the attrition resistance. With increasing amounts of magnesium stearate, this effect is amplified resulting in further decreases in the attrition resistance.

With increasing magnesium stearate concentrations, vibrational amplitudes decreased as before, however, the disintegration time increased. As magnesium stearate is hydrophobic, the introduction of magnesium stearate makes granules and consequently pellets less soluble decreasing the time for tablets to dissolve as indicated by the disintegration time. With increasing amounts of magnesium stearate, a more uniform and complete layer of magnesium stearate is present in the granules increasing the hydrophobicity of the contents. This in turn makes pelletized samples more insoluble resulting in further increases in the disintegration time.

6.2 References

1. United States Pharmacopeia. Tablet friability. North Bethesda, Maryland, United States of America; 2006.
2. Ministry of Health. Determination of the disintegration of tablets. Ottawa, Ontario, Canada; 1989.
3. Jarosz PJ, Parrott EL. Effect of lubricants on tensile strengths of tablets. Drug Dev Ind Pharm. 1984; 10: 259-273.

Curriculum Vitae

Austin Cameron

EDUCATION

Master of Engineering Science   **2017 – 2019**
Chemical Engineering
Western University, London, Ontario, Canada
Thesis Title: "In-line Monitoring of Lubricant Addition Through Passive Vibration
Measurements in a V-blender"

Bachelor of Engineering Science   **2013 – 2017**
Biochemical and Environmental Engineering
Western University, London, Ontario, Canada

AWARDS AND ACCOMPLISHMENTS

Western Graduate Research Scholarship   **2017 – 2019**
Western University, London, Ontario, Canada

NSERC USRA   **2017**
Western University, London, Ontario, Canada

1st Place, 12th Annual Capstone Design and Competition: Petrochemicals   **2017**
Sarnia-Lambton Research Park, Sarnia, Ontario, Canada

Deans Honour List   **2016**
Western University, London, Ontario, Canada

Global Opportunities Award   **2016**
Western University, London, Ontario, Canada

Ivey Foundation Continuing Awards in Environmental Engineering   **2015, 2016**
Western University, London, Ontario, Canada

RELATED WORK EXPERIENCE

Graduate Teaching Assistant   **2017 – 2019**
Western University, London, Ontario, Canada

Undergraduate Research Assistant   **2017**
Western University, London, Ontario, Canada

PUBLICATIONS AND CONFERENCE PRECEEDINGS

Cameron A, Briens L. Monitoring magnesium stearate blending in a V-blender through passive vibration measurements. AAPS PharmSciTech. Published Online July 26, 2019.

Cameron A, Briens L. An investigation of magnesium stearate mixing performance in a V-blender through passive vibration measurements. AAPS PharmSciTech. Published online May 24, 2019.

Non-refereed contributions:
Cameron A. Acoustic Emission Monitoring. Institutional oral presentation at: Chemical and Biochemical Engineering Seminar, Western University. March 26, 2019; London, ON, Canada.